Cover Page

Final Technical Report

Reporting Period: July 1, 2013 to December 31, 2017

Date of Submission of Report: March 31, 2018

Federal Agency/ Organization Element:	DOE/EERE/ Office of Advanced Manufacturing Program (AMO)
Award Number:	DE-EE0005764
Project Title:	RAPID FREEFORM SHEET METAL FORMING: TECHNOLOGY DEVELOPMENT AND SYSTEM VERIFICATION
Project Period:	July 1, 2013 to December 31, 2017
Recipient Organization:	FORD MOTOR COMPANY
DUNS Number:	049967672
Principal Investigator:	Vijitha Kiridena, 313-594-4003, vkiriden@ford.com
	Ravi Verma, 314-545-9679, ravi.verma2@boeing.com
	Timothy Gutowski, 617-253-2034, gutowski@mit.edu
	John Roth, 814-898-7587, jtr11@psu.edu
Business Contact:	Melissa Hendra, 313-594-4714, mhendra@ford.com
Partners:	The Boeing Company, MIT and Penn State Erie
DOE Technology Manager:	David Forrest, 202-586-5725, david.forrest@ee.doe.gov
DOE Project Officer/Manager:	Bill Prymak, 720-356-1754, Bill.Prymak@go.doe.gov
DOE Project Monitor:	John Harrington, 720-356-1276, John.Harrington@go.doe.gov
DOE Contract Specialist:	Scott Schmitz, 720-356-1774, scott.schmitz@go.doe.gov
Submitting Official:	Vijitha Kiridena, Ph.D. Technical Expert Research & Innovation Center Ford Motor Company Telephone: 1-313-594-4003 E-mail: vkiriden@ford.com

Acknowledgment:

This report is based upon work supported by the U. S. Department of Energy's Office of Energy Efficiency and Renewable Energy Advanced Manufacturing under Award No. DE-EE0005764.

Table of Contents

Cover Page ... 1
Table of Contents ... 3
List of Acronyms ... 5
List of Figures ... 6
List of Tables ... 9
Executive Summary ... 10
Chapter 1. Introduction ... 12
Chapter 2. Background ... 15
2.1 State Of The Art ... 15
2.2 Previous Work On Sheet Metal Forming Environmental Impacts and Costs ... 17
2.3 Die-Set And Sheet Metal Impacts And Costs ... 17
2.4 Electricity Impacts, Electricity Costs and Labor Costs ... 18
2.5 Project Goals and Objectives ... 18
2.6 Planned Approach ... 20
Chapter 3. Results and Discussion ... 22
3.1 Task 1: Energy Management & Environmental Impact Modeling ... 22
3.1.1 Overview ... 22
3.1.2 Case Studies ... 22
3.1.3 Electrical Power Measurements ... 23
3.1.4 Global Models ... 24
3.1.5 Extrapolating To A National Level- Automotive ... 25
3.1.6 Further Extrapolations to the National level ... 26
3.2 Task 2: Development, Integration and Verification of RAFFT System ... 27
3.3 Task 3: Tool Path Generation Algorithm, Simulation Modeling and Process Optimization ... 31
3.3.1 Tool path Generation Algorithm ... 31
3.3.2 Tool Path Generation ... 33
3.3.3 Simulation Modeling ... 40
3.3.4 Process Optimization ... 52
3.4 Task 4: Electrically-assisted Freeform Sheet Metal Forming ... 59
3.4.1 Post-deformation EAM treatment investigation ... 59
3.4.2 In-situ EAM Treatment Investigation ... 64
3.5 Task 5: Material Characterization & Performance Validation ... 66
3.5.1 Effect Of Part Geometry, Sheet Alloy And DSIF Process Variables On Formability ... 66
3.5.2 Fatigue Testing Of DSIF Panels ... 69
Chapter 4. Benefits Assessment ... 76

4.1 Applications to the Automotive Industry 77
4.2 Applications to the Aerospace Industry 78
4.3 Savings in Other Sectors 79
4.4 Longer Term Potential 79
Chapter 5. Commercialization 82
Chapter 6. Accomplishments 83
Chapter 7. Conclusions 86
Chapter 8. Recommendations 89
Chapter 9. References 91
Chapter 10. Appendices 95

List of Acronyms

AM	Additive Manufacturing
ANOVA	Analysis of Variance
ANOM	Analysis of Means
BP	Budget Period
CED	Cumulative Energy Demand (primary energy)
DLA	Defense Logistics Agency
DALY	Disability-Adjusted Life Years
DOE	Department of Energy
DOE	Design for Experiment
DOF	Degree of Freedom
DSIF	Double Sided Incremental Forming
EADSIF	Electrically Assisted Double Sided Incremental Forming?
FCF	Fluid Cell Forming
GHG	Greenhouse gas emissions
HRC	Hot Rolled Coil
ISF	Incremental Sheet Forming
J	Joules
kWh	Kilo-Watt-hours
Lb	Pound mass, including million pounds (Mlbs)
PEEQ	Equivalent plastic strain
RAFFT	Rapid Freeform Sheet Metal Forming Technology
RIC	Research and Innovation Center of Ford Motor Company
SMF	Sheet Metal Forming
SPF	Super Plastic Forming
SPIF	Single Point Incremental Forming
t	Metric ton, including kilo-ton (kt) and mega-ton (Mt)
TPIF	Two-point incremental forming
UK	United Kingdom
US	United States
(S/A) CRC	Steel/Aluminum cold rolled coil
FE	Finite Element
3D	Three-Dimensional
ITP	Industrial Technologies Program

List of Figures

Figure 1.1 RAFFT machine 13
Figure 1.2 RAFFT formed panel 13
Figure 2.1 Schematic of a traditional sheet metal stamping process 15
Figure 2.2 DSIF Two Tool Alignment 15
Figure 2.3 Ford’s First DSIF machine 16
Figure 2.4 NU First DSIF machine 16
Figure 2.5 Schematic of planned technical tasks, their interactions and deliverables 20
Figure 3.1 RAFFT machine 27
Figure 3.2 The RAFFT machine installed and powered-on in the Ford RIC in Dearborn. Photograph taken on May 22nd, 2015 28
Figure 3.3 Binder Front view, w/ Cross Bars 29
Figure 3.4 Binder Back View 29
Figure 3.5 Ball-tip forming tools. Tip diameters are 6 mm, 10 mm, and 16 mm 30
Figure 3.6 Flat-tip forming tools. Tip sizes are 12 mm by 6 mm, 15 mm by 6 mm, and 18 mm by 10 mm, respectively 30
Figure 3.7 Moon roof frame 31
Figure 3.8 Mustang GT4 part 31
Figure 3.9 Two forming tool configuration 32
Figure 3.10 Schematic representation of two data structures 34
Figure 3.11 Enhanced RAFFT Toolbar 34
Figure 3.12 RAFFT User Interface panel with updates highlighted 35
Figure 3.13 Truncated Pyramid having concave and convex areas. Right side of the picture shows the generated RAFFT toolpaths of the Pyramid (Convex toolpath) and half spheres (Convex toolpaths) 36
Figure 3.14 Actual display of RAFFT formed mustang hood part showing shallow regions 36
Figure 3.15 Fill layer based on wall angle 37
Figure 3.16 Tool movement inside regions 37
Figure 3.17 Filled layer toolpath of Mustang hood 38
Figure 3.18 Fill layer tool mark on the corner of the Mustang hood 38
Figure 3.19 (a) CAD part (b) the formed part(c) Meshed sheet 41
Figure 3.20 Cross-section geometry comparison among CAD, experiment and simulation 42
Figure 3.21 Geometric comparison between the experiment and simulation (a) global (b) Cross-section 42
Figure 3.22 Simulated reaction force along Z-direction on tools with time(a) Thickness distribution along the wall(b) 42
Figure 3.23 Selected results of the ANOM and ANOVA 44
Figure 3.24 Von Mises stress for CPE4R (stability time=1E-5 sec) (a) 1E-5 sec (b) 1E-8 sec 45
Figure 3.25 Strain history of selected element in thickness direction (a) maximum principle strain (b) middle principle strain (c) minimum principle strain (d) equivalent plastic strain (e) shear strain.... 46

Figure 3.26 Principle of MT approach (a) tool-movement algorithm (b) visualization of toolpath for multiple tools, e.g. 20 pairs of tools shown 47
Figure 3.27 Geometry comparison between experiment and the simulation with 4 pairs of tools (a) global deviations (b) cross-section profile in X-direction (c) cross-section profile in Y-direction 47
Figure 3.28 Simulated part shown in z-displacement (a) Mustang Hood (b) Transit Hood (c) Swing Gate 48
Figure 3.29 Experiments to obtain squeeze factor database (a) truncated pyramids with varying wall angles (b) the deviation between the experiment and the CAD 49
Figure 3.30 DSIF (a) model setup (b) PEEQ strain in front view (c) PEEQ strain in back view 50
Figure 3.31 SPIF (a) model setup (b) PEEQ strain in front view (c) PEEQ strain in back view 50
Figure 3.32 In the back side of the slab for different squeeze factors (a) PEEQ strain history (b) Net force evolution 50
Figure 3.33 Squeeze factor, FEA vs. Experiment 51
Figure 3.34 Tool Parameters 52
Figure 3.35 A set of four "truncated pyramid" parts of varying wall-angles. Each one has a different squeeze factor value applied to each of the four faces 53
Figure 3.36 On the left is an image of the scanning arm, and on the right is a scanned part with colors indicating the deviation from the CAD 54
Figure 3.37 Experimentally determined optimal squeeze factor with respect to wall angle and step size 54
Figure 3.38 Failure limit diagram in single point incremental forming 55
Figure 3.39 Experimental result and simulation minimum principle strain contour for funnel test 56
Figure 3.40 Simulation minimum principle strain contour with fracture model 56
Figure 3.41 Flexible tool model 58
Figure 3.42 Effect of step down size on final part geometry (from left to right - 0.85mm, 0.55mm, ... 59
Figure 3.43 Examples of varying part distortion due solely to Clamping Configuration 59
Figure 3.44 Effect of pulse duration on part springback under v-bend testing conditions (left to right: 59
Figure 3.45 ANSYS model of the incremental forming process 60
Figure 3.46 Applicator for through-thickness spot application of EAM 60
Figure 3.47 Example point locations for through-thickness EAM treatments 61
Figure 3.48 Example positive and negative lead placement locations for path-based EAM treatments 62
Figure 3.49 Path-based EAM treatment fixture 62
Figure 3.50 Example lead locations for Area-based EAM treatments 63
Figure 3.51 Area-based EAM treatment application fixture 63
Figure 3.52 Electrically isolated incremental forming tool 64
Figure 3.53 Tool-to-post and tool-to-frame schematics 65
Figure 3.54 Preliminary In-situ EAM springback results 65
Figure 3.55 Preliminary in-situ EAM formability results 65
Figure 3.56 Panels formed with different variables shown in Table 3.9 67
Figure 3.57 Statistical analysis of formability dependence on various parameters 67
Figure 3.58 Schematic of coupons extracted from formed test panels 68

Figure 3.59 Mechanical properties of pyramid shaped panels formed by DSIF from various automotive and aerospace sheet alloys 70
Figure 3.60 Mechanical properties of panels formed in O-temper and followed by full heat treatment to a harder temper (a) 2024-O formed in O and HT to T42, (b) 7075 formed in O and HT to T62 71
Figure 3.61 Micrographs of formed aerospace alloy Al 7075 for two different ISF step sizes 72
Figure 3.62 Micrographs of formed aerospace alloy Al 7075 showing the inner tool side (left) and the outer side that was in contact with the steel overlay sheet (right) 72
Figure 3.63 High-cycle fatigue results of automotive alloys for specimen orientations parallel to and perpendicular to sheet rolling direction and parallel to rolling direction 74
Figure 3.64 Low-cycle fatigue results of aerospace Al alloys for different ISF step sizes and specimen orientations 75
Figure 4.1 The effect of production number over the die lifespan (N) on per part CED. Generic aluminum part modeled: 1.5 m2, 1.5 mm thick. Forming depth (for ISF calculation): 70 mm. In the case of stretch forming, Batch size, B=Number of parts produced, N. In the 76
Figure 4.2 The effect of production number on per-part cost (including labor and capital depreciation costs). Generic aluminum part modeled: 1.5m2, 1.5mm thick. Forming depth (for ISF calculation): 70mm 77
Figure 4.3 The effect of different “filters” on the addressable market. Distribution from 10,000 simulations 78
Figure 4.4 Total annual energy and cost savings across part prototyping (left column) and car development (right column) assuming ISF displaces zinc die drawing one-to-one in 2030. Distributions from 10,000 simulations 78
Figure 4.5 Potential annual benefits in the USA by 2030 from the development of RAFFT 81
Figure 5.1 High Level RAFFT Deployment & Commercialization Options 82

List of Tables

Table 3.1 Parts formed in the case studies 23
Table 3.2 Summary of electrical energy and power results from the case studies 24
Table 3.3 Mechanical properties of DDQ steel 40
Table 3.4 Simulation parameters and their levels 43
Table 3.5 Analysis cases and relative CPU costs. (The two-dimensional explicit analyses all use CPE4R elements. The three-dimensional explicit case uses C3D8R elements) 45
Table 3.6 Summary for geometric comparison between simulations and experiment data 47
Table 3.7 CPU time comparisons 48
Table 3.8 Maximum forming forces comparison 57
Table 3.9 Post-DSIF mechanical properties of common automotive and aerospace sheet alloys 66
Table 3.10 Sheet alloys, initial tempers, and post-forming heat treatments 68
Table 3.11 Various Zones and tensile specimen orientations 69
Table 3.12 Mechanical properties after forming in O-temper, and after heat treating, as indicated 71
Table 3.13 Fatigue test matrix - aerospace alloys 71
Table 3.14 Fatigue test matrix - automotive alloys 71
Table 3.15 Surface roughness averaged over all 4 faces of all 3 panels (12 measurements) 73

Executive Summary

The objective of this project is to develop a transformational **RA**pid **F**reeform sheet metal **F**orming **T**echnology (**RAFFT**) in an industrial environment, which has the potential to increase manufacturing energy efficiency up to ten times, at a fraction of the cost of conventional technologies. The RAFFT technology is a flexible and energy-efficient process that eliminates the need for having geometry-specific forming dies. The innovation lies in the idea of using the energy resource at the local deformation area which provides greater formability, process control, and process flexibility relative to traditional methods.

Double-Sided Incremental Forming (DSIF), the core technology in RAFFT, is a new concept for sheet metal forming. A blank sheet is clamped around its periphery and gradually deformed into a complex 3D freeform part by two strategically aligned stylus-type tools that follow a pre-described toolpath. The two tools, one on each side of the blank, can form a part with sharp features for both concave and convex shapes. Since deformation happens locally, the forming force at any instant is significantly decreased when compared to traditional methods. The key advantages of DSIF are its high process flexibility, high energy-efficiency, low capital investment, and the elimination of the need for massive amounts of die casting and machining. Additionally, the enhanced formability and process flexibility of DSIF can open up design spaces and result in greater weight savings.

The RAFFT system is the first demonstration system of flexible forming at a large scale in an industrial environment. In addition to Ford and Boeing, the project brought together supplier base from both automotive and aerospace industries during its course, and paved the way for future commercialization of the developed technology. Specific goals include:

a) Design, build and demonstrate the proposed prototype system with unique double-sided incremental forming machine architecture for rapid freeform sheet forming with a sheet size up to 2.0 m x 1.5 m, large enough for most of automobile and aerospace parts.

b) Develop toolpath algorithms for RAFFT process and use the above prototype system to achieve the desired dimensional accuracy (bilateral profile tolerance of 1 mm) and surface finish (Ra < 30 μm);

c) Systematically characterize the performance, fatigue, and microstructure of RAFFT-formed material;

d) Achieve formability 10% higher than that in the conventional incremental forming process using a hybrid Thermally-Assisted Double-Sided Incremental Forming (TADSIF) process;

e) Consistently monitor and manage the energy utilization and environmental impact of RAFFT processes; and

f) Create methodology and evaluation models which link the process planning with energy cost.

The major accomplishments and findings of the RAFFT project are:

- **Energy Management & Environmental Impact Modeling**: Energy management and environmental impact models were developed based on the analysis of case studies for RAFFT and four conventional sheet metal forming processes. This analysis allowed the construction of generalized global models. These models were used to explore a wider range of forming situations which were then used to identify the specific application areas where RAFFT can replace conventional technologies. Techniques like the Bass Diffusion model were employed to estimate how RAFFT would diffuse into these areas.

  The boundaries of the analyses were drawn around the process and included the cost and environmental impacts associated with materials, labor, depreciated equipment, tooling dies,

energy (electricity), and any auxiliary materials (lubricants). The impacts and costs are expressed "per part," with the impacts and costs of a die-set amortized (allocated equally) over the total number of parts produced using that die. The analyses are 'cradle-to-gate' life cycle assessments; the analysis starts from resource extraction (e.g., mining of ore, drilling for natural gas) and ends at the output of the forming process.

- **Development, Integration and Verification of RAFFT System**: A RAFFT machine which can form sheet metal parts without using dies with an effective working (sheet) area of 2.0 m x 1.5 m was conceptualized, designed, manufactured and commissioned in March 2015. It is installed and fully operational at Ford Motor Co. Research and Innovation center in Dearborn MI. This prototype experimental machine has the potential capability of making majority of the sheet metal parts used in ground and aerospace applications.

- **Tool Path Generation Algorithm, Simulation Modeling and Process Optimization**: New algorithms for generating Double-Sided Incrementally Forming (DSIF) toolpaths were developed, implemented, tested and released in second-Generation RAFFT (tool path-generation) software - built within the CATIA environment. Also, a platform for exchanging data among all software applications was developed and is being used for modeling, analysis and testing in order to (1) improve performance & scalability (2) improve robustness (3) employ service-based architecture (4) consolidate source code and (5) ensure easy maintenance

  Additionally, unique simulation methodologies were developed for simulating RAFFT (DSIF) models in Abacus and LS-Dyna. Current models produce results in ~ 30% of the time used by the original models. These models along with results from structured experiments were used to determine and build a database with optimum process parameters.

- **Electrically-assisted Freeform Sheet Metal Forming:** Methods were investigated to understand the effectiveness of post-deformation EAM treatments for reducing part springback by determining the effect of various physical process parameters such as feed rate, step-over, step-down, clamping mechanism, etc. on part distortion. Next, the effectiveness of various EAM process parameters such as current density, duration, etc. were determined via v-bend and 90 degree wiping test configurations for reducing springback in the materials being investigated.

  Once the above EAM testing parameters were determined, probable application test locations/patterns needed to be established along with a process to develop an ANSYS model for approximating the residual stress state after the deformation.

- **Material Characterization & Performance Validation**: Employed the Definitive Screening Designs approach (Jones and Nachtheim, 2013) to develop an optimum Design of Experiments (DOE) for identifying factors that have the most effect on forming by DSIF. Statistical analysis of formability dependence on various parameters was carried out with the results. The analysis returned a model that captured 97% of variation of all the variables ran. The results show that tool radius, wall angle, and sheet temper are the most significant contributors to formability with DSIF.

RAFFT has a great potential to revolutionize the production of freeform sheet metal parts in diverse manufacturing industries. It may stimulate small business development, smart machine tool, and software development firms, and could enhance industrial competitiveness in both mature and emerging industries. The current strategy to commercialize RAFFT technology in three stages begins through Ford's fully own subsidiary Troy Design and Manufacturing (TDM). The leadership from Ford Research is in discussions with the leadership from TDM to find the best way to make RAFFT technology smoothly transition from Research to TDM.

Chapter 1. Introduction

The objective of this project is to develop a transformational **RA**pid **F**reeform sheet metal **F**orming **T**echnology (**RAFFT**) in an industrial environment, which has the potential to increase manufacturing energy efficiency up to ten times, at a fraction of the cost of conventional technologies. The RAFFT technology is a flexible and energy-efficient process that eliminates the need for having geometry-specific forming dies. The innovation lies in the idea of using the energy resource at the local deformation area which provides greater formability, process control, and process flexibility relative to traditional methods.

The traditional sheet metal drawing process utilizes a set of dies under mechanical force generated by a press to deform an initially flat sheet into a three-dimensional (3D) part. A massive die set has to be engineered, cast, and machined even for prototyping or low-volume parts, for which the cost, time, and energy requirements become highly burdensome. In the aerospace industry, up to 95% of parts from high-grade aerospace aluminum alloys are machined out of bulk materials to avoid the construction of dies, with significant cost and material waste.

Double-Sided Incremental Forming (DSIF), the core technology in RAFFT, is a new concept for sheet metal forming. A blank sheet is clamped around its periphery and gradually deformed into a complex 3D freeform part by two strategically aligned stylus-type tools that follow a pre-described toolpath. The two tools, one on each side of the blank, can form a part with both concave and convex shapes, and sharp features. Since deformation happens locally, the forming force at any instant is significantly decreased. The key advantages of DSIF are its high process flexibility, high energy-efficiency, low capital investment, and the elimination of the need for massive die casting and machining. Additionally, the enhanced formability and process flexibility of DSIF can open up design spaces and result in greater weight savings.

The most significant benefit of RAFFT is reducing the engineering and manufacturing time for sheet metal parts from the current 8 ~ 25 weeks to less than one week. RAFFT is ideally suited for small volume production in aerospace industry, prototyping in automotive and appliance industries, on-site repair for military applications, personalized products in the medical industry, and one-of-a-kind creative art products. Once developed, verified, and demonstrated in this project, the implementation and growth of RAFFT will advance machine tool and software industries, create opportunities in emerging industries for clean energy and low-carbon economy, and increase U.S. manufacturing competitiveness.

The technology will enable the manufacture of materials or components with multiple market applications, and new manufacturing technologies that reduce process steps, material waste, or parts count, thereby reducing the embedded energy in the manufacturing value chain.

The technology is expected to revolutionize the production of freeform sheet metal parts in diverse manufacturing industries. It may stimulate small business development, smart machine tool and software development firms, and could enhance industrial competitiveness in both mature and emerging industries. Some examples are:

<u>Automotive</u>

- Prototype Vehicles
- Concept Vehicles
- Vehicle Personalization
- Low-Volume Production
- After-Market Part Service
- Performance Racing

<u>Aerospace and Defense</u>: Low-volume production; in-theater replacement parts.
<u>Biomedical</u>: Customized medical applications (e.g. Cranial plate, ankle support etc.)
<u>Appliance</u>: Prototyping and after-market services
<u>Art and Entertainment</u>: Creative sculptures

Traditionally, prototyping in the car industry has relied on the use of a drawing process that requires multiple cast-and-machined zinc die-sets and a hydraulic stamping press. RAFFT, therefore, presents the opportunity to avoid the die-making process, saving time, money, and energy. It is found that by 2030 it is likely that over 400,000 prototype parts per year will be made with geometries that RAFFT can form. The potential market shrinks to around 300,000 parts when we consider only those components for which RAFFT production will save energy and reduce costs compared to zinc die drawing. The potential market shrinks still further to around 260,000 parts when we consider the likely roll-out of the technology from 2017 onwards (technology diffusion), rather than assuming 100% market penetration. Energy, CO2eq and cost models of RAFFT and drawing are used to estimate potential mean savings of around 100 $TJ_{primary}$, 4.7 kt CO2eq, and 60 million US dollars per year by 2030. Approximately 70% of these savings are derived from the replacement of zinc dies used in early part prototyping. The other 30% derives from the possible use of RAFFT to replace zinc drawing die-sets used in car development (larger batch sizes of 250-units).

Successful commercialization of RAFFT technology is critical to achieving the full potential of energy, environmental and economic benefits. Figure 1.1 shows the RAFFT machine developed under this project, and Figure 1.2 shows a typical RAFFT formed panel.

Figure 1.1 RAFFT machine

Figure 1.2 RAFFT formed panel

We believe the optimal path for successful commercialization is to be carried out in three phases.

Phase 1: Implementing RAFFT technology at Ford's fully own subsidiary that provides stamping engineering and sheet metal prototype products to Ford as well as outside customers. During this phase, RAFFT will be integrated and verified in to a complete sheet metal prototyping eco system that include trimming, hemming, flanging and joining. (24 months)

Phase 2: Ford's fully own subsidiary will be marketing and selling finished sheet metal prototype parts to customers outside of Ford (18 months)

Phase 3: Possibly, setting up a separate business entity for further developing marketing, selling, providing service and customer support for a commercial RAFFT eco system that includes (a) RAFFT machines, (b) RAFFT software platform, and (c) RAFFT simulation methodologies & analytical tools. (18 months)

Chapter 2. Background

2.1 State Of The Art

Sheet metal forming processes have been widely used in various industries, including automotive, aerospace, medical, appliance, beverage containers, etc. Traditional sheet metal stamping die setup. is highly efficient for high-volume productions, with a typical cycle time of fewer than 10 seconds (Kalpakjian and Schmid, 2008), and therefore, is widely used for mass production, examples of which include the making 230 billion metal cans annually, or hundreds of thousands of hoods for a particular model of car. However, when the production volume is fewer than 5000 parts, the traditional sheet metal stamping process becomes highly burdensome in time, energy, and cost since a heavy and massive die set, such as the one shown in Figure 2.1 has to be engineered, cast, machined, and then tried out. To avoid the construction of dies, in the aerospace industry, many parts are produced by machining directly from billet materials. Hence, up to 95% of high-grade aerospace aluminum alloys are machined away, which is a significant material and energy waste (Heinz et al., 2000).

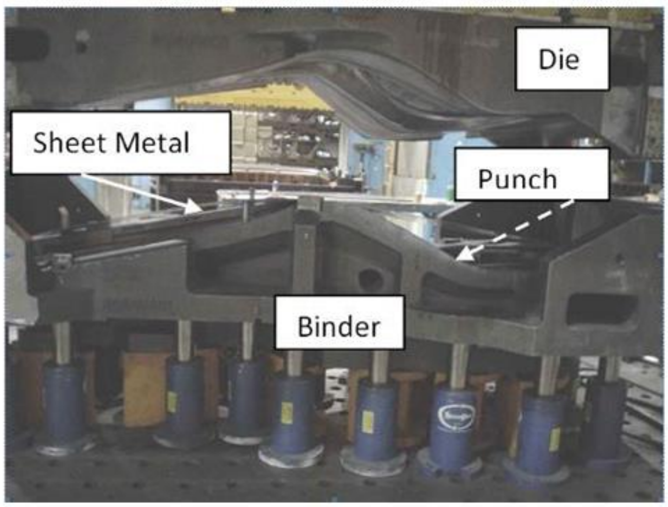

Figure 2.1 Schematic of a traditional sheet metal stamping process

Double-Sided Incremental Forming (DSIF), utilizes two opposing stylus-type tools that follows a predefined toolpath on each side of the blank, which can form a part with both concave and convex shapes. Each tool has three or four degrees of freedom (DOF). Their motions can be independently controlled or synchronized to achieve the desired outcome as shown in Figure 2.2.

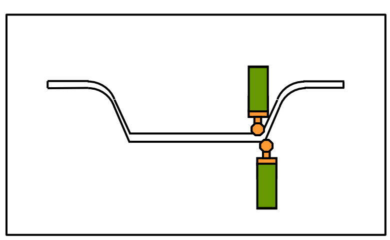

Figure 2.2 DSIF Two Tool Alignment

The key advantages of DSIF are its high process flexibility, high energy efficiency, low capital investment, elimination of the need for massive geometry-specific dies which results substantial reduction in energy and cost. Additionally, the enhanced formability and process flexibility of DSIF can open up design spaces and result in new material choices and greater weight savings.

This DSIF idea was conceived almost simultaneously and independently at Ford and Northwestern University. A medium-size-scale DSIF Lab machine, using two hexapods was designed and built by Ford in 2008 (Figure 2.3). In the same year, these two teams joined the effort and completed a one-year exploratory DOE/ITP project, in which a synchronized control system was developed at Ford, and a DSIF-specific system was built at Northwestern University (Figure 2.3) with the option of passing electricity between the two tools to further enhance the formability (Roth and Cao, 2011). During the same period, Boeing began to research the impact on mechanical performance and formability limits of aerospace aluminum alloys. Furthermore, researchers at M.I.T. evaluated the energy consumption and performed a life-cycle analysis of DSIF systems against other forming processes, showing greater energy efficiency as discussed later.

Figure 2.3 Ford's First DSIF machine

Figure 2.4 NU First DSIF machine

Back in 2013, the two lab-scale DSIF machines mentioned above, to the best of our knowledge, were the only DSIF platforms in the U.S. They have demonstrated the great potential of DSIF and provided the necessary physical means for understanding failure mechanisms, effects of process parameters on formability, microstructure, mechanical properties, and fatigue behavior of DSIF manufactured parts, and for determining the energy benefits. However, the capabilities of these two systems are limited in terms of size, speed, geometric complexity parts that can be made, and dimensional accuracy, which are essential for making DSIF a viable technology for industrial applications.

2.2 Previous Work On Sheet Metal Forming Environmental Impacts and Costs

The forming of complex sheet metal parts is expensive and requires energy-intensive inputs. It is estimated that over 100 billion USD is spent annually in the United States on the design, fabrication, and assembly of stamped parts (Lovell et al. 2006). Improvements in sheet metal forming could therefore result in significant savings in the US economy. The sheet metal parts are typically made from steel or aluminum. Production of these two metals accounts for over 10% of global anthropogenic carbon dioxide emissions (Allwood et al., 2012). Work by Cullen et al. (2012, 2013) suggests that as much as one-fifth of the metal produced (corresponding to 2% of global emissions) is cold rolled into thin sheets for subsequent forming. Additionally, forming processes typically use part-specific die-sets that require energy-intensive casting and machining operations to manufacture. The dies are then pressed into the sheet using mechanisms that rely on electric motors that are often poorly optimized to the load characteristics during the forming cycle (Zhao et al., 2015).

There have been few holistic studies on the environmental impacts of sheet metal forming. Studies that examine the energy required to make a sheet metal part typically ignore the energy invested in the die-making process, and in making the sheet metal and lubricant. In sustainability orientated analysis, Ingarao et al. (2012) state that in sheet metal forming, unlike in machining, there is little “material wastage” and therefore the electrical consumption of the press is the dominant factor to analyze when establishing environmental impacts. However, in a study on the car industry, Omar (2011) finds that on average 35% of the material in a sheet metal blank does not make it into the final part and is scrapped. The impacts of wasted material should therefore not be assumed negligible. In an environmental and cost analysis of stamping low-volume sheet metal car parts, Cooper et al. (2016) find that the impacts of the press electricity are negligible when compared to the impacts of the sheet making or die-making processes.

2.3 Die-Set And Sheet Metal Impacts And Costs

Many researchers make die-set cost comparisons between an emerging technology (FCF, SPF, or ISF) and conventional drawing. In the case of FCF, Peltier and Johannisson (1998) state that the process leads to a 50-90% reduction in tool costs compared to drawing. In a study on the production of aluminum door structures, Luckey et al. (2007) find tool savings of 80% for SPF compared to drawing. Friedman et al. (2004) also compare SPF (in this case of aluminum car hoods) to drawing, finding that SPF is cheaper for batch sizes smaller than 5,000 parts. Despite the apparent cost savings associated with FCF and SPF in the above studies, it is unclear whether these savings correspond to energy savings or a reduction in environmental impacts.

Several authors present a direct cost comparison between conventional deep drawing and ISF. Tuomi and Vihtonen (2007) present the results of discussions with a manufacturer who uses twin-point-incremental-forming (TPIF) to form prototypes prior to production using drawing. For TPIF, the average support tool cost was 1,350 euros and the average related production tooling cost was 31,500 euros. Tuomi and Vihtonen (2007) suggest that for new products where there is uncertainty over part geometry and where the product design is likely to change after product launch, it is economically sensible to start production with ISF small batch production before moving onto matched die-sets.

Theoretical ISF cost analyses are presented by Petek et al. (2007), Ingarao et al. (2012), and Lamminen et al. (2004). Petek et al. (2007) and Ingarao et al. (2012) both calculate the blank size and forming energy in conventional forming using finite element simulations and compare their results to experiments on incremental sheet forming. Both investigations find that the increased formability of ISF could result in smaller metal blanks and lower material costs, with Ingarao et al. (2012) finding an average blank size reduction of approximately 10%. Petek et al. (2007) assume that deep drawing would require a die-set costing 3,000 euros and that the forming rate of conventional forming and ISF are 7 parts/min and 0.125 parts/min respectively. Petek et al. (2007) find that the cost per part is lower for ISF than conventional deep drawing for batch sizes up to approximately 660 parts. Lamminen et al. (2004) performs a theoretical cost comparison for the forming of a shallow metal pan considering two scenarios. In the first, the ISF tool feed rate is 15 m/min, with a 0.2 mm vertical step size. In the second, the feed rate is doubled and the step size is increased to 0.5 mm. In the cost comparison, Lamminen et al., (2004) find that the total cost is less for the case of ISF up to a batch size of 200 parts in the first scenario, and up to 1000 parts in the second scenario (approximately 130,000 euros for the complete batch in both cases).

2.4 Electricity Impacts, Electricity Costs and Labor Costs

A few studies consider the electrical energy needed to form sheet metal. Examples include Zhao et al. (2015) and Cooper et al. (2016) for the case of hydraulic drawing presses, and Branker et al. (2012) and Ingarao et al. (2013) for the case of ISF. Electrical power measurements can, at a minimum, help engineers select appropriate motor sizes. Power measurements can also inform new machine architectures as designers look to minimize electricity costs and environmental impacts. Despite their utility, no electrical power measurements have been found in the literature on stretch forming, FCF, or aluminum SPF.

Several researchers report the electrical energy needed to operate a drawing press. Some express the energy needed per stroke of the forming press (Schuler, 1998; Zhao et al., 2015), and others the energy needed per kilogram of sheet formed (Brown et al., 1985; Burnham et al., 2006; Sullivan et al., 2010; Milford et al., 2011). Cooper et al. (2016) find that a hydraulic single-action press used for prototyping (800 short ton capacity) requires 1.2 kWh of electricity per stroke of the press. The electricity required per stroke is largely independent of the die geometry and material being formed. Subsequently, Cooper et al. deem “electricity requirements per stroke” an appropriate expression of electricity requirements in a hydraulic drawing press. In mass production, mechanical drawing presses are more commonly used. These presses are quicker than hydraulic presses and consume 0.1-0.2 kWh of electricity per part (Schuler GmbH, 1998; Cooper et al., 2016).

Several researchers find ISF machine electrical power requirements to be largely independent of changes in tool speed or incremental step size (Ingarao et al., 2013; Branker et al., 2012). Instead, the baseload power (minimum power required by the machine when on but not in use, frequently referred to as standby mode or idling) dominates the total power requirements (Dittrich et al., 2012; Branker et al., 2012) and the forming time determines overall electricity requirements (Branker et al., 2012; Ingarao et al. 2013). The largest power requirement of an ISF machine identified in the literature is 3 kW (Ingarao et al., 2013).

Several authors have analyzed the cost of incremental sheet forming. Branker et al. (2012) find that the sheet metal cost (approximately $4 per part for forming an aluminum cowboy hat) accounts for over 90% of the material costs (the lubricant and tool cost being minimal) and that the electricity costs are insignificant (around $0.10 per part). The labor costs (assumed to be $60/hour), and therefore the forming time, dominate all other considerations.

2.5 Project Goals and Objectives

The RAFFT system is the first demonstration system of flexible forming at a large scale in an industrial environment. In addition to Ford and Boeing, the project brought together supplier base from both automotive and aerospace industries during its course, and paved the way for future commercialization of the developed technology. Specific goals include:

g) Design, build and demonstrate the proposed prototype system with unique double-sided incremental forming machine architecture for rapid freeform sheet forming with a sheet size up to 2.0 m x 1.5 m, large enough for most of automobile and aerospace parts.

h) Develop toolpath algorithms for RAFFT process and use the above prototype system to achieve the desired dimensional accuracy (bilateral profile tolerance of 1 mm) and surface finish (Ra < 30 μm);

i) Systematically characterize the performance, fatigue, and microstructure of RAFFT-formed material;

j) Achieve formability 10% higher than that in the conventional incremental forming process using a hybrid Thermally-Assisted Double-Sided Incremental Forming (TADSIF) process;

k) Consistently monitor and manage the energy utilization and environmental impact of RAFFT processes; and

l) Create methodology and evaluation models which link the process planning with energy cost.

2.6 Planned Approach

Five (5) coherent "Technical Tasks" were planned as shown in Figure 2.5, to achieve the scientific and technical merits. In addition to the technical tasks, a sixth task was planned for project management.

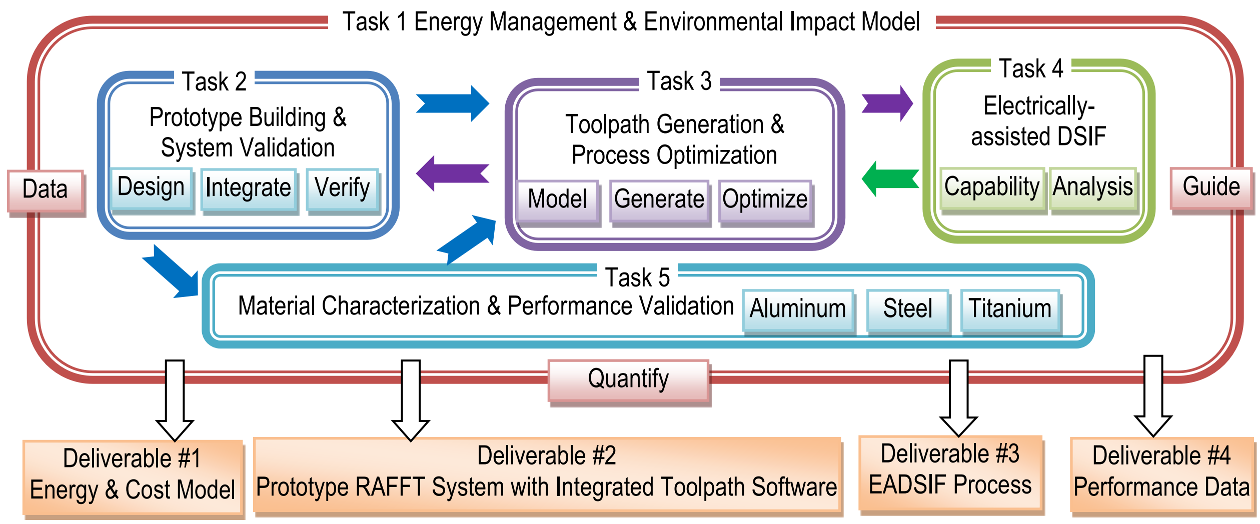

Figure 2.5 Schematic of planned technical tasks, their interactions and deliverables

Task 1: Energy Management & Environmental Impact Modeling

The **objective** of this task is to analyze the energy, cost and environmental impact of the proposed new technology at the prototype stage and at the envisioned scaled-up stage, and compare these results to conventional processes, mostly sheet metal forming processes. This work will take advantage of previously measured lab-scale DSIF data as well as new measurements of **RAFFT, EADSIF** and competing processes. This is needed to clearly state the advantages of the new processes, and to identify opportunities for improvement.

Task 2: Development, Integration and Verification of RAFFT System

The objective of this task is to develop, integrate and verify an industrial-scale, closed-loop prototype RAFFT system with an effective working (sheet) area of 2.0 m x 1.5 m that allows for the production of the majority of sheet metal parts used in ground and aerospace applications. Figure 2.3 and Figure 2.4 show the medium- and small-scale DSIF systems developed at Ford and NU with respective working sheet areas of 675 x 675 mm and 250 x 250 mm. These systems are currently being used to investigate the fundamental characteristics and behavior of DSIF processes. However, for making DSIF a viable technology for industrial applications, we have to overcome the current limitations of these systems regarding size, speed, and geometric complexity and accuracy.

Task 3: Tool Path Generation Algorithm, Simulation Modeling and Process Optimization

The objective of this task is to develop a semi-automated system that generates DSIF toolpaths for a given free-form geometry and desired part accuracy and to establish a validated rapid FEM simulation methodology. Different toolpath algorithms will affect the final shape accuracy as springback is path sensitive. The primary challenges in toolpath generation include: identifying the successful toolpath and path control algorithm that results in a minimum forming time for a given machine configuration, freeform part geometry, and required surface finish and geometric accuracy.

<u>Task 4: Electrically-assisted Freeform Sheet Metal Forming</u>

The objective of this task is to investigate the effect of electricity on material deformation and springback elimination when the sheet is being formed by DSIF.

Our past results showed that passing pulsed electricity through the material under uniaxial tension or compression can extend deformation limit while reducing the forming load. Depending on the material type and applied current density, the extra amount of deformation can be as much as 400% (Roth et al., 2008), so-called 'electroplasticity' effect. In the recent DOE ITP project, for the first time, this team uniquely linked the electrical effect with mechanical deformation in DSIF. DSIF provided a rare mechanism such that electricity can be applied to the sheet metal locally through the two forming tools in a deformation zone. This local effect enables the local current density exceeding the threshold density necessary for the electroplasticity effect, typically in the order of 10s A/mm2, without the need of a heavy-duty power supply.

<u>Task 5: Material Characterization & Performance Validation</u>

The objective of Task 5 is to validate the formability limits, static mechanical, and fatigue performance of DSIF manufactured parts.

Through the previous work Boeing has performed under contract with the Defense Logistics Agency (DLA) on SSIF of 2024 and 7075 aluminum alloys (DLA, 2009), it was discovered that extremely high levels (up to 35%) of reduction in thickness can be achieved while most forming processes are limited to a 5% reduction due to fracture. SSIF has demonstrated that there was a possibility that the required forming could take place at room temperature and employ commonly-used alloys. Also, the DLA study demonstrated that despite the severe deformations achieved, there was no corresponding drop in the mechanical (static and fatigue) performance, which is extremely important for aerospace applications. The downside of the SSIF process is that it requires a geometry-specific tooling for each geometry manufactured, which the proposed DSIF does not.

<u>Task 6: Project Reports and Management</u>

Ford will be responsible for overall project management. It is led by Dr. Kiridena and assisted by the entire team as well as Ford's Business Planning Office.

Chapter 3. Results and Discussion

3.1 Task 1: Energy Management & Environmental Impact Modeling

3.1.1 Overview

The models developed for this study are fundamentally based on our analysis of case studies for the five sheet metal forming (SMF) processes in question; four conventional and one ISF/RAFFT. This analysis allowed the construction of generalized global models which allowed us to explore a wider range of forming situations. We then used this model to identify the specific areas where RAFFT can replace conventional technologies and employed techniques like the Bass Diffusion model to estimate how RAFFT would diffuse into these areas.

The boundaries of the analyses are drawn around the process and include the cost and environmental impacts associated with materials, labor, depreciated equipment, tooling dies, energy (electricity) and any auxiliary materials (lubricants). The impacts and costs are expressed “per part,” with the impacts and costs of a die-set amortized (allocated equally) over the total number of parts produced using that die. The analyses are ‘cradle-to-gate’ life cycle assessments: the analysis starts from resource extraction (e.g., mining of ore, drilling for natural gas) and ends at the output of the forming process. In the Appendix, we address the differences in end of life cycle for these processes.

3.1.2 Case Studies

Case studies were conducted on each of the five SMF processes. Table 3.1 summarizes the key features of the parts and the die-sets used to produce them. The drawing case study presented here is a summarized version of the case study presented in Cooper et al. (2016). Only in the drawing case study could the die cost be confirmed (47,000 USD). Zinc die-sets were used in both the drawing and stretching case studies. Zinc is appropriate for low-volume production in the hundreds or low thousands of parts because it is easier to cast and machine than iron but wears more quickly. FCF is the only process in which multiple parts can be made simultaneously. In the case study, two FCF parts were produced at once; hence their inclusion in Table 3.1. Table 3.1 also includes the batch size (number of parts made sequentially until the next die-set changeover) and the production number over the die lifespan. The production number (N) is used to amortize the impact of die-making over the number of parts produced. The batch size (B) is used to amortize the impacts of batch set-up (for example, pre-heating the SPF die) over the number of parts in the batch.

The production number over the die lifespan (N) may be determined by either physical or economic factors. For instance, zinc drawing dies are likely to wear out and need replacement after being used to make several hundred parts (physical factor), whereas the number of parts made using long-lasting iron SPF dies is likely to be constrained by customer demand (economic factor). The batch size (B) is determined by internal company scheduling, which may be influenced by customer demand. For example, aerospace customers may only require tens of units per year of some aircraft parts, necessitating the manufacturer to either form small batches of parts or stock inventory.

Process		Drawing (750 short ton load)	Stretch forming	Fluid cell forming (30 MPa pressure)		Super-plastic forming	Incre-mental sheet forming
Part made		Truck hood prototype	Large 'U' shaped part	Flanged rectangular part	Flanged semi-circular part	Semi-truck bumper	Truncated cone4
Product-ion number over the die lifespan	(Parts/ Die)	250	750	750	750	750	N/A
Batch size	(Parts/ Batch)	250	8	750	750	90	3
Part	Material	Alum. (AA6014)	Alum. (AA7075)	Alum. (AA7075)	Alum. (AA7075)	Alum. (SP5083)	Low carbon galvanized steel
	Stock sheet area (m2)	3.7	2.14	0.39	0.04	3.3	0.3
	Blank area (m2)	3	2.14	0.39	0.035	3.3	0.25
	Blank thick-ness (mm)	0.95	0.81	1.6	1.6	3	1
	Final part area1 (m2)	2.1	1.87	0.39	0.035	1.92	0.07
	Final part mass (kg)	5.4	4.1	1.67	0.15	15.5	0.55
Lubricant	Type	Lubricant	Lubric-ating oil	Lubric-ating oil	Lubric-ating oil	Graphite	Lubric-ating oil
	Mass (grams/m2 blank)	0.75 (both sides)	100 (one side)	0.5 (both sides)	0.5 (both sides)	160 (one side)	100 (both sides)
Die-set	Material	Zinc2	Zinc2	Alum. (AA7075)	Alum. (AA7075)	Cast iron	N/A
	Mass (kg)	13,190 cast3 1,980 machined-away	4,099 cast 410 machined-away	92.8 block 18.6 machined-away	26.1 block 11.2 machined-away	4,897 cast 331 machined-away	N/A

1. Final part area is approximate, as it assumes no thinning during forming
2. Zinc alloy: Kirksite A
3. The "cast" mass is the total die mass as-cast (minus the removal of any gates)
4. Truncated cone: 300mm large diameter, 150mm small diameter, 80mm height.

Table 3.1 Parts formed in the case studies

3.1.3 Electrical Power Measurements

Part of the case study included collecting data on electrical power measurements. These were taken using a Fluke 434 (Series ii) 3-phase power analyzer using a typical sampling period of one second. The active (real) power, power factor, and cumulative metered energy (in kWh) were recorded. A minimum of three forming cycles was recorded for each process in order to provide reliable averaged results.

The real (or active) power performs work (or is converted to heat). The power factor measures the degree to which the voltage and current waveforms are out of sync and is equal to the ratio of the real power (consumed in the process) to the apparent power (the product of the root mean square voltage and current). A low power factor indicates increased heat losses (poorer efficiency) in transmission lines, transformers, and the load as the current flowing through the system is higher.

The high baseload power requirements of many of the processes mean that even between forming cycles significant electricity is consumed. These energy requirements are attributed to the final parts and labeled as “Part set-up” in Table 3.2. For stretch forming and SPF, significant electrical energy must also be used during “Batch Set -Up.” In the case of stretch forming, the small batch sizes of the aerospace industry (often less than 20 parts) means that the machine is left on while the die is swapped out and adjustments are made to the die Table and gripper. The entire batch set-up takes about 30 minutes. In the case of aluminum SPF, the batch set-up electricity is used to heat the die-set from room to forming temperature, requiring ten hours and 1,560 kWh of electricity in the case study. The energy requirements of “Batch Set-Up” are attributed to individual parts by amortizing them over the number of parts produced in that batch before the next die-set changeover.

Case study	Average cycle time (mins)	Average forming time (mins)	Average cycle power (kW)	Baseload power (kW)	Batch set-up energy (kWh)	Part set-up energy (kWh)	Forming energy (kWh)	Marginal energy of forming (η)	**Energy per part (kWh)**
Drawing	2.8	0.2	26	19	0	1	0.2	11%	**1.2**
Stretch forming	9.8	6.8	99	53	3.5	2.6	10.1	25%	**16.2**
FCF	6.5	1.6	58	52	0	4.2	2.1	11%	**6.3**
SPF	46	41	165	124**	17.4	10.3	98.5	11%	**126.2**
ISF*	135	110	3.2	0.7	0	0.7	6.4	72%	**7.1**

Table 3.2 Summary of electrical energy and power results from the case studies

3.1.4 Global Models

The results from the case studies are specific to the parts considered, ranging in size from 0.15 kg to 15.5 kg. In this section, the case study results are used to help develop generalized global models that allow energy use and environmental impacts to be estimated based on limited information about the final part. The global models are then used to examine each process’s energy (CED) characteristics for varying numbers of parts produced over the die lifespan, and the potential for ISF to save energy when used instead of drawing.

The global models constructed in this section allow environmental impacts to be estimated based on as little information as the process used, the number of parts produced over the die-set lifespan (N), final part material, surface area (X square meters, corresponding to one side), thickness (T meters), and depth (h meters).

Equation 1 and equation 2 present a simple representation of the impacts and costs per part. The impacts of the die are amortized over the total number of parts made using that tool (N).

$$I_{perpart} = I_{sheet} + I_{press\text{-}electricity} + \frac{I_{die}}{N} \quad 3.1$$

$$C_{per\ part} = \left(C_{sheet} - C_{scrap}\right) + C_{press\text{-}elec} + \frac{C_{die}}{N} + C_{dep} + C_{labor} \quad 3.2$$

The die cost (C_{die}) is shown for each process in *Table* 3.7 of Appendix A. The impacts of the sheet metal (I_{sheet}, C_{sheet}, C_{scrap}), press electricity ($I_{press\text{-}electricity}$, $C_{press\text{-}elec}$), die (I_{die}), as well as the equipment depreciation costs (C_{dep}) and labor costs (C_{lab}) can be expressed as equations 3-9, where α is the overall material yield from stock sheet to final part (ratio of mass of the part to mass of the stock sheet); ρ_{metal} is the density of the sheet metal (in kg/m^3); $W_{press\text{-}electricity}$ is the metered electrical energy needed to form a part (in kWh); M_{die} is the mass of the cast die (in kg); $M_{machined\text{-}away}$ is the mass of the cast die that is machined away to produce the final die shape (in kg); $Time_{attr.dep}$ is the amount of the cycle time that is attribuTable to equipment depreciation; and $Time_{attr.lab}$ is the amount of the cycle time that is attribuTable to labor (i.e. labor must be present).

$$I_{sheet} = \frac{X}{\alpha}\left[T\rho_{metal} i_{metal} + i_{galv}\right] \quad 3.3$$

$$C_{sheet} - C_{scrap} = \frac{XT\rho_{metal}}{\alpha}\left(c_{sheet} - c_{scrap}(1-\alpha)\right) \quad 3.4$$

$$I_{press\text{-}elec} = i_{elec} W_{press\text{-}elec} \quad 3.5$$

$$C_{press\text{-}elec} = i_{elec} c_{press\text{-}elec} \quad 3.6$$

$$I_{die} = i_{die-making} M_{die} + i_{die-machining} M_{machined\text{-}away} \quad 3.7$$

$$C_{dep} = c_{dep} \times Time_{attr.\,dep} \quad 3.8$$

$$C_{lab} = c_{lab} \times Time_{attr.\,lab} \quad 3.9$$

Practitioners are free to fill in their own values where available. Otherwise, most of the intrinsic impacts and densities of the inputs (i_{metal}, i_{galv}, ρ_{metal}, $i_{electricity}$, $i_{die\text{-}making}$ and $i_{die\text{-}machining,}$ $c_{sheet},$, c_{scrap}) are set to their default values are expressed in *Table* 3.3 of Appendix A. The precise values of some of these parameters depend on many details of the part shape (e.g., whether the shape has holes or deep "features") and process machine architecture. Such details are neglected in favor of creating a simple model with uncertainty assigned to the variables.

3.1.5 Extrapolating To A National Level- Automotive

In order to estimate the national impact of RAFFT in the automotive industry we make use of the global models to identify the parts that can be made cheaper and more energy-efficiently using RAFFT. We overlay this with a diffusion model in order to generate a realistic estimate of the total environmental and economic impact in 2030.

A typical inventory of sheet metal parts made by a car company and to be used in an American passenger car—including blank dimensions, part sizes and drawing yields—is presented in Omar (2011), and in Appendix A. The metal parts were compared to the ISF specification in order to determine if ISF can form the part geometry.

Historical data on new vehicle production (provided by a leading consultancy on the condition of anonymity) shows that between 1995 and 2014 Ford introduced a mean of 5.4 car models per year (standard deviation: 2.6) and that Ford accounted for a fifth of US domestic production. These numbers correlate well with personal communications the authors had with the Ford team responsible for developing new products. Combined with current US car production growth rates (3.2% per annum) these numbers suggest that by 2030 a mean of 41 new cars will be developed each year across the US (standard deviation of 20), which can be modelled as a normal distribution, N(41,400), truncated below zero parts. The distribution of new parts that ISF could technically make by 2030 ($X_{\text{technical potential}}$) is therefore given by equation 10.

$$X_{Technical\ Potential}\left[\frac{parts}{year}\right] \approx\ 270 \times N(37{,}9) \times N(41{,}400) \qquad 3.10$$

Technology diffusion has often been depicted as a smooth S-curve: first innovators and early adopters use the technology, as time progresses the early majority picks it up, and then the late majority and finally laggards pick it up, at which point it has saturated the market (Rogers, 2003). A popular quantitative method of describing the S-curve is the Bass diffusion model shown in equation 11 (Bass, 1969; Pae and Lehmann, 2003). The Bass model has been found to fit data for most product introductions when appropriately tuned coefficient values have been used in the equation.

$$S(t) = \left(p + q\frac{F(t-1)}{m}\right) \times (m - F(t-1)) \qquad 3.11$$

Where S(t) is the predicted number of sales in year t, F(t) is the cumulative number of sales, p is the coefficient of innovation (including external influence or advertising effect), q is the coefficient of imitation (including internal influence or word-of-mouth effect), m is the potential market size, and t is time measured in years. For a new technology, diffusion parameters must be estimated by looking at analogous technologies for which historical sales data already exists.

The Bass model (equation 11) was used in order to estimate the likely number of parts ISF will be making in 2030. It was assumed that ISF was not used to make any successful parts in 2016: S(2016)=F(2016)=0. The p and q diffusion coefficients were modeled as normal distributions: P ~ N(0.017,0.0066); Q ~ N(0.47,0.09) as derived for industrial innovations by Van Den Bulte (2002). His meta-analysis is the most comprehensive found in the literature; he aggregates over 1,500 diffusion coefficient values and is able to provide confidence intervals on the derived mean values.

3.1.6 Further Extrapolations to the National level

This same approach with slight variations was also applied to the aerospace sector and then to non-transportation sectors with significant sheet-metal usage. More details are given in the next sector and the Benefits Assessment, and in Appendix A and B.

3.2 Task 2: Development, Integration and Verification of RAFFT System

Conceptualizing, designing, manufacturing and commissioning of the RAFFT machine to form sheet metal parts without using any stamping dies are the goals of this task. The machine will have an effective working (sheet) area of 2.0 m x 1.5 m, which allows for the production of the majority of sheet metal parts used in ground and aerospace applications. A flat sheet metal panel will be loaded into a binder and clamps to hold the panel will be actuated. The panel will be formed by two opposing 4 DOF units. On completion of the forming operation, the system will indicate to the operator that the process is complete. The operator can then manually initiate the unload sequence causing the binder to be moved out of the forming area such that the part can be unclamped from the binder and removed.

After careful vetting of potential machine tool suppliers, the contract to undertake the above task was awarded to Ingersoll Production System in Rockford, Illinois in December 2013.

RAFFT Machine Overall Specifications:

- 8 axes with two opposing 4-axis units – Figure 3.1 (X, Y, Z, & A and U, V, W & B)
- Servo controlled linear way slides with linear scale feedback
- Box in a box construction for superior machine rigidity and stiffness
- Siemens 840D control system
- Rapid traverse rates of 18 meters per minute
- HSK 63A spindle tool adaption
- Wireless load force monitoring tool adapters
- Automatic tool changer with a 10 pocket tool rack on each side
- Sheet metal work zone 2.0 meters wide by 1.5 meters high with a form depth of 425mm
- Pivoting binder fixture for easy loading and unloading of sheet metal panels
- Overhead gripping device for loading and unloading panels
- Sheet metal panels range in size from 500 x 500 mm up to 1500 x 2000 mm with a thickness ranging from 0.4 to 2.5mm

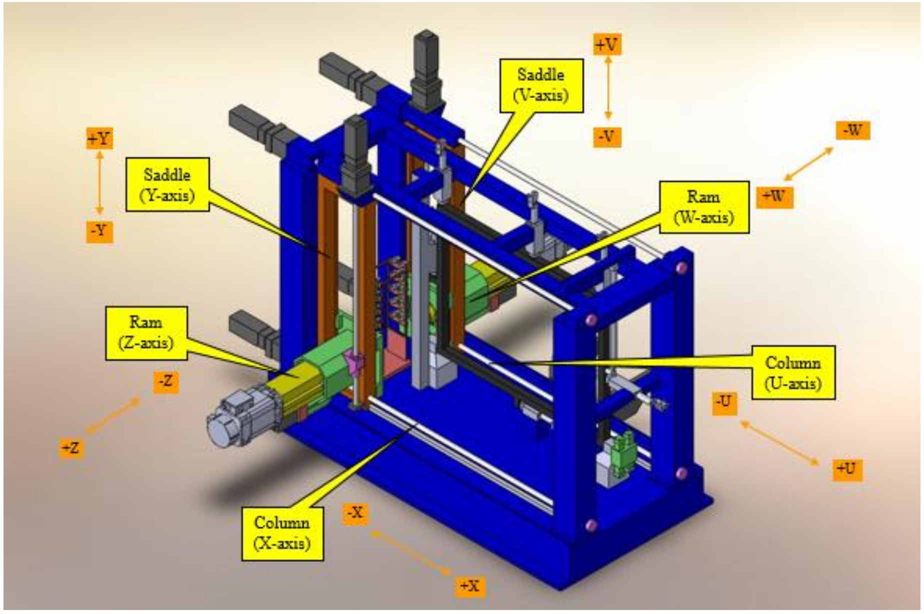

Figure 3.1 RAFFT machine

The RAFFT machine was delivered, installed and calibrated at the Ford Research and Innovation Center (RIC) in Dearborn, Michigan in April 2015. After the machine commissioning event held on March 24th, 2015, in Rockford, Illinois, the RAFFT machine was partially disassembled and prepared for shipment to Dearborn. After delivery and assembly, the lengthy but critically important process of machine calibration and adjustments could begin. Over the months of May and June, a team of technicians and engineers from Ingersoll conducted a multitude of alignment checks and calibration checks on the machine, ensuring that the axes were aligned as precisely as possible to the ideal horizontal, vertical, and depth directions. The axis alignments were verified using a laser interferometer and the RAFFT machine axes met the targets specified by Ford and Ingersoll. After calibrating the machine axes, adjustments were also made to the binder and crossbars of the machine, or in other words, the fixture which clamps the sheet metal blank in place during forming. Figure 3.2 shows the RAFFT machine inside the Ford's Research and Innovation Center. Figure 3.3 is an image of the RAFFT machine binder with reconfigurable cross bars where Figure 3.4 shows the back view of the binder with a full-size sheet attached.

Figure **3.2 The RAFFT machine installed and powered-on in the Ford RIC in Dearborn. Photograph taken on May 22nd, 2015**

Figure 3.3 Binder Front view, w/ Cross Bars

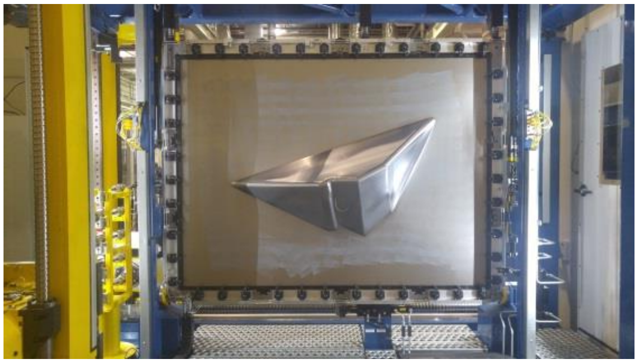

Figure 3.4 Binder Back View

Flat and ball-end stylus are the most typical tools used in RAFFT machine for forming sheet metal panels. Three different ball-tip forming tools are shown in Figure 3.5. The tools shown in Figure 3.5 have tip diameters of 6 mm, 10 mm, and 16 mm, respectively. The tools pictured are made of tungsten carbide and coated in a material called Alcrona Pro, but tools with the same geometry were also made out of A2 tool steel. Figure 3.6 shows three additional forming tool geometries, commonly referred to as flat-tip tools. The tools in Figure 3.6 have tip sizes of 12 mm by 6 mm, 15 mm by 6 mm, and 18 mm by 10 mm, respectively. As with the ball tip tools, the tools pictured are made of tungsten carbide, but tools with the same geometry were also made from A2 tool steel.

Figure 3.5 Ball-tip forming tools. Tip diameters are 6 mm, 10 mm, and 16 mm

Figure 3.6 Flat-tip forming tools. Tip sizes are 12 mm by 6 mm, 15 mm by 6 mm, and 18 mm by 10 mm, respectively

Figure 3.7 is a finished prototype panoramic moon roof used for validating a new conceptual design at Ford whereas Figure 3.8 is a part produced in the same way and installed in Mustang GT4 race car.

Figure 3.7 Moon roof frame

Figure 3.8 Mustang GT4 part

3.3 Task 3: Tool Path Generation Algorithm, Simulation Modeling and Process Optimization

3.3.1 Tool path Generation Algorithm

The CATIA "Z-level machining" function is leveraged to create coordinates and normal vectors on the surface of the CAD model. This surface data is fed into the RAFFT software using the following formulas, based on the "cosine law," to compute the top and bottom tool tip positions. Figure 3.9 illustrates the relationship between top and bottom tools relative to the sheet.

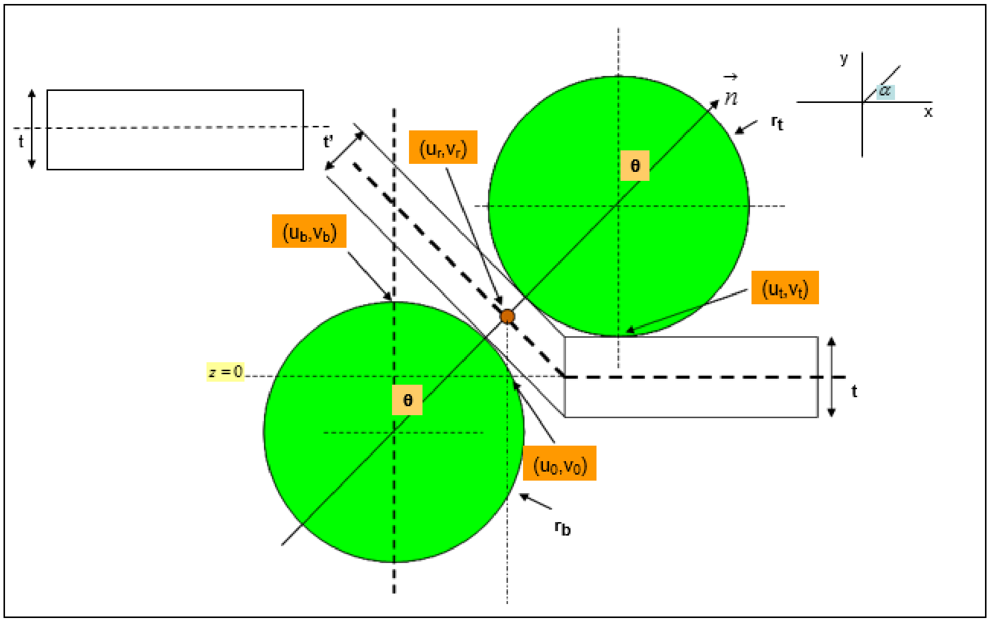

Figure 3.9 Two forming tool configuration

Nomenclature:

P_r: reference point on CAD surface derived from CATIA

P_t: top tool tip point

P_b: bottom tool tip point

$\vec{n}$: a unit normal vector with components (n_x, n_y, n_z) at point P_r derived from CATIA

θ: angle between normal vector $\vec{n}$ and Z axis

α: angle between the projection of normal vector $\vec{n}$ on xy plane and X axis

S_f: squeeze factor

t: nominal thickness of the un-deformed work piece

t': nominal thickness of the deformed work piece (local) following cosine law

r_t: top/front tool radius

r_b: bottom/back tool radius

(u_r, v_r): Coordinates of reference point P_r in UV coordinate system

(u_t, v_t): Coordinates of top tip point P_t in UV coordinate system

(u_b, v_b): Coordinates of bottom tip point P_b inUV coordinate system

(x_t, y_t, z_t): coordinates of top/front tool tip position P_t in XYZ part coordinate system

(x_b, y_b, z_b): coordinates of bottom/back tool tip position P_b in XYZ part coordinate system

$$P_r \equiv (x, y, z, n_x, n_y, n_z) \quad 3.12$$

$$\theta = cos^{-1}(n_z) \qquad 3.13$$

$$\alpha = \pi - tan^{-1}(\frac{n_y}{n_x}) \qquad 3.14$$

$$u_r = 0 \qquad 3.15$$

$$v_r = 0 \qquad 3.16$$

$$u_t = u_r + \left(r_t + S_f \frac{t}{2}\cos(\theta)\right)\sin(\theta) \qquad 3.17$$

$$v_t = v_r + \left(r_t + S_f \frac{t}{2}\cos(\theta)\right)\cos(\theta) - r_t \qquad 3.18$$

$$u_b = u_r - \left(r_b + S_f \frac{t}{2}\cos(\theta)\right)\sin(\theta) \qquad 3.19$$

$$v_b = v_r - \left(r_b + S_f \frac{t}{2}\cos(\theta)\right)\cos(\theta) + r_b \qquad 3.28$$

Top tool tip coordinates are:

$$x_t = x + u_t\cos(\alpha) \qquad 3.21$$

$$y_t = y + u_t\sin(\alpha) \qquad 3.22$$

$$z_t = v_t \qquad 3.23$$

Bottom tool tip coordinates are:

$$x_b = x + u_b\cos(\alpha) \qquad 3.24$$

$$y_b = y + u_b\sin(\alpha) \qquad 3.25$$

$$z_b = v_b \qquad 3.26$$

3.3.2 Tool Path Generation

The “First Generation” of the RAFFT Software had grown exponentially very quickly due to needing for new functionalities. The “Second Generation” of this software has replaced arrays with vectors as the primary data structure. This helped in: (1) improving performance & scalability - vectors allow dynamic memory allocation; (2) improved robustness - new structured classes encompassing vector objects of smaller class as member variables; (3) service-based architecture - methods re-written in a form of services which avoid code duplication; (4) consolidated source code - unwanted try-out codes & commented source codes have been removed; (5) easy maintenance - new visual debugging methods/services are implemented to debug any issues quickly, and code comments have been increased.

A schematic representation of the difference between our old data structure and our new data structure is shown in Figure 3.10 below. With arrays one needs to have a static pre-defined number to indicate the number of memory blocks that will be used. However, with vectors one can assign new memory blocks at run-time.

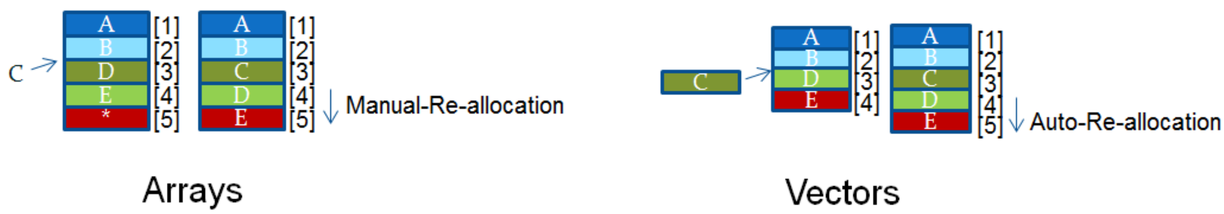

Figure 3.10 Schematic representation of two data structures

First, the "Second Generation" RAFFT software version has been re-implemented with all the functionalities that were present in the "First Generation" of the software. Data collation and integrity checks are now done using vectors, i.e. CATIA Toolpath data is now collected using vectors using new class data structures which have been logically separated & differentiated. All filter functionalities applied to the front toolpath and back toolpaths have been re-implemented using the above vector data structures with filter areas being defined using filter polygon regions. Back toolpath computation is also re-implemented using vectors and stored in vector data structures. Squeeze factor algorithms and optimizations are used for the back toolpath calculations.

Additionally, a new and enhanced RAFFT Toolbar has been released with additional commands. Figure 3.11 below also shows this enhanced toolbar. The commands listed below help the user to simplify the process of creating RAFFT toolpaths starting from CATIA generated Z-Level toolpaths.

Figure 3.11 Enhanced RAFFT Toolbar

a)  New Pocket Project: - When a user clicks on this command button, he/she needs to select a Project folder. All necessary files such as *.CATProcess, *.CATPart and other necessary files are copied into the selected folder. The user will see a sample CATProcess file getting opened with this action. The CATProcess file getting opened is a template Z-level toolpath process file which is created based on a sample CATPart having a Pocket (Convex surface).

b)  New Outer Project: - When a user clicks on this command button, he/she needs to select a Project folder. All necessary files such as *.CATProcess, *.CATPart and other necessary files are copied into the selected folder. The user will see a sample CATProcess file getting opened with this action. The CATProcess file getting opened is a Z-level template toolpath process file which is created based on a sample CATPart having a Outer (Concave surface).

c)  Open Existing Project: - When a user clicks on this command button, he/she needs to select a Project folder which helps the user open an existing CATProcess file which he/she has already created. The purpose of opening this CATProcess file having a Z-level CATIA toolpath is to create RAFFT toolpaths.

d) 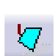 Define Polygon Area: - The purpose of this command button is to help user define Polygon areas for 3 purposes (Define Squeeze Factor Regions, Define Filter regions & Define Fill Layer regions). A dialog box opens helping the user to define the areas and fill the corresponding data along with it. Regions are defined on the CATPart surface by clicking and selecting points on the surface.

e) Toolpath Generation: - This is the button to generate the RAFFT toolpath from the information gathered from CATIA. When a user selects this command button, he/she is given a prompt that allows them to choose process parameters, such as the tools, the sheet thickness, whether or not to include a color map of the squeeze, as well as whether to run a rough or fine pass.

f) Debug Related Tools: - These are debug related commands which help us understand and study the toolpaths generated by RAFFT command and also simulate the toolpath movements along with their tools.

g) MPF Post Processing: - This command helps with auto-editing the mpf file generated from the I-CAM post-processing software. The changes done to the mpf file help with tools mapping verification process on the machine which is explained later in the section *RAFFT Tools Mapping*.

A "Progress Bar" panel was added to the RAFFT software to show which step is currently in progress during RAFFT toolpath generation, and an estimate on how much time it will take to complete. It also allows the user to abort the calculation at any time. Additionally, it is now possible to generate FEA related toolpaths (used in FEA Simulation) using the same RAFFT UI Panel/Dialog. See Figure 3.12 below.

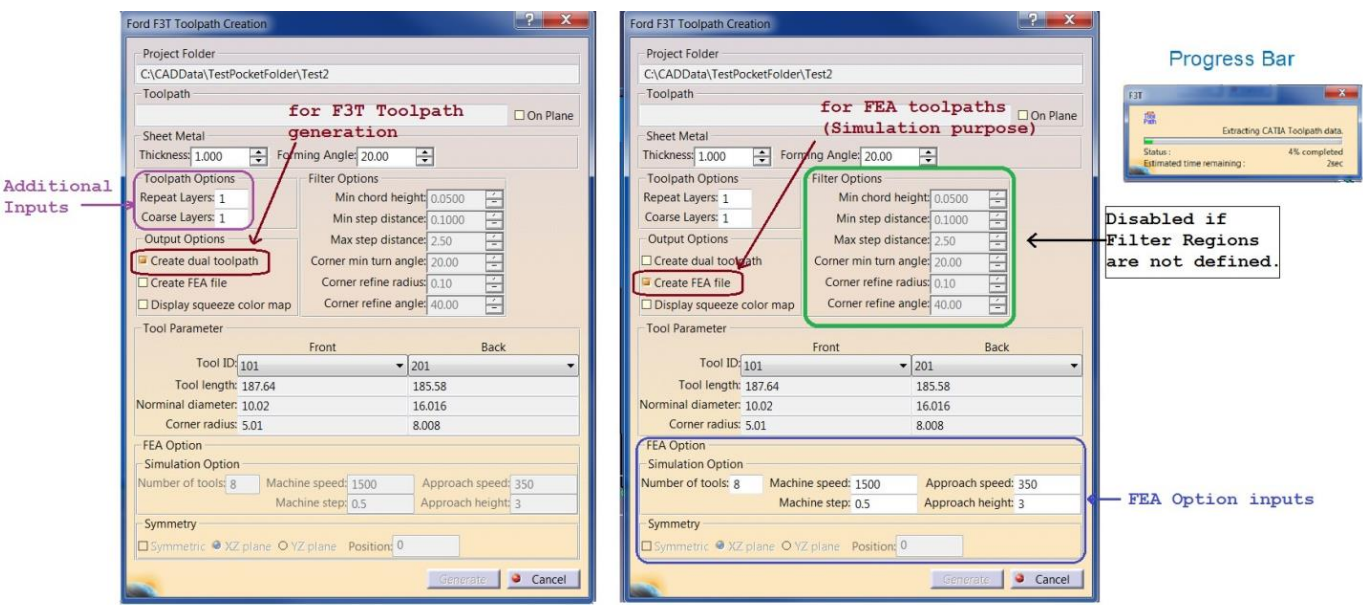

Figure 3.12 RAFFT User Interface panel with updates highlighted

Further, RAFFT software can now generate toolpaths for both convex and concave areas. The software automatically recognizes whether the input CATIA toolpath is concave or convex and thereafter generates corresponding RAFFT (Front and Back) toolpaths using different set of computations thereby making it user-friendly. Figure 3.13 below shows Truncated Pyramid geometry with 4 half spheres thereby having both concave and convex areas and the corresponding RAFFT toolpath generation for both the convex and the concave toolpaths.

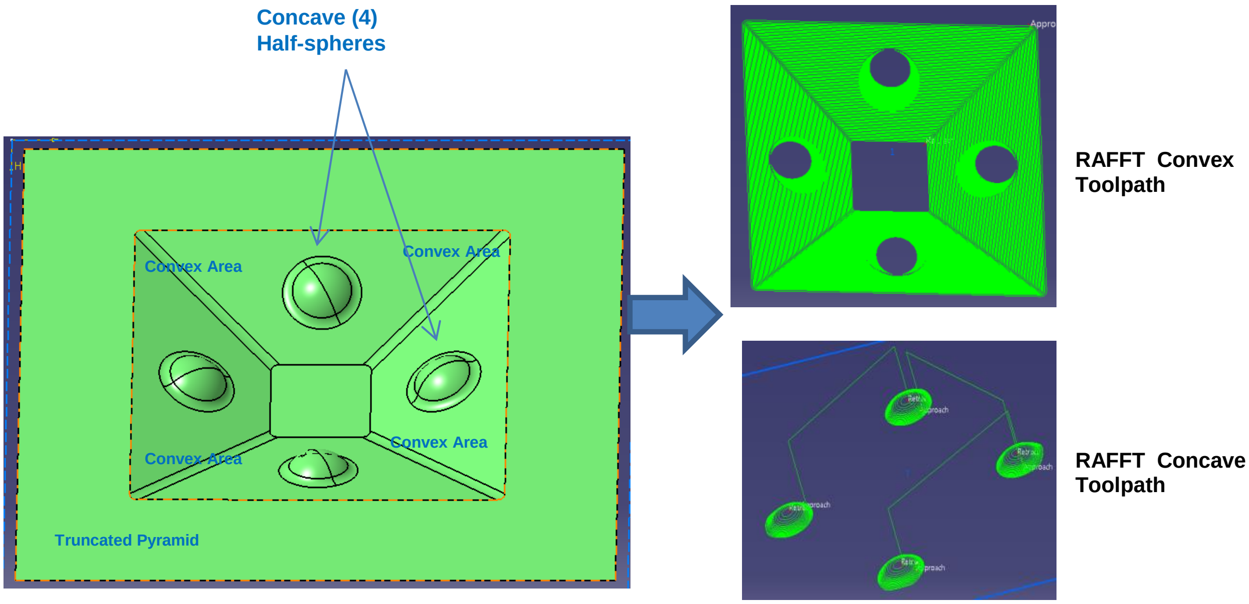

Figure 3.13 Truncated Pyramid having concave and convex areas. Right side of the picture shows the generated RAFFT toolpaths of the Pyramid (Convex toolpath) and half spheres (Convex toolpaths)

With toolpaths generated using the first generation software, one could observe that the gap between toolpath layers was <u>larger in shallow areas</u> (small wall angles) but, they were <u>smaller in steeper areas</u> (steep wall angles). This affected the overall surface finish of the formed part. By decreasing the step-size of overall part (i.e. vertical 'z' distance between each layer), one can get more layers in these shallow areas, but that increases the layers in steep areas as well which may be not required. Also, this would lead to increase in the toolpath size and thereby the machining time.

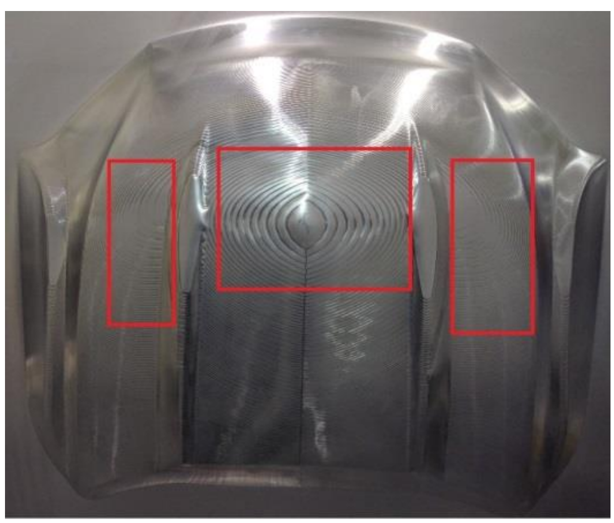

Figure 3.14 Actual display of RAFFT formed mustang hood part showing shallow regions

To address the issue of surface quality versus machine time, a concept called "fill layers" was developed. Inside a particular region, we can have a "dense" or "coarse" toolpath. Two methods were developed. The first is where a user interactively defines a region; the user tells the software if dense toolpath is needed, and where it is needed by defining the regions on the graphical interface with the application "Define Polygon Area" which was developed specifically for this purpose. The second is to treat every 9 consecutive toolpath layers as a region, and use the part surface wall angle to decide where to have dense or loose toolpath. For every consecutive toolpath 9 layers, it would define the regions based on the wall angle. Within each region, the software would automatically decide how many toolpath layers to keep:

- Keep 1
- Keep 3
- Keep 9

Figure 3.15 shows a sample of a filled layer toolpath created from 9 consecutive toolpaths. In some areas, there’s only one layer of toolpath. In some other areas, there are three layers, and in other areas, there’re 9 layers.

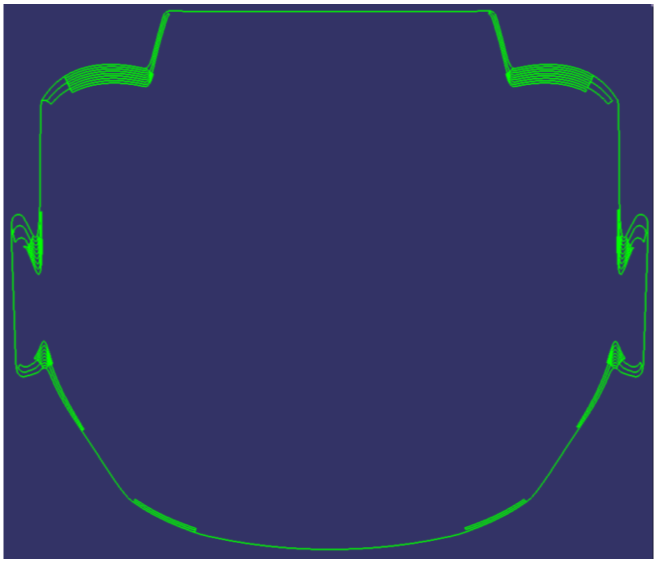

Figure 3.15 Fill layer based on wall angle

Figure 3.16 shows the details of how the tool moves inside the fill layer regions. At the end of each region, the tool will follow the fill layer toolpath end points to the start of the layer. After the fill layer, it will become one new layer. To improve the surface quality, toolpath is reversed for every other layer. It is done by reversing the original toolpaths and use the same algorithm.

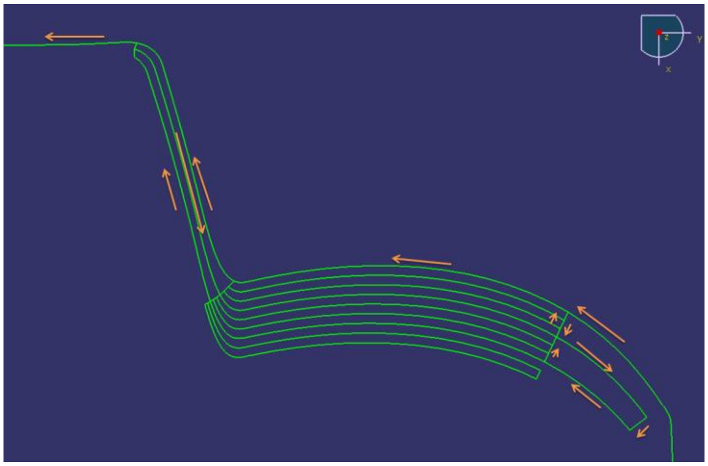

Figure 3.16 Tool movement inside regions

Figure 3.17 is a schematic representation of the Mustang hood toolpath with filled layers. The color represents the amount of squeeze.

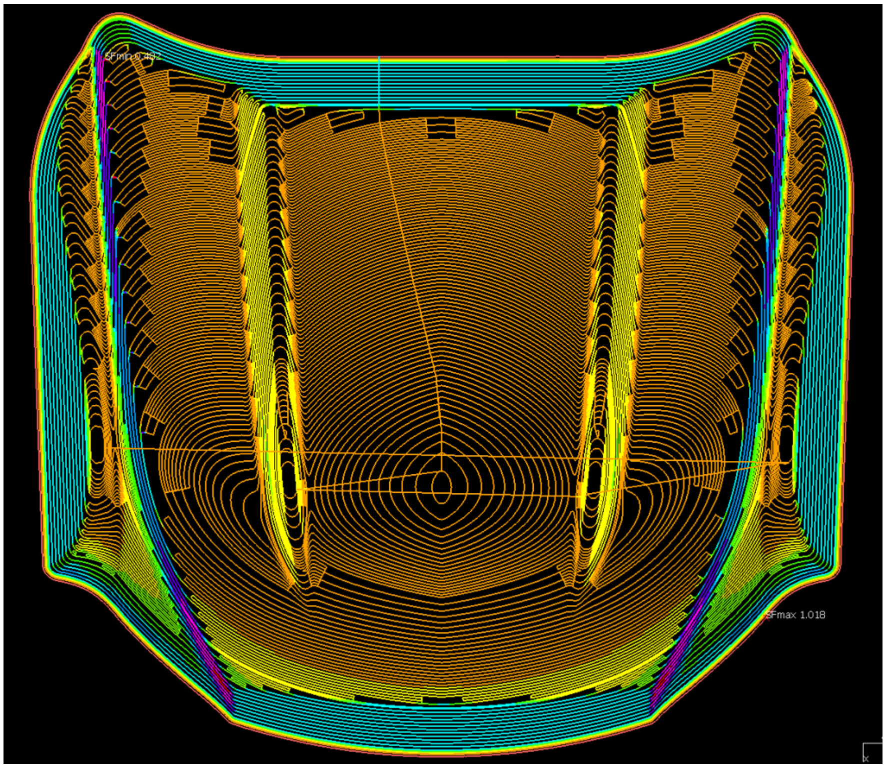

Figure 3.17 Filled layer toolpath of Mustang hood

Figure 3.18 shows the corner of the finished Mustang hood with filled layer tool marks.

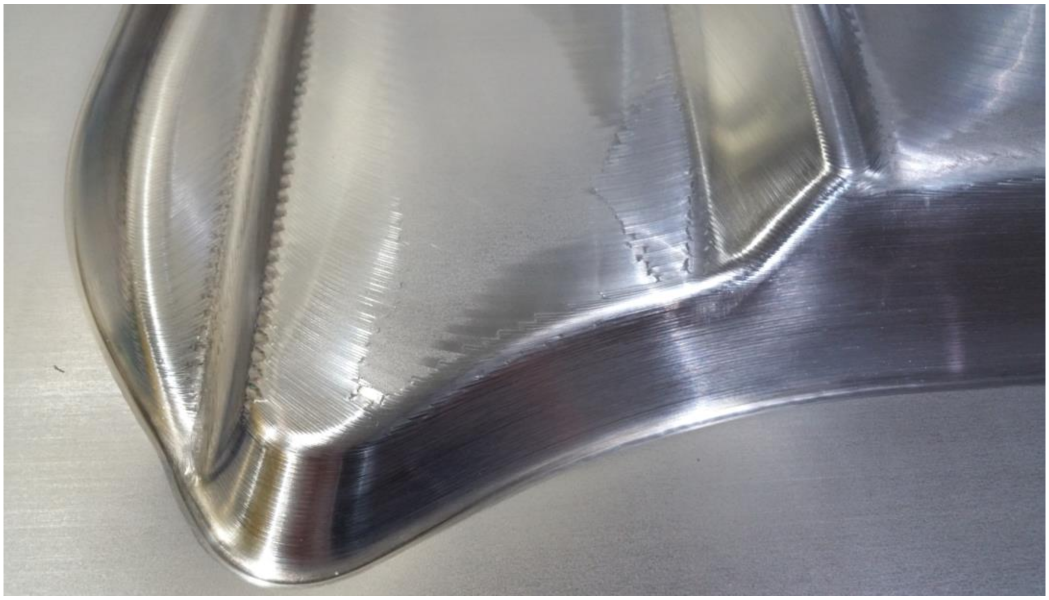

Figure 3.18 Fill layer tool mark on the corner of the Mustang hood

The advantage of this method is that no user interaction is required, and the regions can be relative accurate compared with the first method, without a sacrifice in computation time.

3.3.3 Simulation Modeling

Incremental sheet forming (ISF) is a highly versatile and flexible process for rapid manufacturing of complex sheet metal parts. Compared to conventional sheet forming processes, ISF has evident advantages in manufacturing small batch or customized products. However, most research so far has been based on single point incremental forming (SPIF). With DSIF there are many technical challenges for achieving better geometric accuracy, thickness distribution, and complex shapes.

RAFFT researchers have investigated five different DSIF related simulation methodologies. First, a preliminary modeling methodology was proposed and verified by comparing experimental data and simulation results using a truncated pyramid geometry. Second, to find the optimal stimulation parameters to reduce the computation time and maintain the predicted geometric accuracy, eleven simulation parameters were investigated and optimized using the Taguchi method together with the design of experiment (DOE) and analysis of variance (ANOVA). Third, to investigate the deformation mechanics, a two-dimensional plane strain model and three-dimensional slab model (SM) were simulated and compared. Next, to reduce the computation time in a further way for large automotive panels, an imaginary multiple-tooling method (MT) was proposed, implemented and verified. It turned out that there was a 95% reduction in computation time when simulating with 20 pairs of tools, while still maintaining a reasonable geometry prediction. Finally, a very fast simulation method, based on a simplified truncated pyramid, was developed and used to determine optimum squeeze factor parameters.

3.3.3.1 General Finite Element Model

The purpose of this "general finite element model" is to set up a general finite element model for DSIF, using truncated pyramid geometry.

Method: The double sided incremental forming experiments were performed on RAFFT machine at Ford Research and Innovation Center to collect the data to develop the simulation methodology. A truncated pyramid was formed with 3 mm radius front tool and 5 mm radius back tool, both of which were hemi-spherical headed. The tool path was generated using RAFFT software. In the experiment, the feed rate was kept constant as 83 mm/s, and the step size was set to be 0.1 mm. Lubricating oil was applied between tools and sheet metal to minimize the friction. A ROMER Absolute Arm with an integrated laser scanner was used to develop dense point clouds of the top and bottom surfaces of the formed parts. CAD surfaces were then fitted to these point clouds using the software suite, Polyworks, thus allowing the surfaces to be compared against the desired part and simulation result. The mechanical characteristics of DDQ steel sheet (at a thickness of 1.0mm) from the tensile test were summarized in Table 3.3.

Yield strength (MPa)	160
Density (kg/m^3)	7800
Young's modulus (GPa)	208
Poisson's ratio	0.33
Ultimate tensile strength (MPa)	381
Uniform elongation	0.21
Strength coefficient (MPa)	546
Strain hardening exponent	0.23

Table 3.3 Mechanical properties of DDQ steel

Numerical simulations were conducted in the explicit finite element software ABAQUS, in order to study the effect and sensitivity of simulation parameters. The blank is square in shape with dimensions 500 mm x 500 mm x 1 mm. The blank is discretized with shell element. The nodes along all four edges of the blank are modeled as fully fixed. The contact between the blank and the tools is defined using master-slave contact algorithm. The friction between different contact surfaces are defined using Coulomb's friction law. Table 3.3 shows the base simulation parameters set-up for DSIF.

The sheet is meshed with S4R shell elements. S4R elements are a 4-node doubly curved thin shell, with reduced integration, hourglass control, and finite membrane strains. The element size was set to be 1mm by 1 mm in the deformation center region of 260 mm * 260 mm, while 20 by 20 mm in the four corners, shown in Figure 3.18 (c). For the sheet, all the four edges were fixed in all degrees of freedom, which was based on the observation of insignificant material draw-in phenomena. The tool path generated from the RAFFT software was imported into the ABAQUS code. A tool speed of 1500 mm/s was used in the simulation. Mass scaling was used so that the stable time step is $1*10^{-5}$ second. After the incremental forming ABAQUS/Explicit simulation, the result files are imported for ABAQUS/Implicit simulation to simulate the final shape after springback.

(a) (b) (c)

Figure 3.19 (a) CAD part (b) the formed part(c) Meshed sheet

As to the computation time, the 1 mm reduced integrated shell element mesh used a wall time of 49 hours 58 minutes when using 24 CPU's. As to the cross-section geometry comparison, Figure 3.20 illustrates geometric comparison between the experiment and simulation, in the center cross-section plan. It is clearly found that the simulation considering the springback effect matches with the experiment very well, while there are evident deviations between pre-springback simulations and experiments. Also, there are large deviations at the interface between the unworked sheet and the formed part in comparison with the CAD and experimental data, due to the loss-of-contact of the back tool. Global geometric comparison: Figure 3.21 shows the data color map of deviation between the experiment and the post-springback simulation, using Polyworks commercial software. It was found that the mean deviation was 0.17 mm and the standard deviation was 0.34 mm. One metric for simulation success investigated was a tool force comparison; the simulated reaction force along Z-direction on tools with time, shown in Figure 3.22 (a). It was also found that the back-tool forming force continues to decrease until zero at the depth of about 20 mm. This simulation result matched with the experiment using the same toolpath, in that loss-of-contact occurs at that depth. Another simulation success metric was the sheet thickness comparison. The thickness variation along the wall of the experimentally formed part followed the same trend as predicted by the simulation, shown in Figure 3.22(b). It is the side wall of the truncated pyramid which experiences the maximum reduction in thickness.

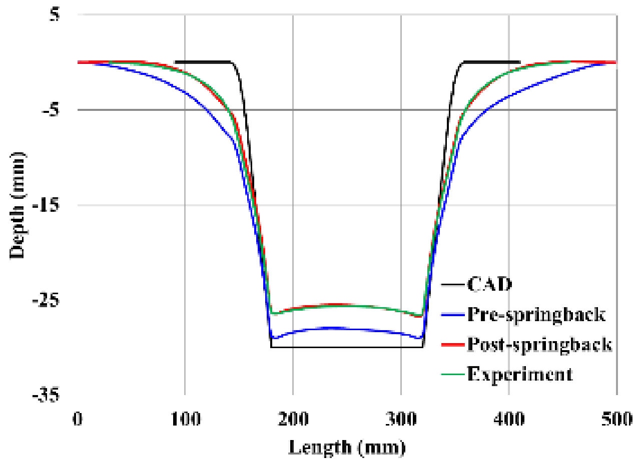

Figure 3.20 Cross-section geometry comparison among CAD, experiment and simulation

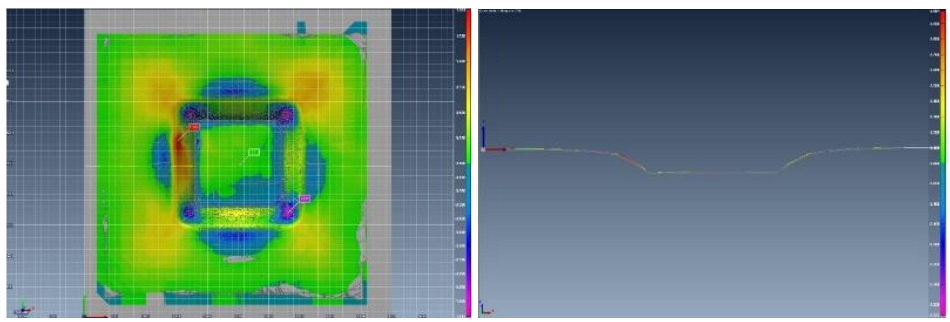

(a) (b)

Figure 3.21 Geometric comparison between the experiment and simulation (a) global (b) Cross-section

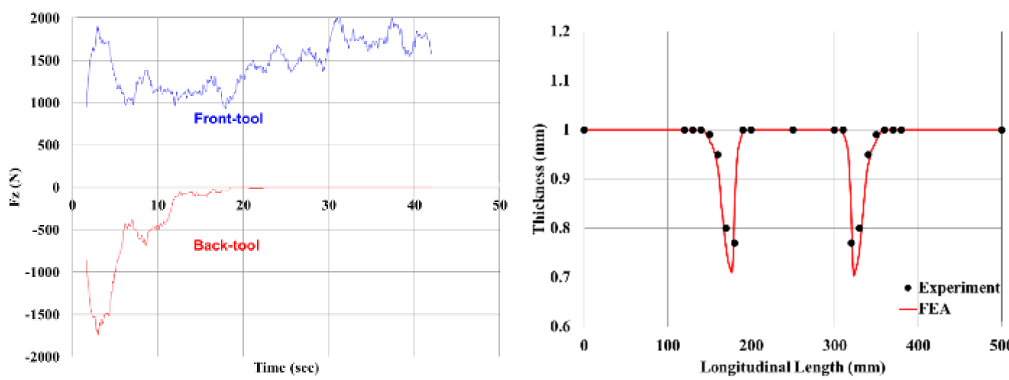

(a) (b)

Figure 3.22 Simulated reaction force along Z-direction on tools with time(a) Thickness distribution along the wall(b)

Conclusion: In the present work, the finite element analysis and validation by ABAQUS are successfully implemented for the double-sided incremental forming process of DDQ steel sheet. It is found that the majority of thickness reduction takes place in the walls of the truncated pyramid but not in the flange or bottom. Experiments were conducted on the RAFFT machine to verify the accuracy of simulated results. The experimental results are in good agreement with the simulated results, with a standard deviation of 0.34 mm. However, two main obstacles for DSIF are found. First, the geometric inaccuracy is a problem due to loss of contact of the back tool. Thus, two possible ways could help: either add extra stiffeners in the un-deformed regions of the sheet metal or apply proper squeeze factors that guarantee a fully-contact during forming. Second, the computation time cost is extremely high. It would be expected to cost from days to weeks for real-world large automotive panels, by conventional modeling procedures. Thus, the development of advanced techniques to reduce computation time would be a must.

3.3.3.2 Taguchi Optimization

The Taguchi optimization methodology was used to optimize simulation parameters to find a balance between simulation efficiency and accuracy. This method was used to look into the simulation computation time by studying eleven simulation parameters including the material properties (yield function and strain rate), mesh size, number of integration points through thickness direction, damping value, friction, mesh topology, number of CPUs, mass-scaling, tool speed, and the use of full or reduced integration. The Taguchi method with ANOVA (Analysis of Variance) to study these simulation parameters on computation time

The Taguchi optimization procedure starts with the selection of an orthogonal array. The minimum number of runs in the array is

$$N_{min} = (L-1)F + 1 \tag{1}$$

Where L and F are the number of levels and number of factors, respectively. In this study, eleven simulation parameters were chosen as factors to study the effect on simulation quality and computation time. Two levels were defined for each of the factors as summarized in Table 3.4. The S/N ratio is a quality control indicator that reflects the influence of changing process parameters on the performance of the process. An S/N ratio of the-smaller-the-better was chosen because the objective was to minimize the output value (mean, standard deviation, and computation time). This was calculated as

$$\eta = -10log(\frac{1}{n}\sum_{i=1}^{n} \quad y_i^2) \tag{2}$$

where η is the S/N ratio, n is the number of experiments taken in one test run, y_i indicates the dimensionless output at the i th experiment with respect to one unit measured.

Factors	Level 1	Level 2
Mass Scaling	1.00E-05	4.00E-05
Yield function	Hill 1948	Von Mises
Strain rate m	0	0.018
IP number	3	9
Damp	0	50
Mesh topology	Mix	Uniform
CPU number	24	48
Integration	S4R	S4
Mesh size	3	5
Friction	0	0.05
Tool speed	750	1500
Segment length	40	800

Table 3.4 Simulation parameters and their levels

In this experiment, three performance characteristics of simulation quality can be measured accurately using the Polyworks and Abaqus software packages. They are the mean difference between the simulation and experimental data, standard deviation between simulations result and scanned data, and computation time

The process of estimating the main effect of each factor is called the analysis of means (ANOM) and the effect of a factor level is the deviation it causes from the overall mean response. The analysis of variance (ANOVA) establishes the relative significance of factors in terms of their percentage contribution to the response. ANOVA is also needed for estimating the error variance for the effects and variance of the prediction error. The results of the ANOM and ANOVA for these parameters are presented in Figure 3.23.

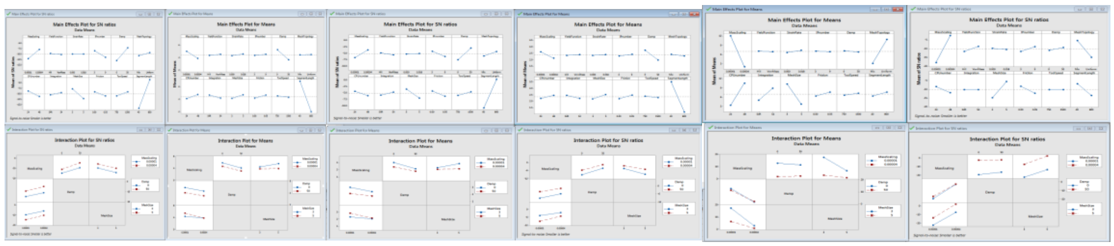

Figure 3.23 Selected results of the ANOM and ANOVA

Conclusion: First, based on the above results, the most important factors are segment length, mesh size and mass-scaling. Second, other optimal parameters considering computation time and accuracy are: yield function= Hill, strain rate=0, IP number=3, damp=50, mesh topology=mixed, integration=S4R, friction=0, tool speed=1500 mm/sec. Finally, the results provide a way for us to perform more efficient DSIF simulations with a reduced set of parameters.

3.3.3.3 Slab Model

The purpose of the "slab model" is to investigate and understand the material deformation mechanism in incremental forming including SPIF and DSIF. The forming process is first investigated using plane strain computations. These results are used to choose the modeling parameters associated with the more computationally expensive three-dimensional analysis.

Method: In this study, a simplified partial model is used for the two reasons below. First, it has been proven by many researchers that incremental forming refers to localized deformation. Second, some researchers already showed the validity and efficiency of the use of a simplified model (Memicoglu et al., 2017; Ma and Mo, 2008). The simplified three-dimensional model is a steel plate of a rectangular cross-section dimensions of 20 mm by 1 mm and a length of 60 mm. The depth of 10 mm for the truncated pyramid is modeled. The tools are assumed to be rigid and is modeled as analytical rigid surfaces. The mesh size is 0.1 mm by 0.1 mm.

For plane strain computations a model with CPE4R elements is used. For the three-dimensional computations a model with C3D8R elements is used. The forming tool is modeled with analytical rigid surfaces for both the two-dimensional and three-dimensional cases. The masses of all elements in the model are scaled so that the stable time step is 1E-8, 1E-7, 1E-6, 1E-5 and 1E-4 second respectively. These scaling values translate into effective tool speeds of 73.3, 733, 7330, 73,300 and 733,000 mm/sec respectively.

Table 3.5 shows the effective tool speeds and the relative CPU cost. The relative costs are normalized with respect to the CPU time for a two-dimensional model with the stability time step of 1E-5 sec. A plane strain calculation allows the user to resolve a number of modeling questions in two dimensions before attempting a more expensive three-dimensional calculation.

Figure 3.24 shows contours of Von Mises stress for the mass scaling of 1E-5 sec and 1E-8 sec. It is found that there is very little difference between the 1E-8 sec and 1E-5 sec. The results of the largest mass scaling case show pronounced dynamic effects. Table 3.5 shows the relative run time of the quasi-static calculation. The mass scaling of 1E-5 sec gives essentially the same results as the quasi-static calculation.

We have ascertained with the two-dimensional calculations that using mass scaling of 1E-5 sec gives results that are essentially the same as a quasi-static solution. Figure 3.25 (a) – (e) show their strains history.

Conclusions: The plane strain assumption is valid for the slab method of simulating double sided incremental forming. There are several interesting findings: (1) the maximum, middle and minimum principle strains of the top element keep constant, 0.28 (±0.001), -0.003 (±0.0008), and -0.28 (±0.001) separately, after the double-sided contact. That is, the strain magnitude in middle direction is 1% of the other directions. (2) the shear strain LE13 of the top element is large, up to -0.48 (±0.012), which is 1.73 times larger than maximum principle strain; (3) the strains of bottom element is always the largest ones.

Analysis type	Stability time step (sec)	Effective tool speed (m/sec)	Relative CPU Time
Explicit, plane strain	1E-8	0.0733	556
Explicit, plane strain	1E-7	0.733	65
Explicit, plane strain	1E-6	7.33	7
Explicit, plane strain	1E-5	73.3	1
Explicit, 3D	1E-5	73.3	11709

Table 3.5 Analysis cases and relative CPU costs. (The two-dimensional explicit analyses all use CPE4R elements. The three-dimensional explicit case uses C3D8R elements)

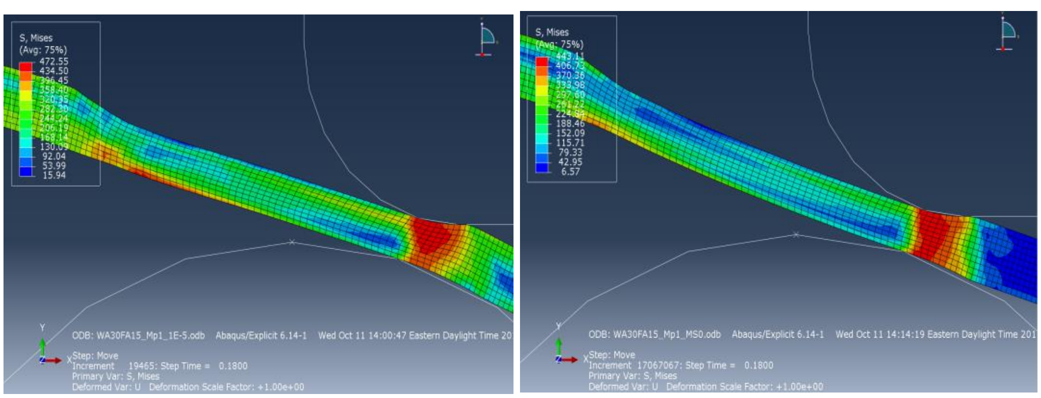

(a) (b)

Figure 3.24 Von Mises stress for CPE4R (stability time=1E-5 sec) (a) 1E-5 sec (b) 1E-8 sec

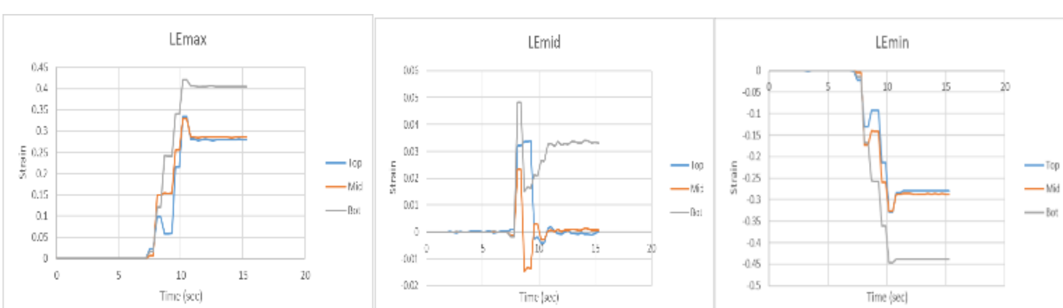

(a) (b) (c)

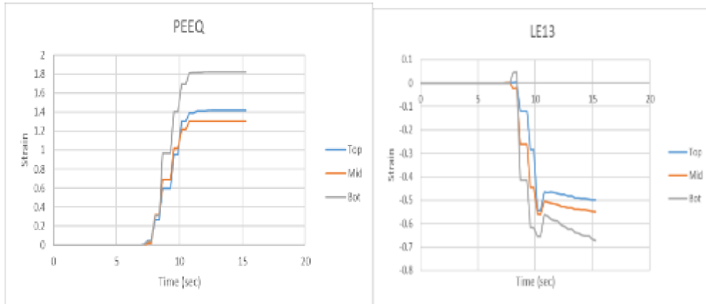

(d) (e)

Figure 3.25 Strain history of selected element in thickness direction (a) maximum principle strain (b) middle principle strain (c) minimum principle strain (d) equivalent plastic strain (e) shear strain

3.3.3.4 Multiple-tooling method

The multiple-tooling methodology was developed to reduce the computation time of DSIF from weeks to one day. The simulation time for the DSIF process is on the scale of weeks. Therefore using the simulation to facilitate in the design of an incrementally formed part is impractical. For example, a full-scale simulation using 8 solid brick elements through the thickness was performed (Smith et al., 2013), which took about 1 month to complete on 56 processors. A total of 24 simplified simulations were carried out (Ren, et al., 2015), and over 4 months of simulation time were necessary for all of the simulations to complete. There are two main factors that contribute to the extraordinarily long computation time: (1) The sheet blank is deformed by forming tools along a sequence of small increments, which cause hundreds of thousands of increments to be calculated when toolpath is long; (2) As the contact area between tools and sheet are very small, a very fine mesh is required in the contact area to ensure accurate contact and deformations calculation, which requires many elements in the simulation. Many researchers work in the field of the reduction of the computation time. A decoupling method is proposed to study the deformation of a localized area (Muresan et al. 2005). It is proposed that a direct sub-structuring method can be used to reduce the computation time, which includes the plastic nonlinear substructures and the elastic pseudo-linear substructures (Hadoush et al., 2009). Another way to reduce the computation time is to simplify the contact model (Bambach, 2013). , None of the methods above can effectively reduce the computation time of IF for large-size real-world automotive panels for practical use.

In this work, a multiple-tooling (MT) method was developed to improve the computational efficiency in FE simulation of IF process. In the proposed approach, the computational efficiency can be increased by adding more forming tools in the FE model. This is achieved by multiple pairs of tools moving simultaneously based on predefined split toolpath segments. In this way, the total forming time involved in the simulation can be reduced without losing the calculation accuracy especially at the plastic deformation area.

Method: Instead of simulating the whole IF toolpath at a time, the toolpath is divided into a number of segments and each pair of tools moves along each segment at the same time. In this way, the total time to form a part is reduced. Figure 3.26 describes the simulation principle of the proposed MT approach.

Once the segment toolpath is assigned to each pair of tools, the next step is to determine how the tools move. Figure 3.26 left shows the tool-movement algorithm of the implemented code combined with CATIA software, where only one front-tool among multiple pairs of tools is shown as an example.

Figure 3.26 right is the visualization result when multiple-tooling method is used. 20-pair of tooling is taken as an example.

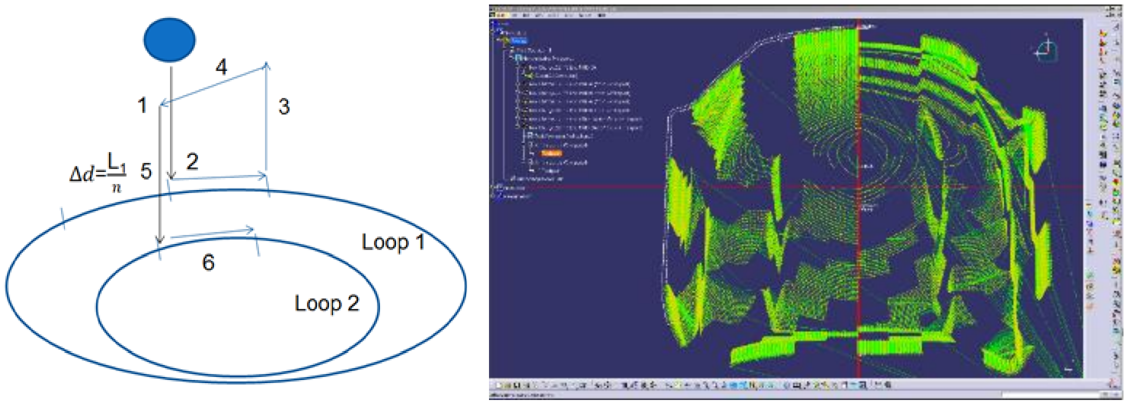

Figure 3.26 Principle of MT approach (a) tool-movement algorithm (b) visualization of toolpath for multiple tools, e.g. 20 pairs of tools shown

In this work, the implementation of the MT approach is achieved via an in-house developed C++ program combined with the commercial software CATIA and ABAQUS.

The MT method achieved almost the same thickness distribution: 0.71 for 4-pair (1.4% error), and 0.72 for 20-pair (2.8% error). It also shows that more tools give lower strain level and less thickness decrease, which is attributed to the more complete plastic deformation as tool number increases, as shown in Table 3.6.

Number of tools	Standard deviation (mm)	Deviation Mean (mm)
1	2.9	1.4
4	2.8	0.1
20	4.0	-1.4

Table 3.6 Summary for geometric comparison between simulations and experiment data

A detailed geometry comparison between the experiment and the simulation with 4 pairs of tools was made with Polyworks and is shown in Figure 3.27. It was found that the largest error between the simulation and the experiment occurs in the opening area along the middle cross-section. That is, the largest vertical error along longitudinal direction reaches 8.572 mm lower than the experiment, while 5.493 mm lower along transverse direction. This error is expected to have been caused by the coarse mesh used for simulation. Further study will be continued to investigate the mesh size effect on opening area geometric accuracy.

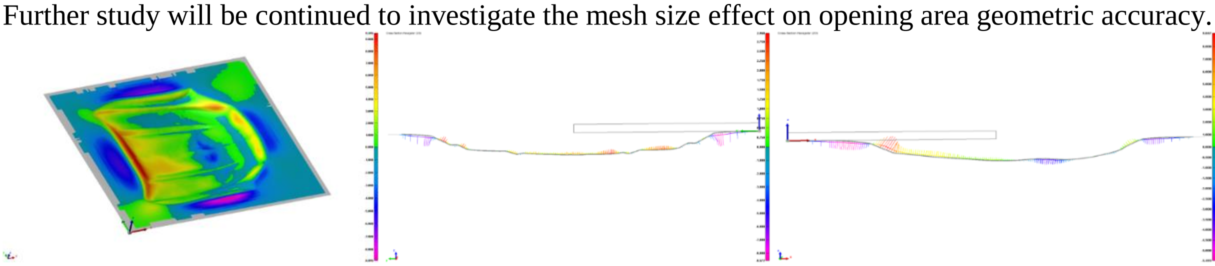

(a) (b) (c)

Figure 3.27 Geometry comparison between experiment and the simulation with 4 pairs of tools (a) global deviations (b) cross-section profile in X-direction (c) cross-section profile in Y-direction

The new multiple-tooling method was used for three geometries using shell element S4R and coarse mesh of 5 mm for simplicity: (1) 0.4 scaled Mustang hood; (2) full size Transit hood; (3) full size swing gate. See Figure 3.28. It was found that the new simulation technique reduced CPU time significantly up to 100 times. See Table 3.7.

Examples	Traditional FEA (days)	New FEA (days)
Mustang Hood (scaled)	6	0.05
Transit Hood	52	0.47
Swing Gate	48	0.46

Table 3.7 CPU time comparisons

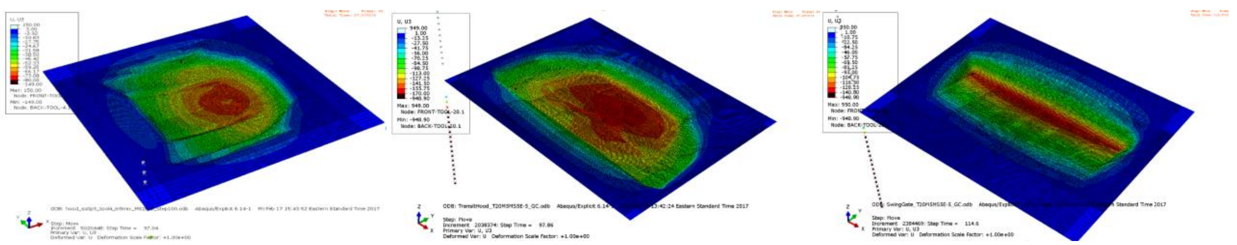

(a) (b) (c)

Figure 3.28 Simulated part shown in z-displacement (a) Mustang Hood (b) Transit Hood (c) Swing Gate

Conclusions: The multiple-tooling approach greatly reduces the computation time for the referenced model, e.g. 68% reduction in time with 4 pairs of tools, or 95% reduction in time with 20 pairs of tools. The achieved geometry by this approach shows a good agreement with the reference model. In addition, the key parameter of number of pairs of tooling, considered in this work, has a noTable influence on the computational efficiency but a less effect on the thickness distribution and the geometric accuracy.

3.3.3.5 Analytical Squeeze Factor Determination

As mentioned previously, computation time is a major problem regarding the use of FEM in the prediction of incremental forming. Based on the previous study, it is clear that continuum shell element SC8R or solid element C3D8R are required to simulate two-sided contact with thickness change. That is, the mesh size in thickness direction should be 0.2 mm, or five layers for 1mm thick sheet metal. Even using Taguchi optimization in Section 3.3.3.2 and multiple-tooling method in Section 3.3.3.4, it is almost impossible to complete the simulation for a large automotive panel model within 1-2 day, with acceptable accuracy.

Experimental results have shown that the squeeze factor between the two forming tools plays a significant role in the DSIF process among some key process parameters, such as tool geometry, step size, sheet thickness, sheet material, etc. Evidence for this is as follows: First, the squeeze factor was found to be strongly associated with the cosine of wall angle, roughly based on cosine law derived from the conservation of volume. Second, in most cases there would be either a loss of contact of back tool resulting in springback if the squeeze factor is small, or over-squeezing resulting surface roughness and material fracture if the squeeze factor is large. It was expected that there would exist an optimal squeeze factor under a specific condition, with a fixed wall angle, tool geometry, step size, sheet thickness, sheet material, etc. We sought to develop a squeeze factor database with parameters such as material, sheet thickness, step size, tool geometry and wall angle, which can be used to determine optimal squeeze factors depending on the forming conditions.

Method: First, several experiments were conducted for truncated pyramid geometries of varying wall angles. Each pyramid has four flat walls where different squeeze factors were applied, shown in Figure 3.29. Then the formed parts were scanned and compared with the CAD model. This is described in detail within section 3.3.3.1 below.

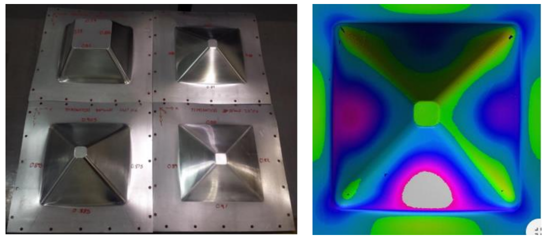

(a) (b)

Figure 3.29 Experiments to obtain squeeze factor database (a) truncated pyramids with varying wall angles (b) the deviation between the experiment and the CAD

Second, the goal is to find a fast and reliable FEM methodology to populate the squeeze factor database under various process conditions, rather than conducting extensive and time consuming experimental trials. Based on the previous simulation study, the slab model with three-dimensional solid elements is the preferred choice.

The modeling procedures begins with a slab model of a sheet metal blank of 60 mm long, 40 mm wide and 1 mm thick. Referring to Figure 3.29 (a), the left edge is fully constrained, while the other three edges are subjected to symmetric boundary conditions, because the incremental forming process is a localized deformation. The tools move back and forth in the Y-direction at a fixed step size in Z-direction. A fast and reliable criterion based on equivalent plastic strains and reaction forces on the front and the back tools is used to determine the optimal squeeze factor

See Figure 3.30 of DSIF and Figure 3.31 of SPIF using the slab model. It is evident that the equivalent plastic strains (PEEQ) of back side in DSIF is different from that in SPIF. For example, PEEQ of 2.3 in the back side of DSIF is much higher than 0.75 in SPIF.

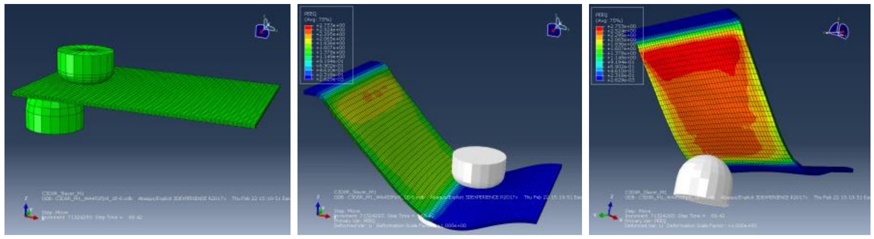

(a) (b) (c)

Figure 3.30 DSIF (a) model setup (b) PEEQ strain in front view (c) PEEQ strain in back view

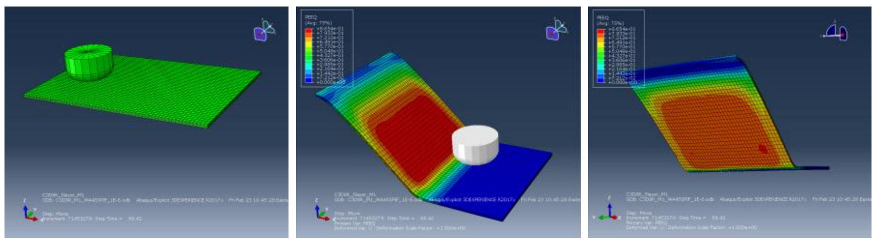

(a) (b) (c)

Figure 3.31 SPIF (a) model setup (b) PEEQ strain in front view (c) PEEQ strain in back view

Consider for example the simulation of forming a 30 degree wall. Figure 3.32 (a) shows the Equalent Plastic Strain (PEEQ) history on the back tool subjected to different squeeze factors. Based on the results (1) for each squeeze factor value the PEEQ strain remains to be nearly constant; (2) the PEEQ strain for DSIF is higher than SPIF due to the squeeze from the second tool; (3) the PEEQ strain increases with the squeeze factor. Figure 3.32 (b) shows the net force evolution, the difference between the force on the front tool and that that on the back tool. It can be seen that (1) the net force starts to increase once the back tool loses the contact with sheet metal, shown as curves of SPIF and squeeze factor of 0.96. (2) there exists an optimal squeeze factor such that the net force nearly equals zero, which are the optimum squeeze factors that are being used in the database.

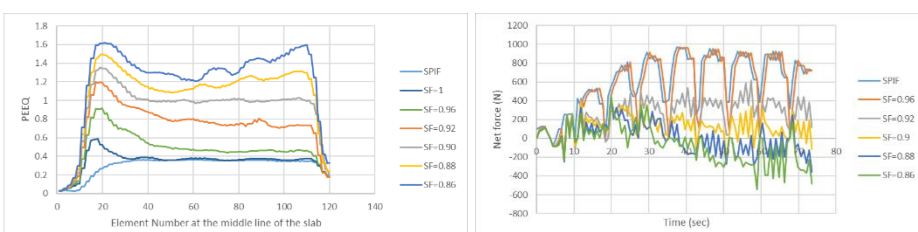

(a) (b)

Figure 3.32 In the back side of the slab for different squeeze factors (a) PEEQ strain history (b) Net force evolution

This method was used to investigate other wall angles from 3.75 degree to 60 degree, the predicated optimal squeeze factors matched with experimental data very well as shown in Figure 3.33. That also verifies the assumption of the force balance between two tools for the springback-free state.

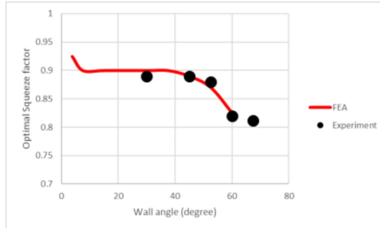

Figure 3.33 Squeeze factor, FEA vs. Experiment

<u>**Conclusions**</u>: First, a new methodology of creating a squeeze factor database to generate a high quality toolpath is proposed and verified. This method can help make the part with minimized springback, in a fast and automated way. Second, a new FEM method was developed to help reduce the number of experimental trials and time required to create such a database. The method combines with the slab model and three-dimensional solid element C3D8R. A new criterion of zero-net-force is proposed and verified by comparing the simulation with experimental data was. Third, this FEM method will be used to establish an expanded squeeze factor database with more related process parameters, such as material, sheet thickness, step size, wall angle, etc.

3.3.4 Process Optimization

3.3.4.1 RAFFT Tools Mapping

Earlier, one needed to verify manually that the tools that are present on the RAFFT machine rack are the same as those which were used in the RAFFT software for the toolpath generation. Any change in tools and their parameters could tear the sheet metal in the machine thereby damaging the tools. Due to this, the need to check and verify that the tools used in both places are indeed the same. Tools are characterized by four parameters, i.e. Tool-ID, Length, Diameter, Radius as seen in Figure 3.34 below.

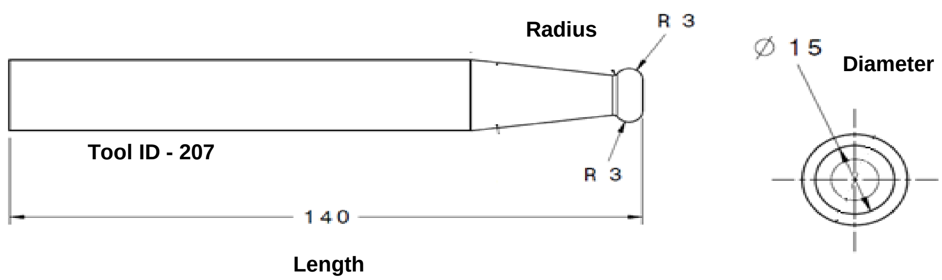

Figure 3.34 Tool Parameters

In order to automate this process, and thereby reduce the chance of human error, the following process was developed:

a) Get the tool information from the machine using the Siemens controller (in form of "*.ini*" file)

b) Run our newly built MS excel macro (created using VBA) to extract just the required tool information / tool parameters from this "*.ini*" file.

The above macro will output a CSV file which contains the tool information, in particular the 4 parameters mentioned earlier. Using the above generated CSV file kept in a specific, windows-based file location, all this data is used in the RAFFT UI panel to choose these existing tools only. In this manner there are no chances of one choosing un-used tools for RAFFT toolpath generation. Further, we make sure that the tools (front & back) used for the RAFFT toolpath generation are printed out in the "*.mpf*" file (ICAM output file). A subroutine is run on the machine to check that the tools & parameters mentioned in this "*.mpf*" file are the same as the ones present in the machine rack. This subroutine is added using "MPF post-processing" command button as mentioned above. If tools are NOT not the same, we immediately stop the machine from incrementally forming the part. The above steps a & b are repeated whenever we have removed / added tools in the machine tool rack.

3.3.4.2 Squeeze Factor Database

As previously mentioned, there exist a large number of process parameters that can be adjusted when making parts using double-sided incremental forming (DSIF). Some of these parameters include the tool geometry, step size, forming feed rate, material to be formed, thickness of the material to be formed, desired target shape after forming, and the squeeze applied by the tools. The material and geometry parameters are what will typically be dictated by the requirements of the desired part, but the others are open to being changed in order to meet specifications (timing, accuracy relative to CAD, etc.). With the aim of reducing the variability and time required in in making accurate parts, it was decided that a database of appropriate parameters would be developed.

To make this database, the first step was to decide which parameters would be controlled and which would be independent. We decided to start with a single material, Deep Draw Quality Steel with a thickness of 1 mm, maintain a standard tool geometry and federate, then ran tests at varying wall angles and step sizes while changing the squeeze factor to look for what squeeze value would result in the smallest discrepancy between the final geometry and the original CAD. A geometry called a “truncated pyramid” was used to emulate parts of varying geometries with assorted wall angles at regular intervals. Each pyramid had four flat faces in which different squeeze factors were applied. Figure 3.35 below shows an example of a few different formed parts.

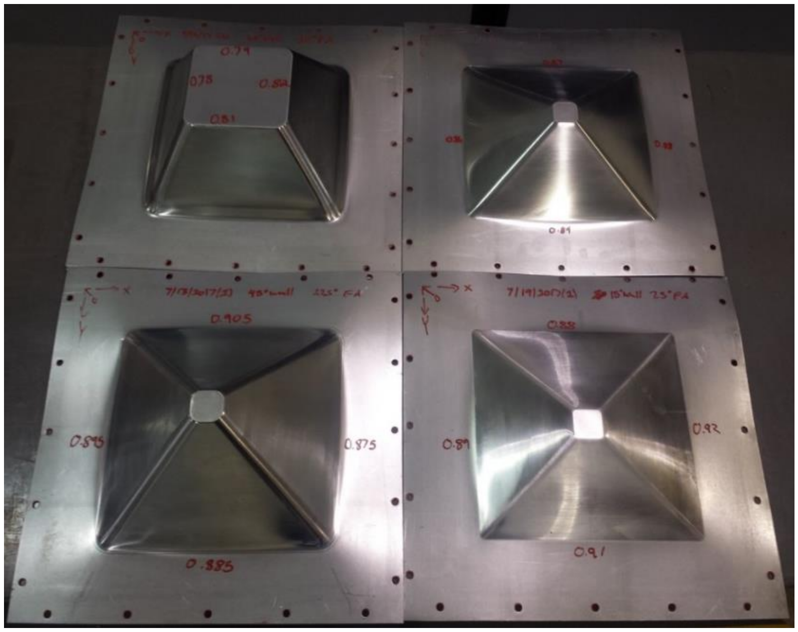

Figure 3.35 A set of four “truncated pyramid” parts of varying wall-angles. Each one has a different squeeze factor value applied to each of the four faces

To acquire the raw geometry data, the formed truncated pyramid parts were scanned into a point cloud using a ROMER Absolute Arm and the Polyworks software. This software also was used to import CAD model and record the deviations between the targeted and measured geometries. Figure 3.36 below shows an example of a comparison image between a formed truncated pyramid and the CAD model it was based off of.

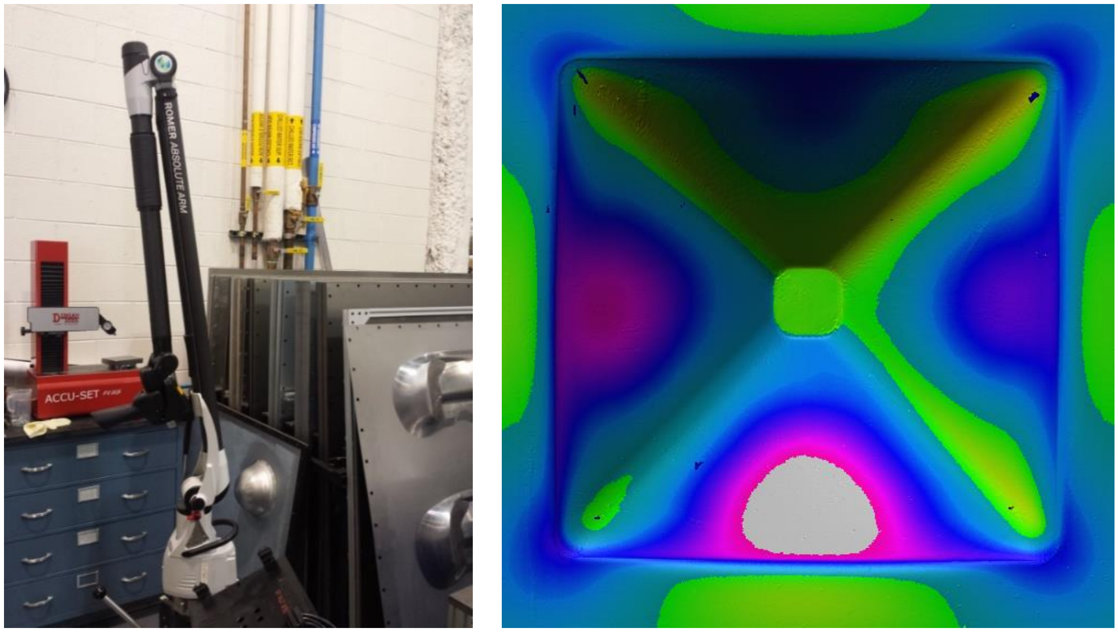

Figure 3.36 On the left is an image of the scanning arm, and on the right is a scanned part with colors indicating the deviation from the CAD

The deviations between the CAD model and the formed part can be exported on a per-wall basis, and then run through a statistics software package to determine which choice in squeeze factor resulted in the geometry closest to the target.

Once the optimal squeeze from one test is established, the test is repeated with refined squeeze values around the optimal value from the last test in order to more closely approach the true optimal values. After the experiments have been run to a sufficient granularity, the optimal value is recorded. When the optimal squeeze values are plotted against Figure 3.37 below shows a sample chart of accumulated data from these experiments at three different squeeze factors. This database can be integrated directly into the toolpath generation software for the RAFFT process to the point where for any set of material, thickness, step size, and geometry, the part should come out as close to the target shape as possible.

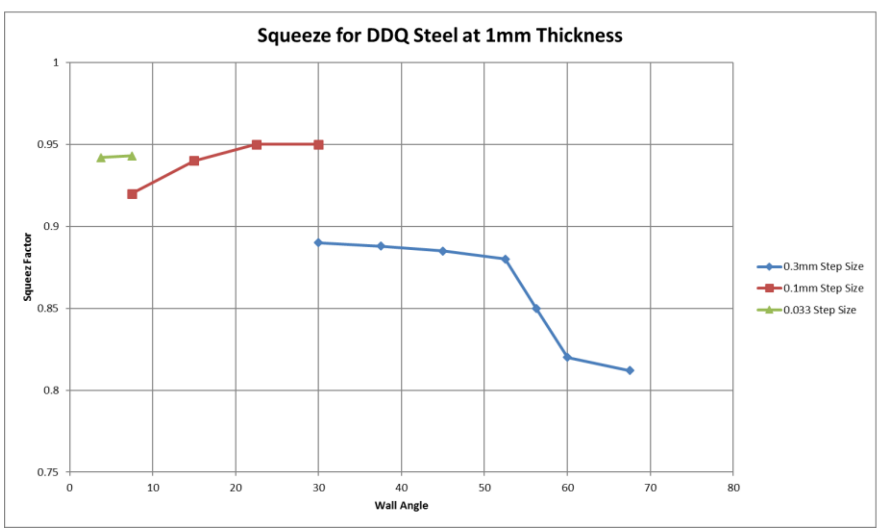

Figure 3.37 Experimentally determined optimal squeeze factor with respect to wall angle and step size

The next step in this process is to continue to build the database for other materials and thicknesses by running more experiments. The experimental data that is being obtained through these trials is being fed into simulation work to validate the models under development. It is our goal that given appropriate conditions, that simulations can accurately populate the parameter database rather than requiring the extensive testing currently required. This would save both time and material resources moving forward.

3.3.4.3 Development Of Theoretical Models To Predict Fracture In DSIF

A critical part of the incremental forming process is to predict what toolpath strategies will result in a successful part regarding both geometric accuracy and sheet failure. There are various pre/post strategies that attempted to correct or even prevent the potential inaccuracy of the DSIF process, while there are fewer available tools that addressed the issue of understanding as well as predicting material failure. While not inclusive, in-general for sheet metal forming processes, Finite Element Methods (FEM) are usually implemented with a failure criterion that is predominantly governed by either strains or stresses. Our focus is to determine the appropriate failure criterion that strikes a balance between 1) the number of independent variables that must be defined through experimental measures, 2) accuracy of the results with respect to the actual formed part, and 3) the computational efficiency of the model that is to be programmed within the finite element code.

To begin the tests, we considered a rather simple thinning criterion where failure is determined by the current value of the thickness strain. If it dips below the measured failure strain in the thickness direction, then the material is assumed to have failed and the appropriate elements are deleted. Mathematically, this criterion is expressed as:

$$\varepsilon_1 + \varepsilon_2 = -\varepsilon_3 < -\varepsilon_f$$

where ε_1 and ε_2 are the in-plane true strains, ε_3 is the thickness true strain, and ε_f is the failure true strain in the thickness direction. This formula is based off the conservation of volume during plastic flow. The motivation behind the formulation is from the line-fit (with a slope of -1) that can be often used to approximate the failure strains within strain space as shown in Figure 3.38.

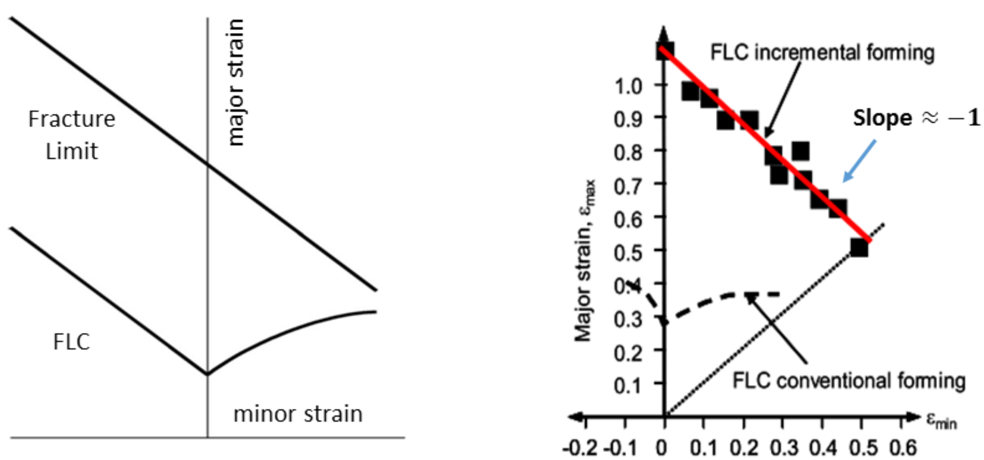

Figure 3.38 Failure limit diagram in single point incremental forming

A preliminary study has been implemented to investigate the feasibility of this thinning criterion in the incremental forming process. A funnel test with no failure criterion is first implemented to check the model accuracy with respect to the contact and damping parameters. The simulation result matches well with the experimental results for both formed part geometry and thinning point relative to the tool as shown in Figure 3.39.

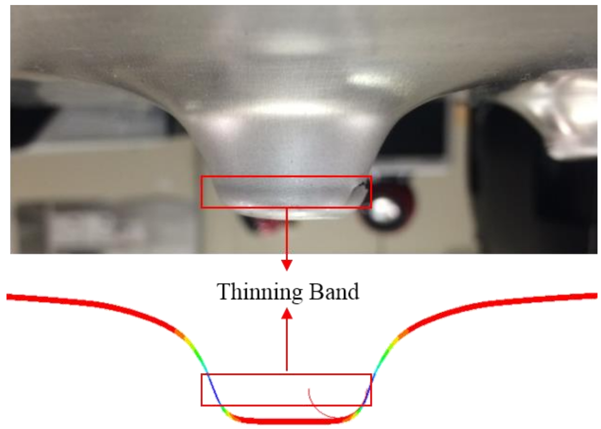

Figure 3.39 Experimental result and simulation minimum principle strain contour for funnel test

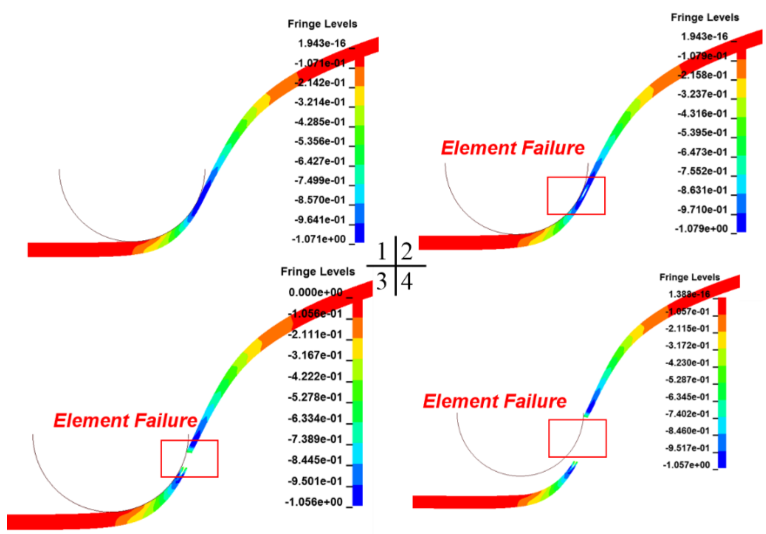

Figure 3.40 Simulation minimum principle strain contour with fracture model

Based on the calibrated simulation model, a thinning criterion is added into the simulation model and the model is capable of simulating the element failure as shown in Figure 3.40. A complete element deletion and failure process could be simulated completely. In this model, the critical minimum principle strain is set to be -1.1 for initial guess. A more accurate ε_f is need to be captured in order to get the same wall angle in the simulation part as the real experimental part after failure.

The current work is mostly based on single point incremental forming. Although there are lots of similarities between these two processes, we do think that the DSIF process requires for independent data since this criterion is not accurate under all stress states that can occur during incremental forming. Current work is investigating progressive damage laws that try to emphasize that materials fail over time rather than instantly due to void growth, void coalescence and ultimately crack propagation. Additionally, this type of formulation will be able to account for pressure and shear stresses, which were both presented in DSIF.

3.3.4.4 Machine Compliance Modeling In Simulation

One of most critical process parameters in the DSIF is tool gap, which characterizes how much the squeeze effect is offered by both tools, and distinguishes the DSIF process with SPIF. However, the tool gap largely depends on the system compliance, i.e. machine compliance and tool compliance, due to the large forces encountered during the process. In the rigid tool simulation model, the force profile for SPIF can be captured accurately as shown in Table 3.8. However, for the DSIF, the forming forces in the simulation are much larger than the experimental one, which is because the tools are rigid, and the tool gap is small as the input value from the tool path in the simulation. However, in experiment, the tool gap will become larger under the influence of large compliance, which reduces the forming forces in DSIF. Due to this sometimes only one tool is forming the metal sheet and there is no squeezing effect which will be influenced by the compliance. In this condition, there is no difference in forming forces from the SPIF.

In DSIF, the enlarged tool gap will reduce the forming forces, which influence the geometry accuracy and change the fracture behavior. In Table 3.8, the difference of forming forces in simulation and experiment mainly exists in the horizontal forces (parallel to the sheet metal). The reason is that in the current machine, the major compliance is in the horizontal direction, which causes the tool position changes in the horizontal direction.

	SPIF		DSIF	
	Z Force (N)	Horizontal Force (N)	Z Force (N)	Horizontal Force (N)
Experiment	670	350	820	400
Simulation	800	350	850	1400

Table 3.8 Maximum forming forces comparison

The influence of machine compliance should be investigated carefully in order to achieve better geometry accuracy, and prevent fracture in the DSIF. The machine compliance can be directly measured from the experiment. Thus, the tool position changes can be roughly estimated. However, in order to capture the geometry changes and stress state difference caused by the tool position changing, a dedicated simulation model is needed to investigate the process. Therefore, an explicit simulation model was developed to incorporate the tool compliance into the original rigid-tool simulation model. In the simulation, the tool hemisphere is still rigid since it helps to accelerate the contact algorithm and the whole simulation process. An artificial tool body is added to the tool hemisphere as a cantilever beam. The Young's Modulus of the tool is calibrated with the measured compliance. A rigid tool holder is attached to the end of the tool body to impose the tool motion. The tool structure is shown in Figure 3.41. The tool compliance model has been validated in a tool motion simulation with tool speed increasing and mass scaling. In future, the flexible tool model will be put into the original simulation model.

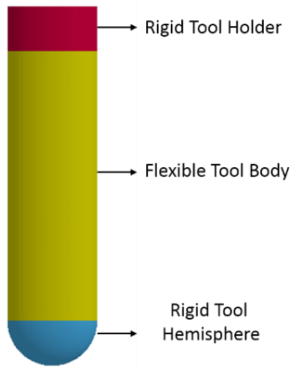

Figure 3.41 Flexible tool model

3.4 Task 4: Electrically-assisted Freeform Sheet Metal Forming

3.4.1 Post-deformation EAM treatment investigation

In order to investigate the effectiveness of post-deformation EAM treatments for reducing part springback, it was first necessary to determine the effect of various physical process parameters (such as feed rate, step-over, step-down, clamping mechanism, etc.) on part distortion. Figure 3.42 shows the effect of decreasing step-down size and Figure 3.43 demonstrates the effect of varying the clamping technique.

Figure 3.42 Effect of step down size on final part geometry (from left to right - 0.85mm, 0.55mm, 0.25mm step down sizes)

Figure 3.43 Examples of varying part distortion due solely to Clamping Configuration

Having established the effect of various physical process parameters on springback, it was then necessary to determine the effectiveness of various EAM process parameters (such as current density, duration, etc.) with respect to reducing springback for the materials being investigated. These effects were established via v-bend (Figure 3.44) and 90 degree wiping test configurations (not shown).

Figure 3.44 Effect of pulse duration on part springback under v-bend testing conditions (left to right: 2, 3, and 4 second pulse durations at 40A/mm2)

Once the preliminary EAM testing parameters were determined, probable application test locations/patterns needed to be established. The first step of this process was to develop a model for approximating the residual stress state after the deformation. Using ANSYS, a quarter slice of the pyramid was investigated by using a stepwise deformation loop that progressively deformed the material corresponding to each pass of the incremental forming tool. The results of this model (Figure 3.45) established where the highest stress concentrations (top of the pyramid corners) and greatest part displacement occurred (middle of the pyramid walls).

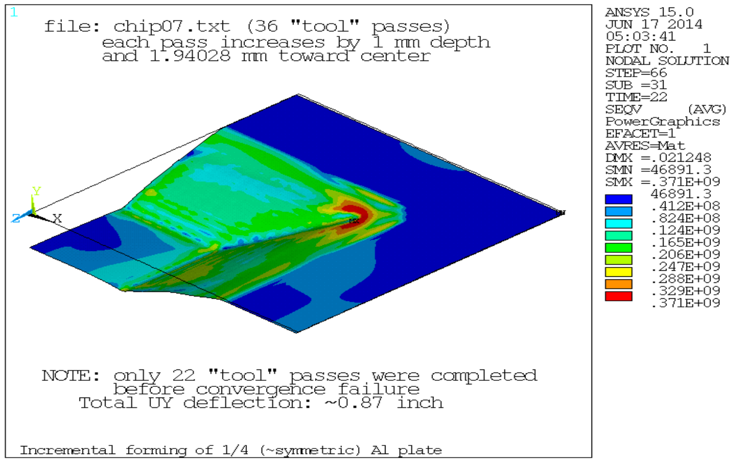

Figure 3.45 ANSYS model of the incremental forming process

Based on the residual stress profile, several testing protocols were examined:

3.4.1.1 Through-Thickness EAM Treatments

This treatment technique involved aligning the flow of the electrical current through the part's thickness via the use of co-linear applicators applied normal to the part's surface, similar to a spot-welding configuration (Figure 3.46 shows the fixture developed for this treatment approach). In this configuration, single and multiple treatments were applied to the high-stress regions (corners) of the pyramids at various current densities for different lengths of time. When looking at Figure 3.47, an example single treatment would be placing the applicators solely at location 2 in each corner of the pyramid, whereas an example multiple treatment would entail treating first point 1 and then point 3 for each corner of the pyramid. After treatment, the clamping was removed and the resultant part geometry was scanned for comparison against the desired geometry.

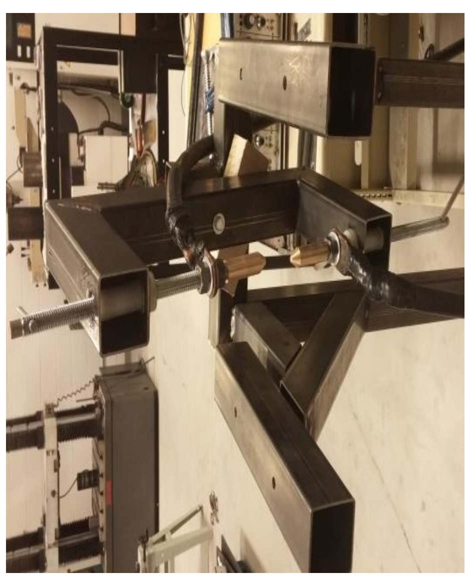

Figure 3.46 Applicator for through-thickness spot application of EAM

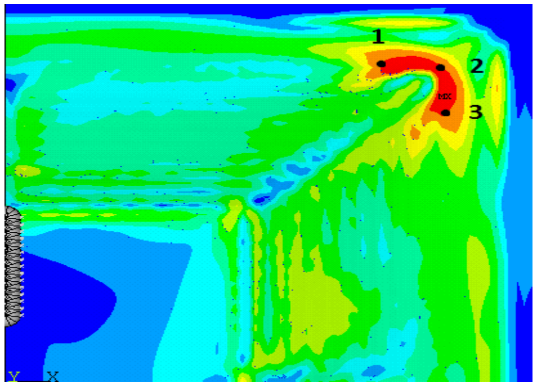

Figure 3.47 Example point locations for through-thickness EAM treatments

3.4.1.2 Path-based EAM Treatments

For the path-based treatment technique, electricity flowed along the sheet from one point to a second point. For instance, in Figure 3.48, a few example paths include flow from: point 1 to point 3, point 2 to point 4, or point 4 to point 5, as applied to the corresponding location on all four sides/corners of the pyramid. In addition, testing individual paths, multipath options were investigated wherein combinations of each path were investigated. When examining the combinations, tests were also conducted to determine if the order of application altered the effectiveness (that is, were different results obtained if the electricity was applied first from 1-to-3 and then 2-to-4, rather than the reverse 2-to-4 and then 1-to-3.

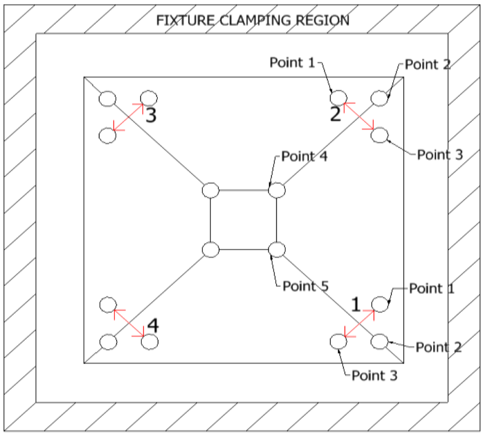

Figure 3.48 Example positive and negative lead placement locations for path-based EAM treatments

The application system for the path-based treatment technique can be seen in Figure 3.49, wherein the positive and negative leads are connected to the two different applicators, allowing the electricity to flow between them. The 2-part independent multi-degree of freedom alignment system shown in Figure 8 allowed the applicators to be adjusted to be normal to the part surface for complex geometries where the normal to the surface at the two application points was not parallel.

Figure 3.49 Path-based EAM treatment fixture

3.4.1.3 Area-based EAM Treatments

As an alternative to the sequential testing above, area-based EAM treatments were also investigated. For this treatment technique, positive and negative leads were applied to multiple applicators simultaneously, allowing the electricity to flow across large areas of the part (for instance from the left to the right of the part).

Figure 3.50 presents a few representative examples of the lead arrangements. These configurations were achieved via the grill arrangement shown in Figure 3.51. Two applicator tip configurations were investigated: rounded and swivel-jointed tips (the swivel-jointed tips are shown in Figure 3.51).

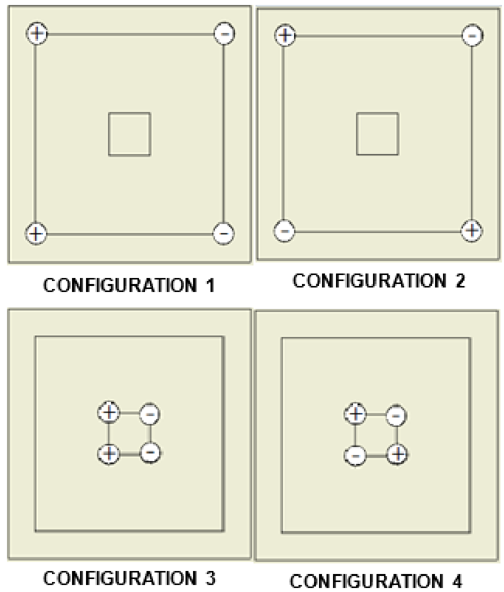

Figure 3.50 Example lead locations for Area-based EAM treatments

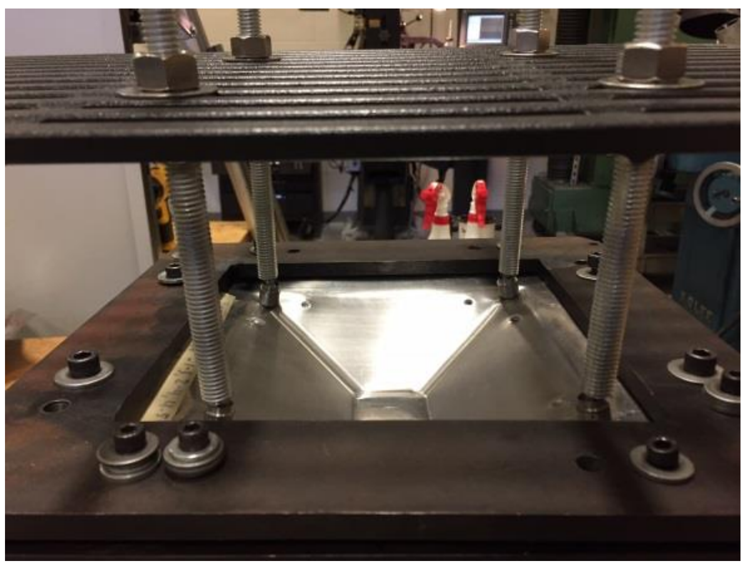

Figure 3.51 Area-based EAM treatment application fixture

Brief summary of findings

For each treatment technique, it was demonstrated that, through tuning, part distortion could be completely eliminated. However, different advantages and disadvantages existed for each technique. For instance, the area-based treatment technique required the least tuning but was the least energy efficient and could be quickly applied to different part geometries with minimal changes. Alternatively, the through-thickness technique required the least electrical energy while requiring the greatest amount of tuning based on the stress pattern and part geometry. The path-based technique presented a compromise between the two approaches. More in-depth descriptions of the testing and the findings for the various conditions tested can be found in the project's monthly reports.

3.4.2 In-situ EAM Treatment Investigation

While the post-deformation EAM techniques effectively reduced springback and part distortion, it is often desirable to also improve the material's maximum achievable elongation (especially when light-weighting or when producing complex geometries). In addition, when optimizing a process for minimal production costs, reducing process forces/energy and equipment size are also frequently important. In these cases, in-situ EAM treatment techniques are favorable. In-situ EAM treatment techniques involve the application of the EAM process during part formation, rather than post-deformation. As such, these techniques are, by their very nature, more complicated to set-up and employ since electrical current is flowing through the part during deformation. While this is not extremely difficult for traditional forging and stamping operations, in-situ EAM application is more complicated with incremental forming.

While the primary focus of the project was to examine post-deformation EAM techniques, an initial investigation into the effectiveness of in-situ EAM treatments for incremental forming operations was undertaken. For this investigation, three application configurations were examined: tool-to-frame EAM technique, tool-to-post EAM technique, and the Energized Workpiece (frame-to-post) EAM Technique. A fourth technique, specifically suited for double-sided incremental forming operations, the Tool-to-Tool EAM technique, was not specifically examined as a part of this project due to issues with the isolation of the RAFFT and RAFFT machining platforms.

For the two technique involving the tool, it was necessary to design a system that allowed the forming to become energized while electrically isolating the tool from the rest of the forming machine. This was achieved by wrapping an electrically insulative layer around the tool spindle that then extended to a secondary tool post (refer to **Figure** 3.52). Schematics of the two set-ups can be found in **Figure** 3.53. The third technique combined the two set-ups, wherein the tool was not energized but the frame and post were. The preliminary findings from this testing are shown in **Figure** 3.53 and

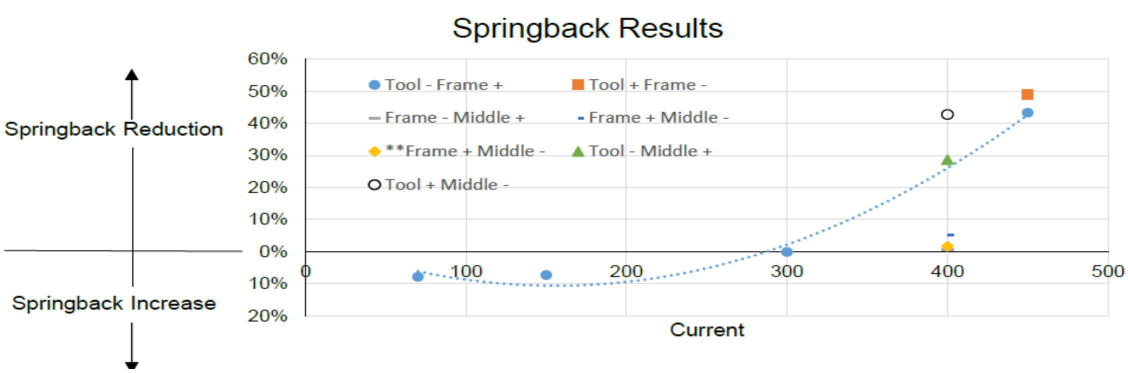

Figure 3.54.

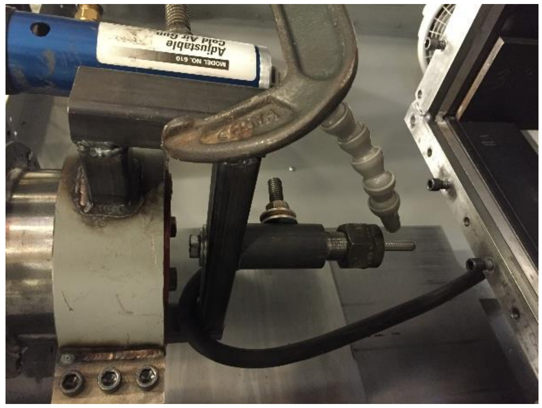

Figure 3.52 Electrically isolated incremental forming tool

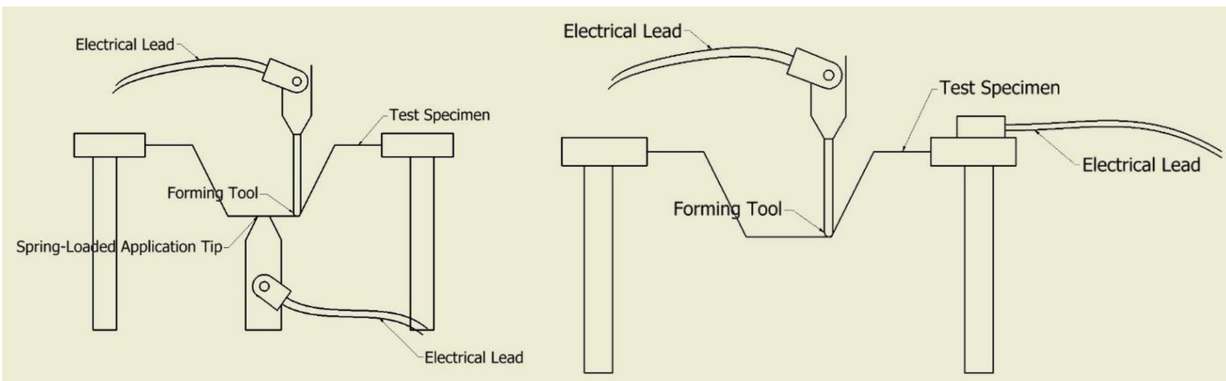

Figure 3.53 Tool-to-post and tool-to-frame schematics

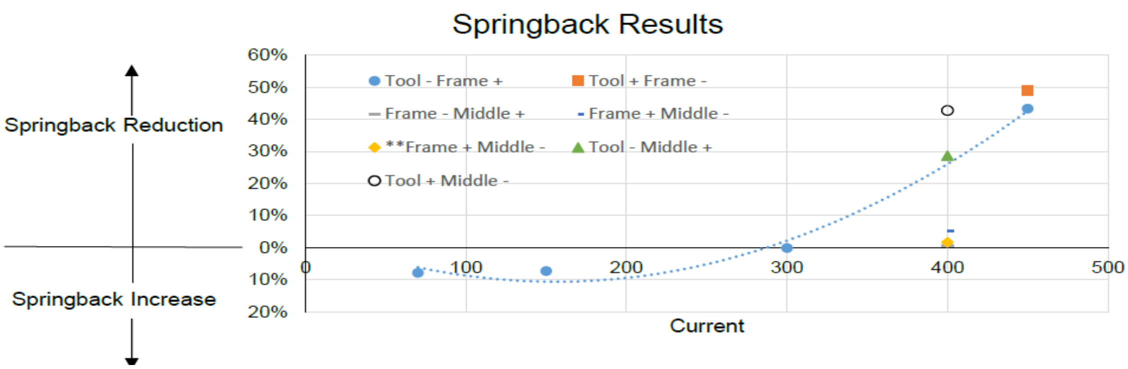

Figure 3.54 Preliminary In-situ EAM springback results

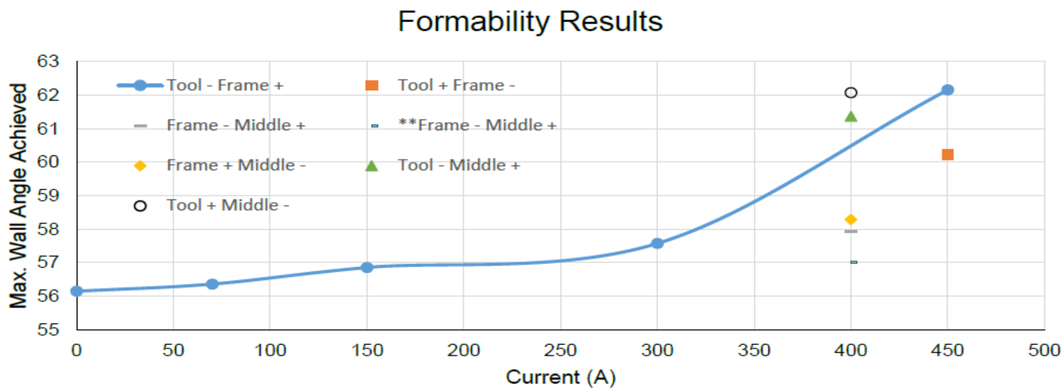

Figure 3.55 Preliminary in-situ EAM formability results

3.5 Task 5: Material Characterization & Performance Validation

3.5.1 Effect Of Part Geometry, Sheet Alloy And DSIF Process Variables On Formability

The Definitive Screening Designs approach (Jones and Nachtheim, 2013) was employed to develop an optimum DOE for identifying factors that have the most effect on forming by DSIF. A subset of this DOE, along with results of the forming runs, are reported in Table 3.9 and Figure 3.56. The formed parts were subjectively ranked on their formability on a scale of 1-5, 1 being the best. The results are shown in the last 2 columns of Table 3.9. Statistical analysis of formability dependence on various parameters was carried out with the results of just the 8 runs in Table 3.9. The analysis returned a model that captured 97% of variation of all the variables ran. The results in Figure 3.57 show that tool radius, wall angle, and sheet temper are the most significant contributors to formability.

Run	Stylus Dia.	Fillet Radius	Wall Angle	Thickness	Material	Temper	Coating	Step Size	Feed Rate	Formability Ranking	Survivabiltity ranking
2	10	8	15	0.813	2024	O	bare	0.1	2500	3	2
3	15	16	15	0.813	7075	T	clad	0.1	2500	3	5
5	15	8	37.5	0.813	2024	O	clad	0.4	5000	1	2
10	6	24	15	0.813	7075	O	clad	0.25	5000	3	4
12	6	24	15	0.813	2024	T	bare	0.4	3750	4	5
16	6	8	60	0.813	7075	O	bare	0.1	5000	2	4
21	10	16	37.5	1.5495	2024	O	bare	0.25	3750	2	2
22	10	16	37.5	1.5495	7075	T	clad	0.25	3750	3	3

Ranking from 1 (best) to 5 (worst)

Table 3.9 Post-DSIF mechanical properties of common automotive and aerospace sheet alloys

A summary of sheet alloys and associated tempers are shown in Table 3.10. All DDQ steel and 5754 panels were formed in O temper and tested for mechanical properties in the as-formed condition. All 6111 panels were formed in T4 temper and tested in the as-formed condition. The aerospace alloy 2024 was formed in O and T3 tempers, and alloy 7075 was formed in O and T6 tempers. Some of the 2024-O and 7075-O formed panels were further solution treated, quenched, and aged to T42 and T62 tempers, respectively.

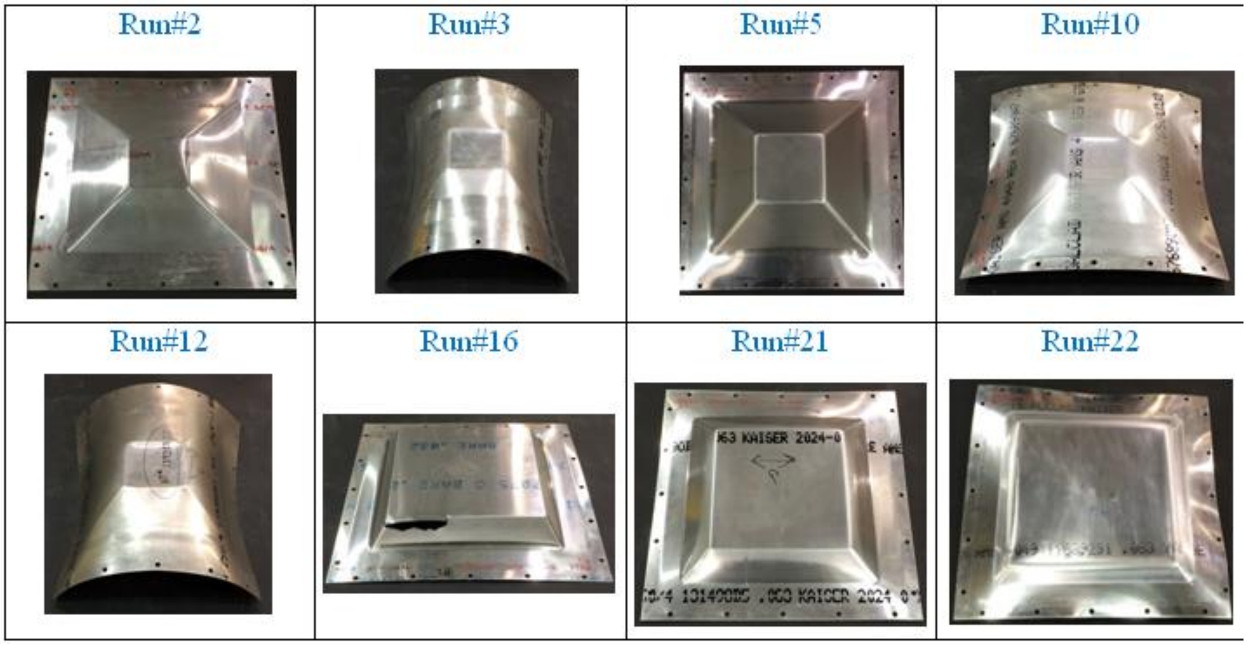

Figure 3.56 Panels formed with different variables shown in Table 3.9

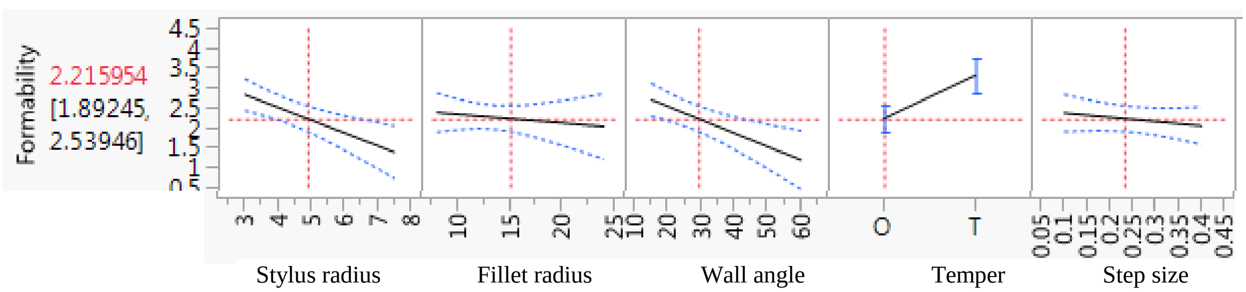

Figure 3.57 Statistical analysis of formability dependence on various parameters

A schematic of a test panel is shown in Figure 3.58 with various zones identified and the tensile specimens cut from these zones indicated. The zone identities, types, and specimen orientations are also listed in Table 3.11.

Alloy	Forming Temper	Post Form HT
DDQ Steel	Annealed	-
Al 5754	O	-
Al 6111	T4	-
Al 2024	O	-
Al 2024	O	T42
Al 2024	T3	-
Al 2024	T3	T81
Al 7075	O	-
Al 7075	O	T62
Al 7075	T6	-

Table 3.10 Sheet alloys, initial tempers, and post-forming heat treatments

Quasi-static tensile tests were performed on all the specimens. Figure 3.59 exhibits test results of all sheet alloys in the as-formed condition. The reported test results are averages of at least 3 specimens. The properties in the formed regions (areas deformed by stylus tools) are compared with those in the unformed regions (parent metal). All formed regions exhibit increased ultimate strength and yield strength and decreased percent elongation, compared to the corresponding parent materials, indicating work hardening in the formed regions. The sheet materials are highly isotropic as evidenced by small differences in the results for L and LT orientations. Yield strength is more than doubled and percent elongation reduced to less than half in DDQ, 5754-O and 2024-O alloys. Hard sheet tempers, 6111- T4, 2024-T3, 7075-T6, exhibit smaller strength increases post forming.

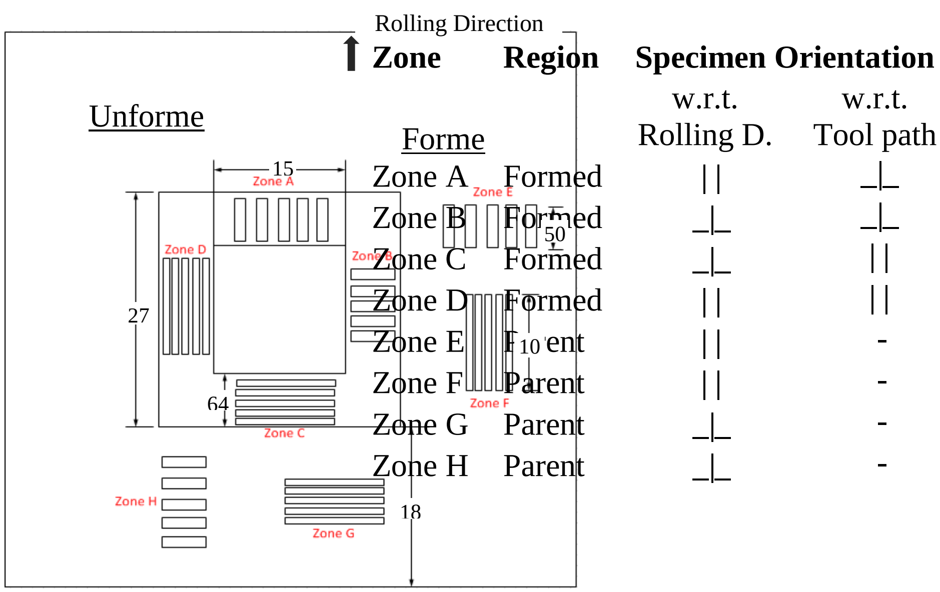

Figure 3.58 Schematic of coupons extracted from formed test panels

<table>
<tr><th>Zone</th><th>Region</th><th>Specimen Orientation</th><th></th><th></th></tr>
<tr><td></td><td></td><td>w.r.t. Rolling D.</td><td>w.r.t. Tool path</td><td></td></tr>
<tr><td>Zone A</td><td>Formed</td><td>| |</td><td>_|_</td><td></td></tr>
<tr><td>Zone B</td><td>Formed</td><td>_|_</td><td>_|_</td><td></td></tr>
<tr><td>Zone C</td><td>Formed</td><td>_|_</td><td>| |</td><td></td></tr>
<tr><td>Zone D</td><td>Formed</td><td>| |</td><td>| |</td><td></td></tr>
<tr><td>Zone E</td><td>Parent</td><td>| |</td><td>-</td><td></td></tr>
<tr><td>Zone F</td><td>Parent</td><td>| |</td><td>-</td><td></td></tr>
<tr><td>Zone G</td><td>Parent</td><td>_|_</td><td>-</td><td></td></tr>
<tr><td>Zone H</td><td>Parent</td><td>_|_</td><td>-</td><td></td></tr>
</table>

Table 3.11 Various Zones and tensile specimen orientations

Some panels made from aerospace alloys 2024-O and 7075-O were heat treated by full solutionizing, quenching and aging treatment to T42 and T62 tempers, respectively. The mechanical properties in Figure 3.60 and Table 3.12 show that heat treating 2024-O aluminum panel to T42, as expected, greatly increases ultimate and yield strengths, as well equalizes both strength and elongation properties between the un-formed and formed regions of the panel. Heat treating 7075-O aluminum panel to T62 exhibits similar results, where large increases in ultimate and yield strengths equalize properties between the parent and formed regions of the panel.

3.5.2 Fatigue Testing Of DSIF Panels

A separate set of truncated pyramid panels with wall angle of 35° were formed at a tool speed of 6000 mm/min for extracting fatigue coupons. Table 3.13 and Table 3.14 show the test matrices for the aerospace and automotive panels. The aerospace panels for this purpose were formed by using a thin-gage steel overlay sheet as a buffer between the Al sheet being formed and the outer forming tool. The steel overlay sheet prevents localization of load on the outer surface, and provides acceptable surface smoothness in these O-temper (soft) sheet materials. Metallography of cross sections cut from the 7075-O panels, Figure 3.61, shows more grain refinement with the smaller step size. This was observed in both aerospace alloys. Another observation in the 7xxx alloy micros (Figure 3.62) is the difference in surface roughness caused by the overlay sheet vs the forming tool alone. The use of the overlay sheet resulted in a much smoother surface. Surface roughness measurements were carried out on the aerospace panels. The results in Table 3.15 show that the roughness of the outer surface, which is protected by steel overlay sheet, varies in a narrow range with little effect due to change of alloy, step size, or measurement direction (parallel or perpendicular to the tool path). For example, 2024 panel formed with 0.05 mm step size shows a roughness of 35 Ra parallel to the tool direction and 32 Ra in the perpendicular direction.

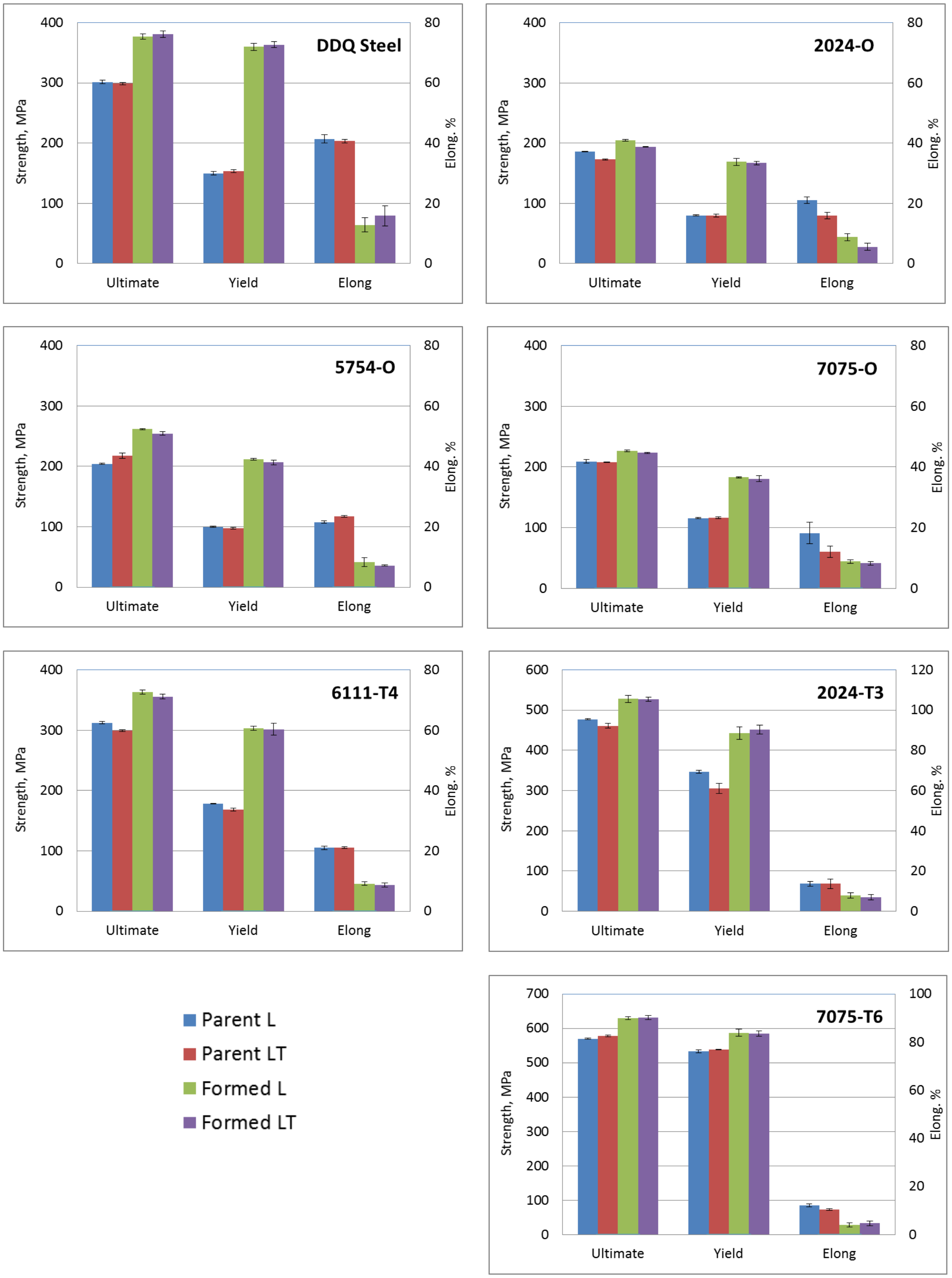

Figure 3.59 Mechanical properties of pyramid shaped panels formed by DSIF from various automotive and aerospace sheet alloys

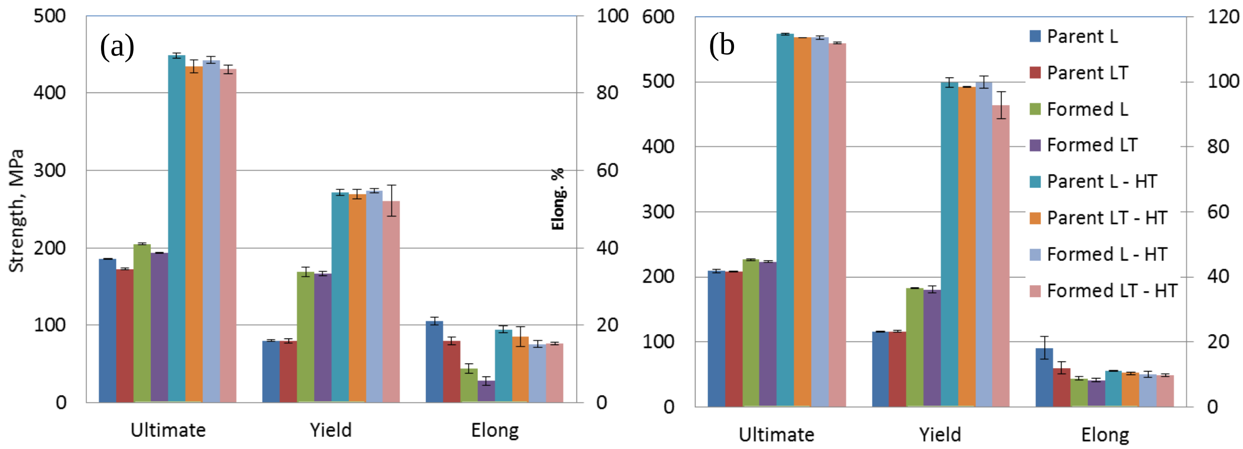

Figure 3.60 Mechanical properties of panels formed in O-temper and followed by full heat treatment to a harder temper (a) 2024-O formed in O and HT to T42, (b) 7075 formed in O and HT to T62

	AA 2024			AA 7075		
	US, Mpa	YS, Mpa	El %	US, Mpa	YS, Mpa	El %
Parent L	186	80	21	209	116	18
Parent LT	173	80	16	208	116	12
Formed L	205	169	9	226	183	9
Formed LT	194	167	6	223	181	8
Parent L – HT T42	449	271	19	573	499	11
Parent LT – HT T42	434	270	17	568	492	10
Formed L – HT T62	443	273	15	568	499	10
Formed LT – HT T62	431	261	15	559	464	10

Table 3.12 Mechanical properties after forming in O-temper, and after heat treating, as indicated

Alloy	Thickness (mm)	Step Size (mm)	# of Panels
2024-O	1.6	0.05	3
2024-O	1.6	0.20	3
7075-O	1.6	0.05	3
7075-O	1.6	0.20	3

Table 3.13 Fatigue test matrix - aerospace alloys

Alloy	Thickness (mm)	Step Size (mm)	# of Panels
DDQ steel	1.0	0.01	6
5754-O	1.0	0.01	6
6014-T4	1.0	0.01	6

Table 3.14 Fatigue test matrix - automotive alloys

The inner surface of panel, which directly comes in contact with the tool, however, exhibits sharp differences in surface roughness along the two directions. For example, the inner surface of 2024 panel, formed with 0.20 mm step size, shows a roughness of 13 Ra parallel to the tool direction and 61 Ra perpendicular to the tool direction. Further, the Ra is affected by the alloy and the step size.

Sheet thinning in both alloys essentially follows the cosine law, with thickness reduced by cosine of the wall angle of 35 degree. The sheet thickness is reduced from 1.6 mm to 1.3 mm in the pyramidal faces.

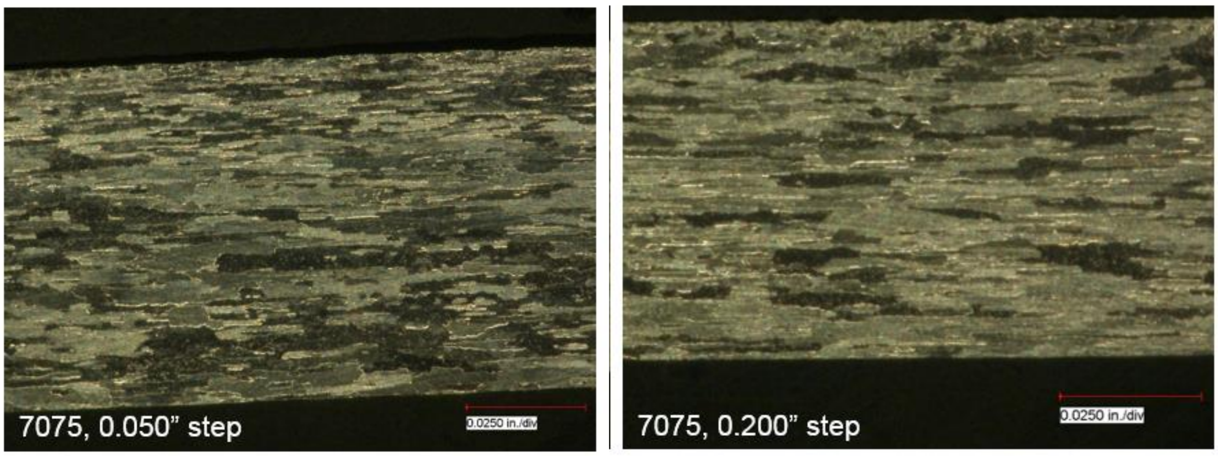

Figure 3.61 Micrographs of formed aerospace alloy Al 7075 for two different ISF step sizes

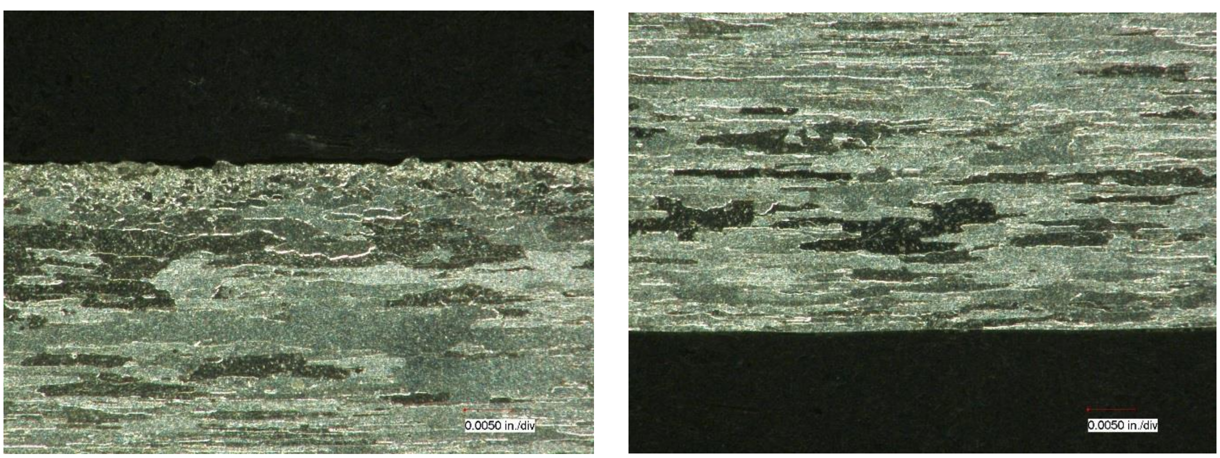

Figure 3.62 Micrographs of formed aerospace alloy Al 7075 showing the inner tool side (left) and the outer side that was in contact with the steel overlay sheet (right)

Alloy		AA 2024				AA 7075			
Step Size		0.05 mm		0.2 mm		0.05 mm		0.2 mm	
		Avg. Ra	S. Dev	Avg. Ra	S. Dev	Avg. Ra	S. Dev	Avg. Ra	S. Dev
Outer surface	ǁ	34.6	1.8	31.5	2.1	27.0	2.8	25.9	3.4
	⊥	31.5	4.0	40.7	3.4	36.0	5.4	26.2	4.1
Inner surface	ǁ	9.0	2.9	12.8	5.2	32.6	9.9	9.6	1.5
	⊥	32.5	6.9	60.5	13.3	84.4	10.1	39.5	7.0

Table 3.15 Surface roughness averaged over all 4 faces of all 3 panels (12 measurements)

Fatigue specimens were machined to 4” length and 0.50” grip width from the four inclined faces of the truncated pyramids. Axial fatigue testing was conducted per ASTM E466-15 at room temperature in load control employing a 60 hertz sinusoidal waveform with an R-ratio of 0.02. Run out was defined as 2,000,000 cycles and any test reaching run-out was discontinued. Boeing provided the stress levels for the aerospace alloys and Ford for the automotive alloys. The Boeing stress levels fell in the low cycle (high stress) fatigue regime, whereas the Ford stress levels were in the high cycle fatigue regime. Figure 3.63 and Figure 3.64 plot fatigue test results for the automotive and the aerospace alloys under high-cycle and low-cycle regimes, respectively. The plots compare results for L and LT orientations and orientations parallel and perpendicular to the tool path direction with those of the unformed material. In case of the aerospace alloys, the plots also compare results for the two step sizes used.

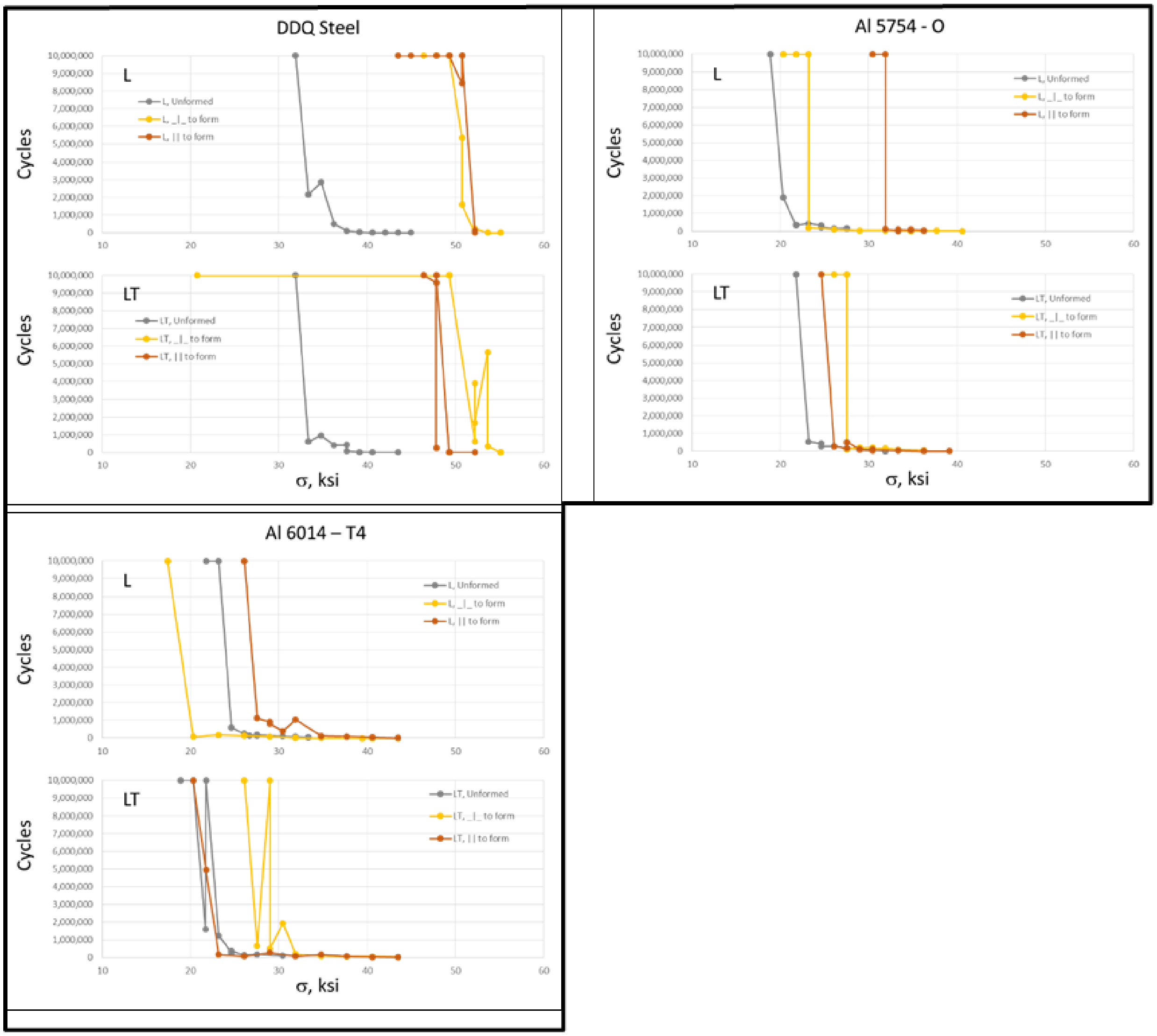

Figure 3.63 High-cycle fatigue results of automotive alloys for specimen orientations parallel to and perpendicular to sheet rolling direction and parallel to rolling direction

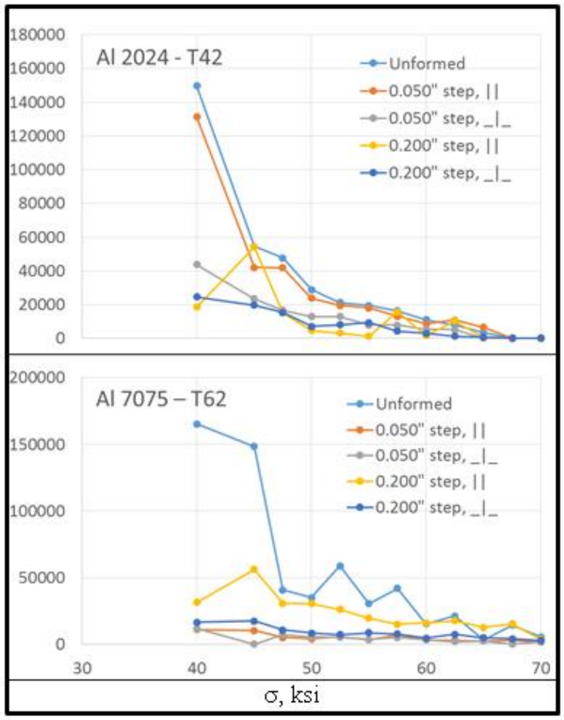

Figure 3.64 Low-cycle fatigue results of aerospace Al alloys for different ISF step sizes and specimen orientations

Under a low-cycle regimen, interaction with the ISF tool shows to significantly reduce fatigue life, especially in test direction perpendicular to the tool path. In case of the automotive alloys under high-cycle regime, interaction with the ISF tool appears to increase fatigue strength of the sheet material. The effect of specimen orientation relative to tool path is not very clear.

Chapter 4. Benefits Assessment

The analysis conducted for this project shows that RAFFT presents large opportunities to save on tooling costs during low-volume sheet metal part production. In addition, RAFFT presents large lead-time savings for extremely low-volume production (20 parts or less). It is difficult to assign a monetary value to the time saved in production, but the saving could be used for additional design time and testing or to reduce overall product development time. Shortened lead-time represents a substantial competitive advantage for those companies that pursue this strategy. Like other flexible manufacturing technologies (such as additive manufacture), RAFFT is particularly suiTable when custom parts are required or where replacement parts are hard to come by (i.e., when the original tooling has been lost or if the product is situated in a remote location).

The Figure 4.1 below shows the predicted Cumulative Energy Demand (CED) for Incremental Sheet Forming (ISF) compared to four conventional sheet metal forming processes for a generic aluminum part using each process. The error bars in this Figure correspond to one standard deviation away from the mean. For details on the uncertainty analysis readers are referred to Section 3.2.2 in Appendix A. Several trends can be established by examining Figure 4.2, despite large uncertainties in the predictions.

When only a few parts are required (less than 20), ISF can potentially save significant amounts of energy compared to the other processes. As the number of parts increases, the die-set impacts are quickly amortized and per part impacts have reduced to the level of ISF by 1,000 parts. As the number of parts required approaches 1,000, the energy curve for several of the conventional processes plateaus and remains above ISF, except for Fluid Cell Forming which becomes less energy intensive than ISF at around 170 parts

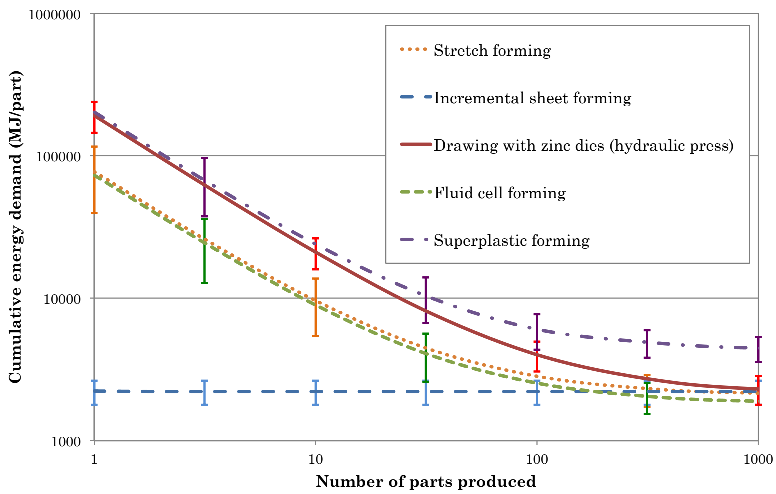

Figure 4.1 The effect of production number over the die lifespan (N) on per part CED. Generic aluminum part modeled: 1.5 m2, 1.5 mm thick. Forming depth (for ISF calculation): 70 mm. In the case of stretch forming, Batch size, B=Number of parts produced, N. In the

A similar analysis for cost shows a comparable trend but now with a cross-over occurring in the range of 100’s of parts. See Figure 4.2.

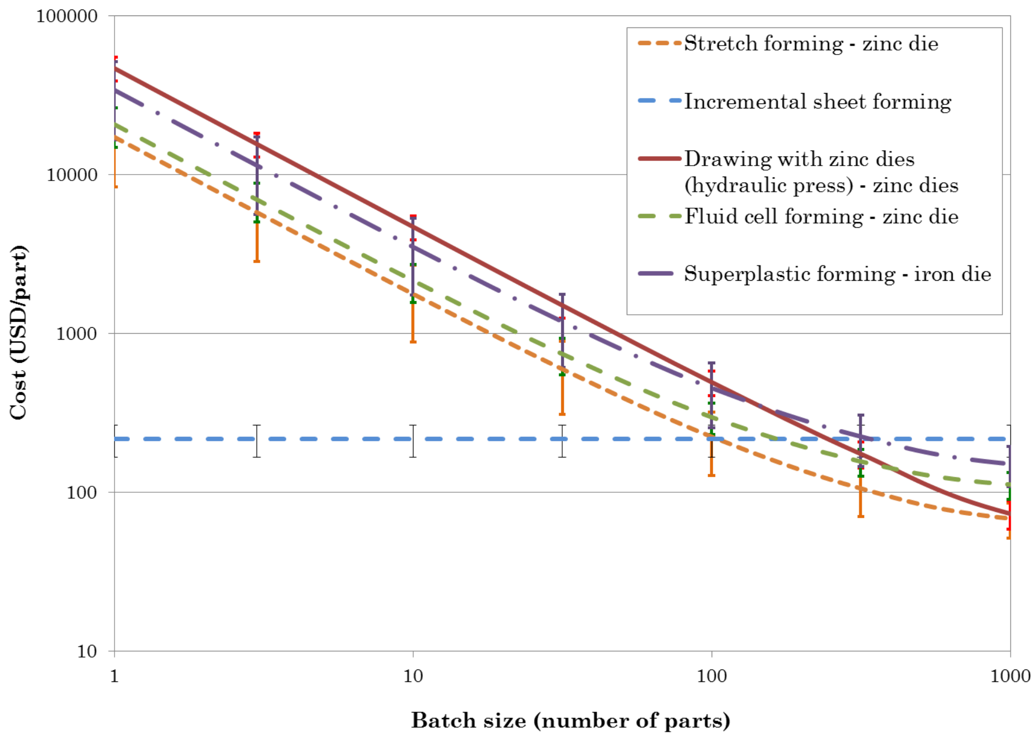

Figure 4.2 The effect of production number on per-part cost (including labor and capital depreciation costs). Generic aluminum part modeled: 1.5m2, 1.5mm thick. Forming depth (for ISF calculation): 70mm

This Figure shows that the RAFFT break-even volume for cost is generally lower than the RAFFT break-even volume for energy if equipment depreciation and labor are included in the cost analysis.

4.1 Applications to the Automotive Industry

Traditionally, prototyping in the auto industry has relied on the use of a stamping process that requires multiple cast and machined zinc die-sets and a hydraulic stamping press. ISF therefore presents the opportunity to potentially avoid the die-making and try-out processes, thus saving on time, money, and energy. This section presents calculations on the potential costs and environmental impacts of using RAFFT in the US car industry by 2030. It is found that by 2030 it is likely that over 400,000 prototype parts will be being produced with geometries that ISF can form. The potential market shrinks to around 300,000 parts when we consider only those parts for which ISF production will save energy and costs compared to zinc die drawing, and around 260,000 parts when we consider technology diffusion. Energy and cost models of ISF and drawing are used to estimate potential mean savings of **around 100 $TJ_{primary}$ and 60 million USD per year by 2030**.

These conclusions are reached by identifying potential parts that can be created using RAFFT and then applying filters to only consider parts where energy and costs are saved. Finally, a diffusion model is applied to these findings. *Figure* 4.3 below illustrates the effects of these filters and of the diffusion model. Full details of this methodology can be found in Section 4 of Appendix A.

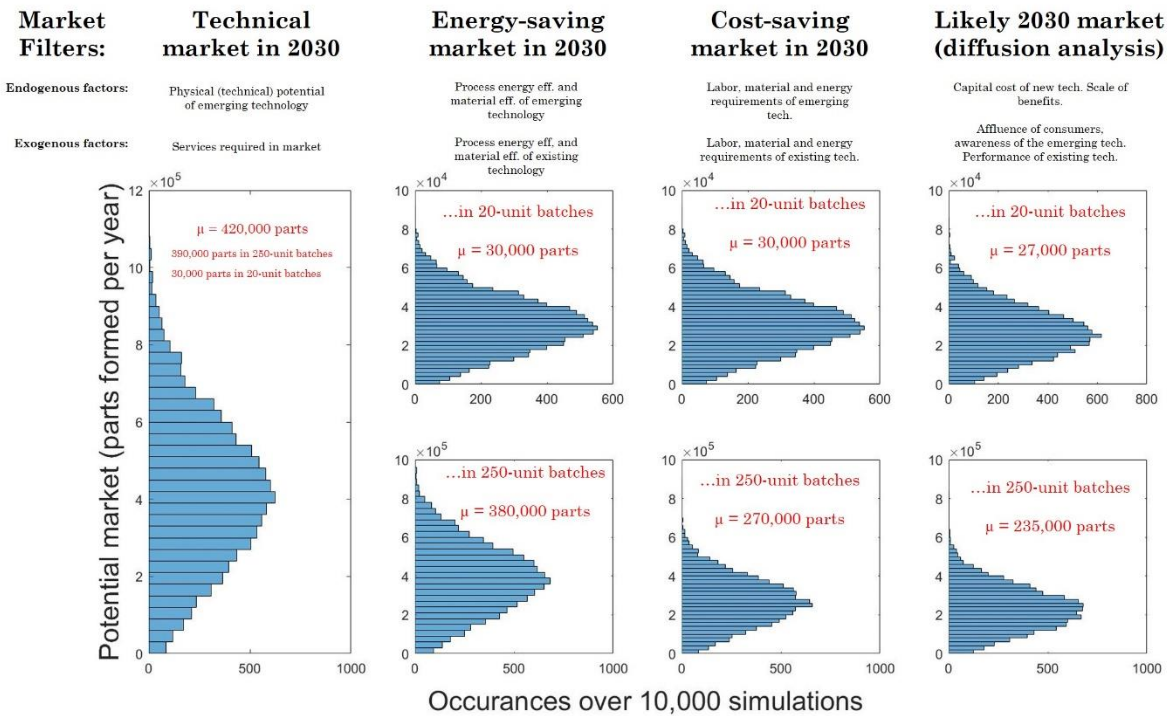

Figure 4.3 The effect of different "filters" on the addressable market. Distribution from 10,000 simulations

Figure 4.3 focuses on the market size. Figure 4.4 attempts to translate this market size to environmental and economic impact of RAFFT in 2030.

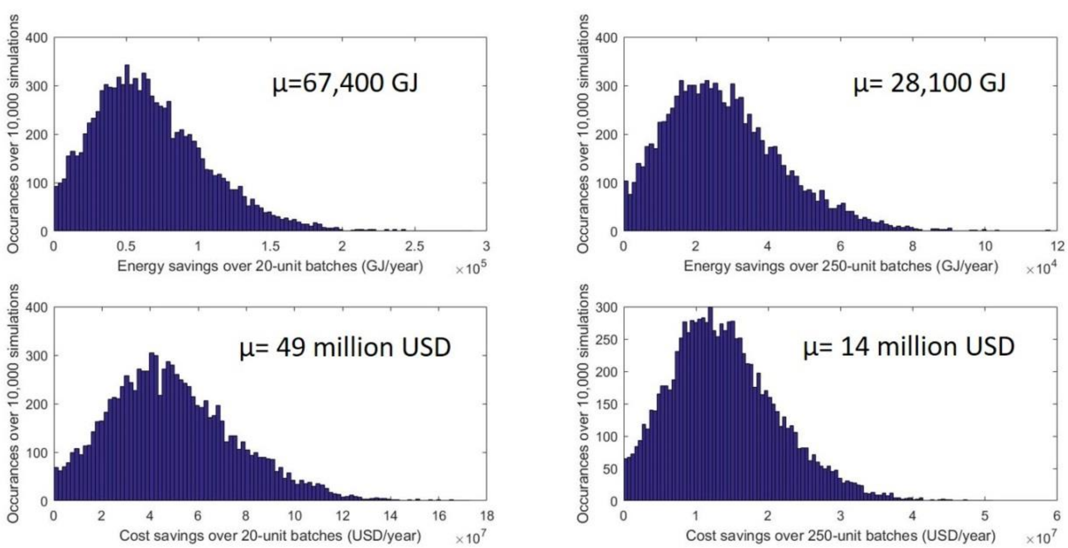

Figure 4.4 Total annual energy and cost savings across part prototyping (left column) and car development (right column) assuming ISF displaces zinc die drawing one-to-one in 2030. Distributions from 10,000 simulations

4.2 Applications to the Aerospace Industry

At the beginning of this project, it was assumed that all production rates in aerospace were low enough that RAFFT could be used to meet any need. However, the total production number for each part design is difficult to know because aircraft stay in production for decades. For example, while just 45 Apache helicopters were made in 2014 (Rossie, 2015), over 2,000 have been made since the program's inception in the early 1980s. Additionally, often incremental changes and different models are introduced over the years, making it difficult to know the duration for which a given part will be produced. For example, currently 737 models are under the "Next Generation" umbrella (produced since the mid-1990s) but are transitioning to the "Max" umbrella. It seems that much of the aircraft will be the same with no reason to make different dies (Boeing, 2014). In Rossie's analysis, representative low-volume aerospace production is taken to be 25 parts per year for 30 years; 750 parts total. The upper limit is taken to be 15,000 based on the fact that Boeing has so far received a lifetime total of 12,649 orders for the 737 Next Generation and Max (as of the end of 2014), and the 737 is expected to undergo major redesign in the 2020s (Boeing, 2014; Red, 2014). The results of the process cost and energy comparisons (see Section 3.2 in Appendix A for more detail) show that RAFFT becomes more expensive than rival processes when producing 100's rather than 1000's of parts, it is unsurprising that RAFFT is not theoretically cost competitive for even the modest production numbers considered by Rossie. However, in Low-volume Production, Field Support, and Prototyping and Special Projects, RAFFT could be useful for very low-volume production, particularly when the demand is sporadic or original tooling has been lost.

4.3 Savings in Other Sectors

The benefits of RAFFT in the auto industry (transport) can be scaled to estimate potential savings in other applications. A sensible scaling factor is the relative quantity of sheet metal used in different sectors of the economy. No data on the use of sheet metal at the national level has been found; therefore, global annual data on the use of steel (Cullen et al., 2012) and aluminum (Cullen and Allwood, 2013) sheet metal is used instead.

Allwood et al. (2005) claim that ISF can only be used to form metal sheets less than 1.5mm thick. Given this restriction, it is likely that RAFFT will be able to form aluminum foil, electrical steel sheet, and steel and aluminum cold rolled coil (CRC). The majority of aluminum foil is used in packaging applications where no further forming is required, and electrical sheet is typically stacked to form the cores of transformers and motors, with no further forming. Subsequently, it is likely that RAFFT is mainly going to be used to form cold rolled coil. By mass, steel is the dominant material, and therefore we scale the potential benefits of using RAFFT to form steel parts to obtain additional benefits of **83.2 TJ avoided energy use, $54.9 M USD saved and 5.0 kt CO2eq avoided.**

4.4 Longer Term Potential

Potential to use smaller blanks:

In stamping, material around the edge of the dies must be 'drawn-in' to prevent the sheet from tearing. An unconstrained sheet would wrinkle; therefore, the edges of the blank are held in blank holders that control the flow of the sheet towards the center of the part. The result of this forming process is a final part that has excess material around the edge (corresponding to the last material that was held between the die holders) and a wall thickness that is similar to that of the original blank. In contrast to conventional forming, the higher forming limits in RAFFT allow the sheet to be fixed around the edge, with the potential to reduce trimming losses. This advance would mean that, in comparison to conventional forming, a smaller blank would be required in order to form the same part.

The relative sizes of blanks required in ISF and conventional forming is investigated by Ingarao et al. (2012). They use ISF to form two different components from two different aluminum alloys and two different sheet thicknesses. They compare the required blank sizes for these processes to those for conventional forming, which they calculate using simulation software.

Ingarao et al. (2012) find that the blanks required for ISF are typically 10% smaller than those required for conventional stamping. Assuming a 10% saving is applied to the forming of the car and plane parts yields an additional savings of **24.1 TJ energy, $395,000 USD, and 2.01 kt CO2eq**

Potential for thickness control:

In conventional forming, the wall thickness of a formed part is approximately equal over most of its area to the thickness of the original blank (DIN, 2003). The resulting localized thinning means that parts are typically heavier than necessary; given that the thinnest section must meet a minimum specification, the remaining sections are generally thicker than required. In RAFFT, the sheet can experience much larger in-plane strains, and this global thinning of the sheet may be able to reduce the excess thickness of formed parts. The wall thickness of a part formed by RAFFT is approximately given by the sine law (Jackson and Allwood, 2009).

The ability to use RAFFT to form lightweight parts is, however, an unproven concept. In addition, the applicability of the sine law has been called into question by several authors investigating the mechanics of ISF, such as Jackson and Allwood (2009). In light of this, in this report it is assumed that RAFFT could reduce the mass of a formed part by only 5%.

The potential for RAFFT to create lighter components means potential use phase savings in transport applications.

It was estimated previously that in 2014 there were 90,000 (609 planes x 150 parts per plane = 91,350) aluminum commercial plane parts manufactured that could, technically, have been made using RAFFT. Applying the 9% growth rate, in 2017, there will be 118,000 parts made which RAFFT could, technically, produce. Assuming a typical part dimension of 1x1x0.001m, applying the potential 5% weight saving as discussed above implies that RAFFT could reduce the total mass of all aircraft being produced in 2017 by 16 t.

The fuel required to move 1 t by plane can vary, but for modern long haul aircraft it is approximately 2 MJ/t.km (Smil, 2008; Lee, 1992). Hence, the estimated 16 t saved per year could result in an energy saving of 32 MJ/km. Assuming that airplanes travel an average of 9,600 km daily (equivalent to a US coast to coast return flight), 6 days per week, 48 weeks per year, implies that airplanes travel an average of 2.8×10^6 km each year. A reduction in the total mass of all aircraft produced in a year by 16 t will therefore result in an annual energy saving of 89.6 TJ.

Combined potential effect:

In 2030, RAFFT may potentially be used to reduce primary energy requirements in the USA by up to around 4 PJ (3,800,000 MMBtu), reduce greenhouse gas emissions by 280 kt (620 million lbs) of CO2eq, and save US companies around 220 million $USD_{2016\ dollars}$. These potential savings were all calculated assuming that researchers will overcome the technical challenges posed. *Figure* 4.5 shows a summary of the results. The potential savings have been plotted against a logarithmic axis in order to visually weigh the potential savings in each sector against growing uncertainty. During the project, most resources were put into understanding how RAFFT might be used in the car industry. As such, we are much more confident about the numbers relating to the car industry than, say, non-transport applications. If RAFFT could be used to locally control part thickness in lightweight aerospace components, then the potential savings are vast. However, this ability has yet to be demonstrated.

In addition to the uncertainty described above, these savings assume one-to-one displacement of existing forming processes with the RAFFT process. As mentioned previously and as discussed in some detail in Section 4.1 in Appendix A, it may be possible that displacement will be less than one-one and there may also be potential for rebound effects in certain applications.

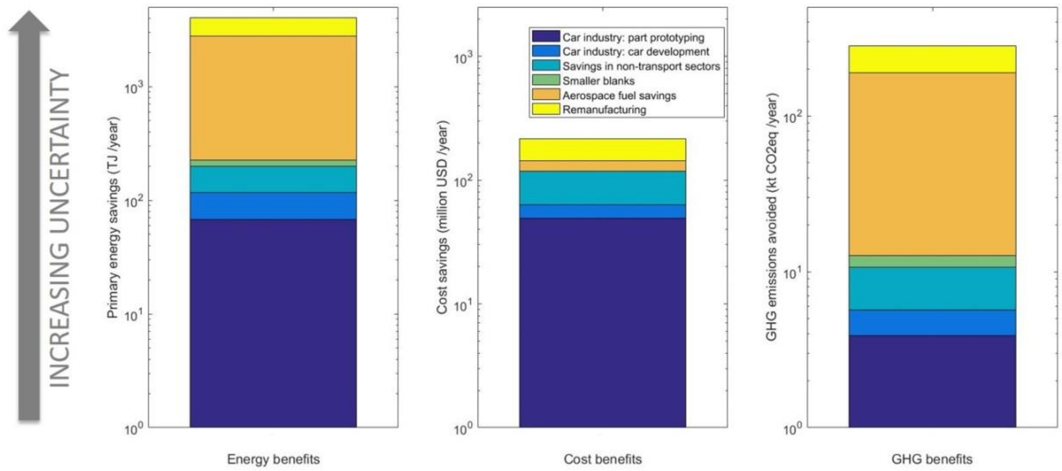

Figure 4.5 Potential annual benefits in the USA by 2030 from the development of RAFFT

Chapter 5. Commercialization

A successful, well planned and well executed commercialization is necessary to gain the full potential regarding the (a) energy saving, (b) time saving, and (c) financial benefits that RAFFT can offer. Ford Motor Company, who is the lead in this project, is committed to undertake this responsibility and propose to do so in three phases. The high level vision/options for RAFFT commercialization is illustrated in Figure 5.1

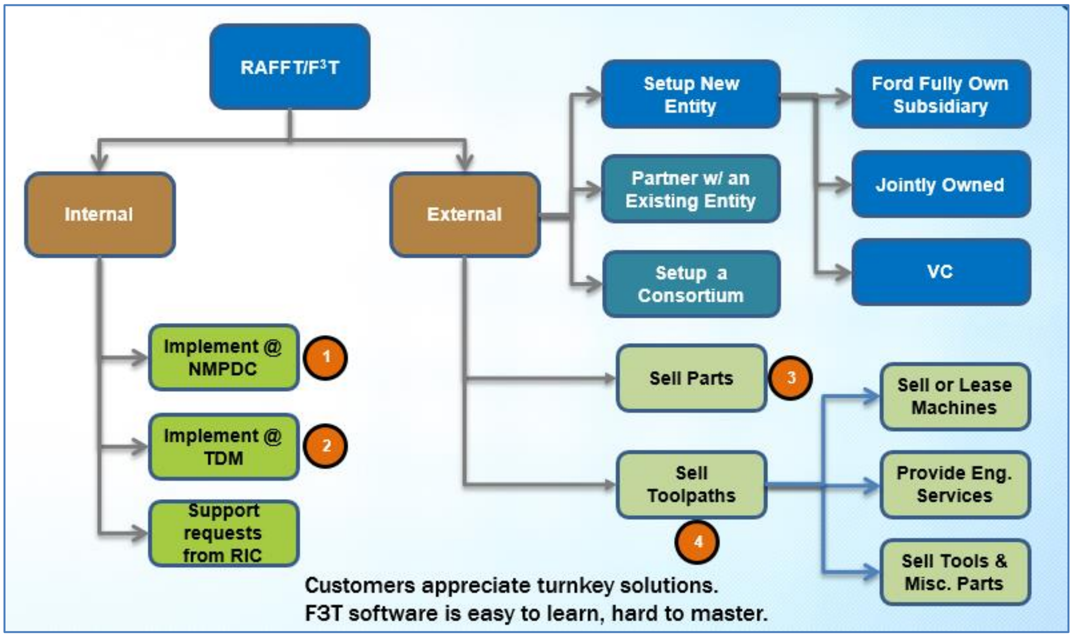

Figure 5.1 High Level RAFFT Deployment & Commercialization Options

We believe the optimum path for successful commercialization is to be carried out in three phases.

Phase 1: Implementing RAFFT technology at Ford's fully own subsidiary that provides stamping engineering and sheet metal prototype products to Ford as well as outside customers. During this this phase, RAFFT will be integrated and verified in to a complete sheet metal prototyping eco system that include trimming, hemming, flanging and joining. (24 months)

Phase 2: Ford's fully own subsidiary will be marketing and selling finished sheet metal prototype parts to customers outside of Ford (18 months)

Phase 3: Possibly, setting up a separate business entity for further developing marketing, selling, providing service and customer support for a commercial RAFFT eco system that includes

i. Service for marketing and selling toolpaths,
ii. RAFFT machines,
iii. RAFFT software platform, and
iv. RAFFT simulation methodologies & analytical tools.
v. Tool and misc. parts

Chapter 6. Accomplishments

Publications:

1. Rossie, KE. 2015. An energy and environmental analysis of aerospace sheet metal part manufacturing. Massachusetts Institute of Technology Master's thesis

2. Cooper, DR., Rossie, KE., and Gutowski, TG. 2017. An Environmental and Cost Analysis of Stamping Sheet Metal Parts. Journal of Manufacturing Science and Engineering: vol: 139, issue 4,

3. Cooper, DR., Rossie, KE., and Gutowski, TG. 2017. The energy requirements and environmental impacts of sheet metal forming: an analysis of five forming processes. Journal of Materials Processing Technology, vol: 244, pages 116-135

4. Cooper, DR. and Gutowski, TG. 2017. Prospective environmental analyses of emerging technology: a critique, a proposed methodology, and a case study on incremental sheet forming. Accepted in Journal of Industrial Ecology

5. Verma R., Thomas E., Martinek B., Gillard A., Kiridena V., 2017, "Post-forming mechanical properties of double-sided incrementally formed sheet alloys", Contributed Papers from Materials Science and Technology 2017, pp. 97 – 104.
6. Huaqing Ren, Newell Moser, Zixuan Zhang, Ebot Ndip-Agbor, Jacob Smith, Kornel F.Ehmann, Jian Cao, 2015, "Effects of Tool Positions in Accumulated Double-Sided Incremental Forming on Part Geometry", Journal of Manufacturing Science and Engineering, 137 (5), 0510081-051008.
7. Moser, N., Ndip-Agobr, E., Ren, H., Zhang, Z., Ehmann, K., Cao, J., 2014, "Challenges and Process Strategies Concerning Multi-Pass Double Sided Incremental Forming", Key Engineering Materials, 651-653.
8. Moser N, Pritchet D, Ren H, Ehmann KF, Cao J. 2016, "An Efficient and General Finite Element Model for Double-Sided Incremental Forming", ASME. J. Manuf. Sci. Eng., 138(9):091007-091007-10. doi:10.1115/1.4033483.
9. Moser, N., Zhang, Z., Ren, H., Ehmann, K., Cao, J., 2016, "An Investigation into the Mechanics of Double-Sided Incremental Forming using Finite Element Methods," AIP Conference Proceedings, 1769, art. no. 070021.
10. Ndip-Agbor, E., Smith, J., Ren, H., Jiang, Z., Xu, J., Moser, N., Chen W., Xia Z.C., Cao, J., 2016, "Optimization of relative tool position in accumulative double sided incremental forming using finite element analysis and model bias correction", International Journal of Material Forming, 9 (3), pp. 371-382.
11. Ndip-Agbor, E.E., Smith, J., Ren, H., Xu, J., Jiang, Z., Chen, W. and Cao, J., 2014, "Optimization of CAD-based Toolpath Generation in Accumulative-DSIF", Proceedings of ISFA2014. 2014 International Symposium on Flexible Automation, Japan.

12. Qiang Zeng, Kornel F. Ehmann and Jian Cao, 2014, “Tri-pyramid Robot: Design and Kinematic Analysis of a 3-DOF Translational Parallel Manipulator,” Elsevier, Robotics and Computer-Integrated Manufacturing, 30, pp. 648-657.
13. Qiang Zeng, Kornel F. Ehmann and Jian Cao, 2014, “Tri-pyramid Robot: Stiffness Modeling of a 3-DOF Translational Parallel Manipulator,” Cambridge University Press, Robotica, FirstView Article, pp. 1-20.
14. Qiang Zeng, Kornel F. Ehmann, Jian Cao, 2016, “Design of General Kinematotropic Mechanisms,” Elsevier, Robotics and Computer-Integrated Manufacturing, 38, pp. 67-81.
15. Ren H, Moser N, Zhang Z, Ehmann KF, Cao J., 2016, Effects of Tool Deflection in Accumulated Double-Sided Incremental Forming Regarding Part Geometry. ASME. International Manufacturing Science and Engineering Conference, Volume 1: Processing (): V001T02A069. doi:10.1115/MSEC2016-8839.
16. Zhang Z, Ren H, Xu R, et al. A Mixed Double-Sided Incremental Forming Toolpath Strategy for Improved Geometric Accuracy. ASME. J. Manuf. Sci. Eng. 2015;137(5):051007-051007-7. doi:10.1115/1.4031092.
17. Rui Xu, Xiaoting Shi, Dongkai Xu, Rajiv Malhotra, and Jian Cao, 2014, “A preliminary study on the fatigue behavior of sheet metal parts formed with accumulative-double-sided incremental forming”, SME Manufacturing Letter, 2, pp. 8-11.

Patent and Invention Disclosures:

1. Company: Ford
   Inventor(s): Feng Ren, Cedric Xia, Vijitha Kirideana
   Title: Interference Detection in Double Sided Incremental Forming

2. Company: Ford
   Inventor(s): Feng Ren, Cedric Xia, Vijitha Kirideana
   Title: High Stiffness Incremental Forming Tool

3. Company: Ford
   Inventor(s): Alan Gillard
   Title: Method of Incrementally Flanging a Workpiece and Creating Channel Features with Vertical Walls

4. Company: Northwestern
   Inventor(s): Jian Cao, Ebot Ndip-Agbor
   Title: An Automated Toolpath Generation Method for Double-Sided Incremental Forming of Three-Dimensional Freeform Shapes from Sheets

5. Company: Boeing
   Inventor(s): Justin Peters, & Brian Martinek, Brian
   Title: Programmable Tool Length Adjustment for DSIF Dual Sided Incremental Sheet Forming

6. Company: Boeing
   Inventor(s): Justin Peters
   Title: Method for generating continuous helix sweeping intersection (HIS) tool paths for parts presenting more than one central axis

Chapter 7. Conclusions

Energy Management & Environmental Impact Modeling:

- Based on the analysis conducted by this team, RAFFT presents large opportunities to save money on tooling costs during low-volume sheet metal part production. In addition, RAFFT presents large lead-time savings for extremely low-volume production (20 parts or less).
- At this early state of the technology, it is difficult to assign a monetary value to the time saved in production, but the saving could be used for additional design time and testing or to reduce overall product development time. Shortened lead-time represents a substantial competitive advantage for those companies that pursue this strategy. Like other flexible manufacturing technologies (such as additive manufacture), RAFFT is particularly suiTable when custom parts are required or where replacement parts are hard to come by (i.e., when the original tooling has been lost or if the product is situated in a remote location).
- The primary energy requirements associated with forming a part using RAFFT are dominated by the energy needed to make the sheet metal, much of which is scrapped and does not make it into the final part. In the authors' experiences, a low material yield is typical in ISF/RAFFT; however, as the technology matures there is potential to improve matching between the frame size and shape and the desired part size and shape.
- The cost of forming parts using RAFFT is dominated by equipment depreciation. Equipment depreciation may be reduced if forming times can be shortened.
- Electrical power consumption of the DSIF process while forming parts on RAFFT machine is strongly correlated to the forming time, which is determined by the size of the final part, the tool speed, and the vertical step size. In general, the baseload power of RAFFT is very low compared to the other processes. The approximately 0.7 kW corresponds to running the computer, controller, and lighting. However, after set-up, an additional 1.1 kW of power is required to run the hydraulic blank holding mechanism. The cooling system for the controller also intermittently increases the power requirements by an additional 1 kW. The power draw rises and falls in sync with the vertical rise and fall of the forming tools (the plane of the blank surface is vertical in this ISF machine). An average power factor of 0.31 implies that the motors used to move the indenters are over-sized for this application. It should be noted that as an emerging technology there has been less time and emphasis so far on design optimization of RAFFT than on design optimization of the more traditional processes.
- For the case of the RAFFT machine used in the case study, a hydraulic blank holder system runs continuously throughout the forming process. A passive blank holding system (such as nuts and bolts or a quicker snap-fit system) would eliminate the need for this continuous power draw.

Development, Integration and Verification of RAFFT System:

- RAFFT machine which can form sheet metal parts without using dies with an effective working (sheet) area of 2.0 m x 1.5 m is fully operational at Ford Motor Co. Research and Innovation center in Dearborn MI, since May 2015.
- This prototype experimental machine has the potential capability of making majority of sheet metal parts used in ground and aerospace applications.
- Panels have been successfully formed using six (6) different aluminum alloys and three (3) different steel alloys. However, panels made using aluminum alloys with low formability is more

susceptible to galling, fracture and lack of dimensional accuracy. An attempt to make panels with titanium alloys wasn't successful.

- Typical range of sheet thickness used for panels made with RAFFT is between 0.75 – 1.5 mm. Beyond 1.5 mm sheet thickness, the panels will be subjected to substantial non-local elastic and plastic deformation resulting poor dimensional accuracy.
- Use of shorter forming tools are better for maintaining dimensional accuracy. Similarly, tungsten carbide tools perform better than forming tools made with tool-steel.
- Use of Teflon grease along with coated tools proved to be a very effective way to lubricate and maintain low (coefficient of) friction during DSIF.

Tool Path Generation Algorithm, Simulation Modeling and Process Optimization:

- Second-Generation RAFFT (tool path-generation) software is fully integrated into CATIA environment. CATIA is the choice for CAD/CAM software for most large-scale automotive and aerospace companies worldwide.
- User interface of the Second-Generation RAFFT (software) tool-bench has the same feel as a native CATIA tool-bench making it an easy transition for an average CATIA user to start using RAFFT software for generating toolpaths.
- The knowledge gained during the last four years on making better DSIF parts is fully integrated in to the core of the RAFFT software. As the research continues in the years to come, we will continue to improve and enhance the core based on the new knowledge we gain on DSIF.
- Automation and templates are extensively used in RAFFT software in order to improve user experience and efficiency.
- Multiple methods and redundancies are built in to the software to protect the RAFFT machine while forming.
- Time to complete a DSIF simulation was substantially reduced through the development of new FEA simulation methodologies. However, it is still not practical to use such FEA simulations to plan for making parts that more closely conform to target dimensions.
- It seems that a database with optimum process parameter can be a more viable way to use simulations to guide forming parameters using simulations to produce parts with better dimensional accuracy.

Electrically-assisted Freeform Sheet Metal Forming:

- Achieved a good understanding of the effectiveness of post-deformation EAM treatments for reducing part springback, based on the effect of various physical process parameters such as feed rate, step-over, step-down, clamping mechanism, etc on part distortion.
- Also, the effectiveness of various EAM process parameters such as current density, duration, etc on part distortion is being understood

Material Characterization & Performance Validation:

- Both the automotive and aerospace sheet alloys subjected to DSIF exhibit highly isotropic propoerties as evidenced by small differences in the results for L and LT orientations.

- There is little difference in mechanical properties parallel to and transverse to the forming tool path in DSIF. Forming increases ultimate and yield strengths and reduces elongation.
- In DDQ, 5754-O and 2024-O alloys, yield strength is more than doubled and percent elongation reduced to less than half upon forming. As expected, the higher strength sheet tempers, 6111-T4, 2024-T3, 7075-T6, exhibit smaller strength increases post forming.
- In age-hardenable aluminum alloys, forming in the O-temper followed by full heat treatment by solutionizing, quenching, and aging to harder tempers, not only tremendously increases sheet strength, it also equalizes both strength and elongation properties between the unformed and formed regions of the panel. All formed regions with parts made using DSIF exhibit increased ultimate strength and yield strength and decreased percent elongation, compared to the corresponding parent materials, indicating work hardening in the formed regions.
- The aerospace aluminum panels for mechanical and fatigue testing were formed using a thin-gage steel overlay sheet as a buffer between the Al sheet being formed and the outer forming tool. The steel overlay sheet prevents localization of load on the outer surface, and provides acceptable surface smoothness in O-temper (soft) sheet materials.
- Metallography of cross sections cut from the 7075-O panels, shows more grain refinement with the smaller step size.
- The use of the overlay sheet resulted in a much smoother surface. For example, a 2024 panel formed with 0.05 mm step size shows a roughness of 35 Ra parallel to the tool direction and 32 Ra in the perpendicular direction. The inner surface of panel, which directly comes in contact with the tool, however, exhibits sharp differences in surface roughness along the two directions. As an additional example, the inner surface of 2024 panel, formed with 0.20 mm step size, shows a roughness of 13 Ra parallel to the tool direction and 61 Ra perpendicular to the tool direction. Further, the Ra is affected by the alloy and the step size.
- Sheet thinning in both alloys essentially follows the cosine law.
- Under low-cycle regime, interaction with the RAFFT tools shows to significantly reduce fatigue life, especially in test direction perpendicular to the tool path. Compared to aerospace alloys, automotive alloys under high-cycle regime, interaction with the ISF tool appears to increase fatigue strength of the sheet material. At this stage, the effect of specimen orientation relative to tool path is not very clear – further study in fatigue is required.

Chapter 8. Recommendations

- Create RAFFT sheet metal prototyping "ecosystem" where RAFFT systems are fully integrated with sheet metal finishing processes - trimming, hemming, flanging and joining.
- Develop a family of next generation RAFFT machine with three standard work volumes based on the same machine architecture. Current RAFFT machine has a workspace of 2 m x 1.5 m which is still not large enough to produce automotive parts such as body sides and large hoods. Similar examples can be seen across automotive and other industries. The recommendation is to build a family of machines based on work volumes of 1 m x 1m x 0.4 m (small), 2 m x 1.5 m 0.6 m (medium) and large 3.0 m x 2 m 0.8 m (large).
- Expand the study and evaluation of material properties, formability and, fatigue for a broad range of materials used with RAFFT process beyond steel and aluminum alloys used during this project..
- Investigate new ways to reduce the full model (with higher fidelity) simulation time at-least comparable with actual forming time by adopting new FEA software which are more suited for DSIF simulations and rely on faster multi-processing computers.
- Develop an integrate hardware and process for automated loading of blanks and unloading of formed panels.
- Innovate new sheet clamping method that does not require to use picture frame-based clamping of sheet blanks
- Use only the industry leading controllers and associated controller hardware in order to reduce operator and maintenance training.
- Design and build force feedback in to the machine. wireless measuring and recording the forming forces does not appear to be at a mature stage
- Investigate strategy for automated or semi-automated method for application of sheet stiffeners to reduce sheet metal springback.
- Enhance the squeeze factor database for new materials.
- Continue to improve and enhance toolpath generation algorithms.
- Utilize parallel processing to reduce time to generate first toolpath based on CAD model with a very fine tolerance, which makes a huge difference in dimensional accuracy and surface quality.
- Develop automated or semi-automated CAD software tools to generate addendums surfaces can potentially decrease the amount of engineering design work that needs to go into the creating a part using the RAFFT process.
- Adopt remote video monitoring and recording by installing cameras on the machine and on the spindle to watch the act of forming with the RAFFT machine. Having visual data associated with part failures may help both with understanding the failure mechanisms, and through remote monitoring may be able to alert operators of issues.
- Incorporate hardened security measures with the next generation of RAFFT machines, so they can be networked.
- Can eliminate the rotational capabilities of the spindle during forming. Most of the time, rotating the spindles during DSIF forming lead to part. Also, it is possible to save about 15% of the cost of the machine by eliminating the rotating spindles.

- Develop RAFFT's own Z-level machining capabilities. Licenses for CATIA are very expensive so in the interest of commercialization, the decoupling between CATIA and the RAFFT software may be very advantages.

Chapter 9. References

- Allwood, J. M., Childs, T. H. C., Clare, A. T., De Silva, A. K. M., Dhokia, V., Hutchings, I. M.,

- Allwood, J. M., King, G. P. F. and Duflou, J. (2005) ‘A structured search for applications of the incremental sheet-forming process by product segmentation’, Proceedings of the Institution of Mechanical Engineers, Part B: Journal of Engineering Manufacture, 219(2), pp. 239–244. doi: 10.1243/095440505X8145.

- Allwood, J., Cullen, J., Carruth, M., Cooper, D., McBrien, M., Milford, R., Moynihan, M. and Patel, A. (2012) ‘Sustainable Materials with Both Eyes Open’, Cambridge: UIT.

- Bambach, M. (2013). ‘Fast simulation of asymmetric incremental sheet metal forming’, AIP Conference Proceedings, 1567(1), pp. 844-847.

- Bass, F. M. (1969) ‘A New Product Growth for Model Consumer Durables’, Management Sience, 15(August), pp. 215–227. doi: 10.1287/mnsc.1040.0264.

- Branker, K., Adams, D. and Jeswiet, J. (2012) ‘Initial analysis of cost, energy and carbon dioxide emissions in single point incremental forming - producing an aluminum hat’, International Journal of Sustainable Engineering, 5(3), pp. 188–198.

- Brown, H., Hamel, B. and Hedman, B. (1985) Energy analysis of 108 industrial processes. Fairmont Press.

- Burnham, A., Wang, M. and Wu, Y. (2006) ‘Development and Applications of GREET 2.7 — The Transportation Vehicle-Cycle Model’, Energy, pp. 124. doi: 10.2172/898530.

- Cooper, D. R., Rossie, K. E. and Gutowski, T. G. (2016) ‘An environmental and cost analysis of stamping sheet metal parts’, Journal of Manufacturing Science and Engineering. doi: 10.1115/1.4034670.

- Cullen, J. M. and Allwood, J. M. (2013) ‘Mapping the global flow of aluminum: from liquid aluminum to end-use goods’, Environmental science & technology, 47(7), pp. 3057–64. doi: 10.1021/es304256s.

- Cullen, J. M., Allwood, J. M. and Bambach, M. D. (2012) ‘Mapping the global flow of steel: from steelmaking to end-use goods’, Environmental science & technology, 46(24), pp. 13048–55. doi: 10.1021/es302433p.

- Jones, B., and Nachtheim, C. (2013) ‘Definitive Screening Designs with Added Two-Level Categorical Factors’, Journal of Quality Technology, 45(2).

- Dittrich, M. a., Gutowski, T. G., Cao, J., Roth, J. T., Xia, Z. C., Kiridena, V., Ren, F. and Henning, H. (2012) ‘Exergy analysis of incremental sheet forming’, Production Engineering, 6(2), pp. 169–177. doi: 10.1007/s11740-012-0375-9.

- Final program report for DLA IBIF program entitled, ‘Incremental Sheet Forming for Aging Department of Defense Asset Sustainment ’, Contract SP4701-09-C-0011.

- Friedman, P. a., Luckey, S. G., Copple, W. B., Allor, R., Miller, C. E. and Young, C. (2004)

'Overview of Superplastic Forming Research at Ford Motor Company', Journal of Materials Engineering and Performance, 13(6), pp. 670–677. doi: 10.1361/10599490421277.

- Hadoush, A. and Van Den Boogaard, A. H. (2009) 'Substructuring in the implicit simulation of single point incremental sheet forming', International Journal of Material Forming, 2, pp. 181-189.

- Heinz, A., Haszler, A., Keidel, C., Moldenhauer, S., Benedictus, R. and Miller, W.S. (2000) 'Recent development in aluminum alloys for aerospace applications', Material Science Engineering, A280, pp.102-107.

- Ingarao, G., Ambrogio, G., Gagliardi, F. and Di Lorenzo, R. (2012) 'A sustainability point of view on sheet metal forming operations: material wasting and energy consumption in incremental forming and stamping processes', Journal of Cleaner Production. Elsevier Ltd, 29–30, pp. 255–268. doi: 10.1016/j.jclepro.2012.01.012.

- Ingarao, G., Kellens, K., Behera, A., Vanhove, H., Ambrogio, G. and Duflou, J. (2013) 'Electric energy consumption analysis of SPIF processes'.

- Jackson, K. and Allwood, J. (2009) 'The mechanics of incremental sheet forming', Journal of Materials Processing Technology, 209(3), pp. 1158–1174. doi: 10.1016/j.jmatprotec.2008.03.025.

- Kalpakjian, S. and Schmid, S.R. (2008). 'Manufacturing processes for engineering materials', 5th ed.

- Lamminen, L., Wadman, B., Kutter, R. and Svinning, T. (2004) ProSheet: Prototyping and low-volume production of sheet metal components.

- Lee, S. (1992) Handbook of Composite Reinforcements. New York: John Wiley & Sons.

- Lovell, M., Higgs, C. F., Deshmukh, P. and Mobley, a. (2006) 'Increasing formability in sheet metal stamping operations using environmentally friendly lubricants', Journal of Materials Processing Technology, 177(1–3), pp. 87–90. doi: 10.1016/j.jmatprotec.2006.04.045.

- Luckey, S. G., Subramanian, S., Young, C. and Friedman, P. a. (2007) 'Technical and Cost Study of Superplastic Forming of a Lightweight Aluminum Door Structure', Journal of Materials Engineering and Performance, 16(3), pp. 266–273. doi: 10.1007/s11665-007-9047-x.

- Ma, L. W., Mo, J. H. (2007) 'Three-dimensional finite element method simulation of sheet metal single-point incremental forming and the deformation pattern analysis', the Proceedings of Institution of Mechanical Engineers, 222, Part B: Journal of Engineering Manufacture.

- Memicoglu, P., Music, O., Karadogan, C. (2017) 'Simulation of incremental sheet forming using partial sheet models', Procedia Engineering, 207, pp. 831-835.

- Milford, R. L., Allwood, J. M. and Cullen, J. M. (2011) 'Assessing the potential of yield improvements, through process scrap reduction, for energy and CO2 abatement in the steel and aluminum sectors', Resources, Conservation and Recycling. Elsevier B.V., 55(12), pp. 1185–1195. doi: 10.1016/j.resconrec.2011.05.021.

- Muresan, I., Brosius, A., Homberg, W., Kleiner, M. (2005) 'Finite element analysis of incremental sheet metal forming', Proceedings of ESAFORM, pp. 105-108.

- Omar, M. (2011) 'The Automotive Body Manufacturing Systems and Processes'. New York: John Wiley & sons.

- Pae, J. H. and Lehmann, D. R. (2003) 'Multigeneration Innovation Diffusion: The Impact of Intergeneration Time', Journal of the Academy of Marketing Science, 31(1996), pp. 36–45. doi: 10.1177/0092070302238601.

- Peltier, D. J. and Johannisson, T. G. (1998) 'Flexforming of Prototype and Low-Volume Parts (SAE Technical Paper Series (982398))', in Proceedings of the IBEC '98, Volume 5, Body Manufacturing, Assembly, and Advanced Manufacturing, pp. 334.

- Petek, A., Gantar, G., Pepelnjak, T. and Kuzman, K. (2007) 'Economical and Ecological Aspects of Single Point Incremental Forming Versus Deep Drawing Technology', Key Engineering Materials, 344, pp. 931–938. doi: 10.4028/www.scientific.net/KEM.344.931.

- Red, C. (2014) 'The market for OOA Aerocomposites, 2013-2022', High-Performance Composites, (Jan 2014), pp. 42–49.

- Rogers, E. M. (2003) Diffusion of Innovations. 5th edition. Edited by F. Press. New York.

- Rossie, K. (2015) 'An energy and environmental analysis of aerospace sheet metal part manufacturing'' Massachusetts institute of technology.

- Roth, J. T., Loker, I., Mauck, D., Warner, M., Golovashchenko, S., Krause, A. (2008) 'Enhanced formability of 5754 aluminum sheet metal using electric pulsing', Trans.NAMRI/SME, 36, pp. 405.

- Roth, J., Cao, J. (2011) 'Electrical-assisted Double Side Incremental Forming and Processes Thereof', US Patent application.

- Schuler GmbH (1998) Metal forming handbook. New York: Springer-Verlag.

- Smil, V. (2008) Energy in nature and society. Cambridge: MIT Press.

- Smith, J., Malhotra, R., Liu, W. K., Cao, J. (2013) 'Deformation mechanics in single-point and accumulative double-sided incremental forming', International Journal of Advanced Manufacture Technology, 69, pp. 1185-1201.

- Tuomi, J. and Vihtonen, L. (2007) 'Incremental sheet forming (ISF) as small batch production method', in Paulo Jorge da Silva Bartolo, Mateus Artur Jorge, Fernando da Conceicao Batista, Henrique Amorim Almeida, Joao Manuel Matias, Joel Correia Vasco, Jorge Brites Gaspar, Mario Antonio Correia, Nuno Carpinteiro Andre, Nuno Fernandes Alves, Paulo Parente Novo, R. A. C. (ed.) Virtual and Rapid Manufacturing: Advanced Research in Virtual and Rapid Prototyping. CRC Press, pp. 611–617.

- Van Den Bulte, C. (2002) 'Want to know how diffusion speed varies across countries and products? Try using a Bass model', PDMA Visions, XXVI (4), pp. 5.

- Zhao, K., Liu, Z., Yu, S., Li, X., Huang, H. and Li, B. (2015) 'Analytical energy dissipation in large and medium-sized hydraulic press', Journal of Cleaner Production. Elsevier Ltd, 103, pp. 908–915. doi: 10.1016/j.jclepro.2014.03.093.

Chapter 10. Appendices

- **Appendix A**: Daniel Cooper, Alex van Grootel, and Timothy Gutowski, 2017 Rapid Freeform Sheet Metal Forming: Potential environmental and economic benefits, DE-EE0005764 (134 pages) (https://www.dropbox.com/sh/qkjof6n8el9y0h3/AAC7SFxJkPZw1CEm2axoQRMda?dl=0)

- **Appendix B**: Kathleen Eaton Rossie, M.S. Thesis 2015, An Energy and Environmental Analysis of Aerospace Sheet Metal Parts Manufacturing, (347 pages) (https://dspace.mit.edu/handle/1721.1/101487)